HOKKAIDO UNIVERSITY

Title	Development of a Robot Combine Harvester Based on GNSS
Author(s)	張, 澤
Citation	北海道大学. 博士(農学) 甲第11394号
Issue Date	2014-03-25
DOI	10.14943/doctoral.k11394
Doc URL	http://hdl.handle.net/2115/56100
Type	theses (doctoral)
File Information	Zhang_Ze.pdf

Instructions for use

Hokkaido University Collection of Scholarly and Academic Papers : HUSCAP

Development of a Robot Combine Harvester based on GNSS

GNSS を用いたロボットコンバインの開発に関する研究

2014

北海道大学　　大学院農学院

環境資源学専攻　　博士後期課程

張　澤

Zhang Ze

Development of a Robot Combine Harvester based on GNSS

BY

Zhang Ze

Dissertation

Submitted to Department of Environmental Resources in the

Graduate School of Agriculture

Hokkaido University, Sapporo, Japan, 060-8589 in partial fulfillment of

the requirements for the degree of

Doctor of Philosophy

2014

TABLE OF CONTENT

ACKNOWLEDGEMENT

I would like to express my deep gratitude to Dr. Noboru Noguchi, my research supervisor, for his patient guidance, enthusiastic encouragement and useful critiques of this research work. His passion and knowledge has always been like a beacon, which influenced and guided me throughout the whole process of study. Without his help, the study would not have been possible.

My grateful thanks are also extended to Dr. Kazunobu Ishii. I would like to thank him for sharing his knowledge in programming and robot control, especially his guidance in during the field experiments.

I also would like to extend my thanks to Dr. Yutaka Kaizu and Dr. Hiroshi Okamoto for their advice and their help. In addition, I would like to express my gratitude to Mr. Sato and Mr. Wada from Hokkaido University and Mr. Wataru Nakagawa and Mr. Toshi Furuta from Yanmar Co., Ltd. for their help in building and maintenance the platform in this study.

I am also grateful to Mr. Jongmin Choi, Mr. Liangliang Yang, Mr. Xiang Yin, Mr. Ryosuke Takai, Mr. Fumisato Kawahara, Mr. Chi Zhang and Mr. Ziyi Fan for their participation in the field experiments.

Furthermore, I would like to thank Dr. Minzan Li, my supervisor in master's study, for recommending me to further my study in Laboratory of Vehicle Robotics. Without his support, I would not have had the opportunity to study in the top laboratory in the field of off-road vehicle robotics.

Finally, I would like to thank my parents and my girlfriend Ms. Xin Li for their love, understanding and support.

LIST OF FIGURES

LIST OF TABLES

NOTATION

A	The vector from the GPS antenna to the center of the crawlers	
a_k	A boundary in the Golden Section Search	
b_k	A boundary in the Golden Section Search	
d	The lateral error in a navigation	[m]
d_0	The initial lateral error in a navigation	[m]
d_N	The vector that points at north	
E	The compensation matrix of the robot's position	
E^2	The Euclidian two-dimensional space	
E^3	The Euclidian three-dimensional space	
g_h	The heading gain of the robot vehicle	
g_l	The lateral gain of the robot vehicle	
L	The look-ahead distance of the robot vehicle	
k	The step index in the Golden Section Search	
l	The lever angle of the robot vehicle	
N	The number of navigation points in Ω	
N^*	The number of navigation points in Ω^*	
P	The position data obtained from the GPS receiver	
$\mathbf{P}'$	The compensated position of the robot	
R	The turning radius of the vehicle	[m]
v_s	The velocity of the vehicle in a straight movement	[m/s]
v_t	The velocity of the vehicle in a turning movement	[m/s]
x_0	The coordinate on *x* axis in the beginning	

x_c	The absolute value of the compensation vector on *x* axis	
x_g	The coordinate on *x* axis received by GPS receiver	
x_h	The coordinate on *x* axis of the combine harvester's header	
x_t	The coordinate on *x* axis at time *t*	
y_0	The coordinate on *y* axis in the beginning	
y_c	The absolute value of the compensation vector on *y* axis	
y_g	The coordinate on *y* axis received by GPS receiver	
y_h	The coordinate on *y* axis of the combine harvester's header	
y_t	The coordinate on *y* axis at time *t*	
Δt	A short period time to calculate position of the vehicle	[s]
$\Delta\phi$	The heading error in a navigation	[degree]
ε	Precision requirement in the Golden Section Search	
δ	The steering angle of the robot vehicle	
η	The robot vehicle's position	
θ_p	The pitch angle received from the IMU	[degree]
θ_r	The roll angle received from the IMU	[degree]
λ	A parameter on the interval [0,1]	
λ_k	A calculated candidate gain	
μ_k	A calculated candidate gain	
ξ	A navigation point on the interval $[\omega_{c1}^*, \omega_{c2}^*]$	
$\xi_{closest}$	The calculated closest point on the navigation map	
ξ_t	A calculated point on the interval $[\omega_j^*, \omega_{j+1}^*]$	
ϕ	The heading of the robot vehicle in a navigation	[degree]
ϕ_0	The heading of the robot vehicle in the beginning	[degree]

ϕ_d	The desired heading of the robot vehicle in a navigation	[degree]
ϕ_t	The heading of the robot vehicle at time *t*	[degree]
Ω	A set of navigation points	
Ω^*	A sub set of navigation points of Ω	
ω	The angular velocity of the robot vehicle	[rad/s]
ω_i	A navigation point in Ω	
ω_{c1}^*	The closest navigation point to the robot vehicle	
ω_{c2}^*	The second closest navigation point to the robot vehicle	
ω_j^*	The farthest navigation point in the look-ahead distance	
ω_{j-1}^*	The closest navigation point out of the look-ahead distance	

ACRONYMS AND ABBREVIATIONS

2D	Two Dimensional
CAN	Controller Area Network
DGPS	Differential GPS
ECU	Electronic Control Unit
FDS	Full-time Drive System
FOG	Fiber Optical Gyroscope
GDS	Geomagnetic Direction Sensor
GNSS	Global Navigation Satellite System
GPS	Global Positioning System
HG	Heading Gain
IMU	Inertial Measurement Unit
LG	Lateral Gain
MAFF	Ministry of Agriculture, Forestry and Fishery (of Japan)
PDA	Personal digital assistant
RMS	Root Mean Square
RTK-GPS	Real-Time Kinematic GPS
USCB	United States Census Bureau
UTM	Universal Transverse Mercator (coordinate system)
VRS	Virtual reference station

CHAPTER 1

INTRODUCTION

1.1 Research background

1.1.1 Necessity of the research

According to a statistic given by the United States Census Bureau (USCB), the world population exceeded 7 billion on March 12, 2012. (http://www.worldometers.info/world-population/). By November, 2013, this number has exceeded 7.2 billion. What problems has the booming population brought us? The most serious one might be how to feed it. This is probably a big challenge to modern agriculture as well.

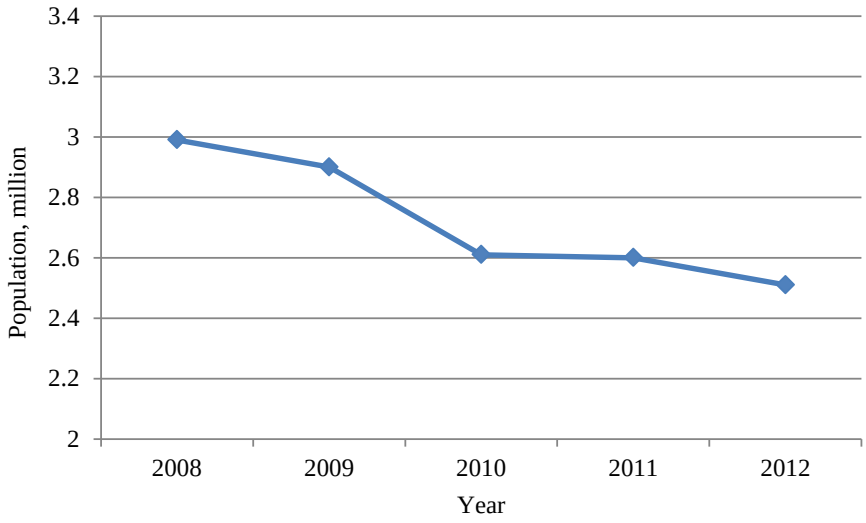

Figure 1-1 Agricultural population in Japan from 2008-2012

Another problem arisen with the growth of population is that the number of agricultural population did not grow. It even decreased in the developed countries, such as Japan. Aging of the population has been an issue that made the problem more serious.

According to a census conducted by the Ministry of Agriculture, Forestry and Fishery (MAFF) of Japan, the number of agricultural population decreased, but its average age increased in the past 5 years. Figure 1-1 shows that in the past 5 years, the number of the agricultural population in Japan has decreased from 3 million to 2.5 million, while the average age of the population increased, as shown in Figure 1-2, from 65.2 to 66.2. (http://www.maff.go.jp/ j/tokei/ sihyo/data/08.html)

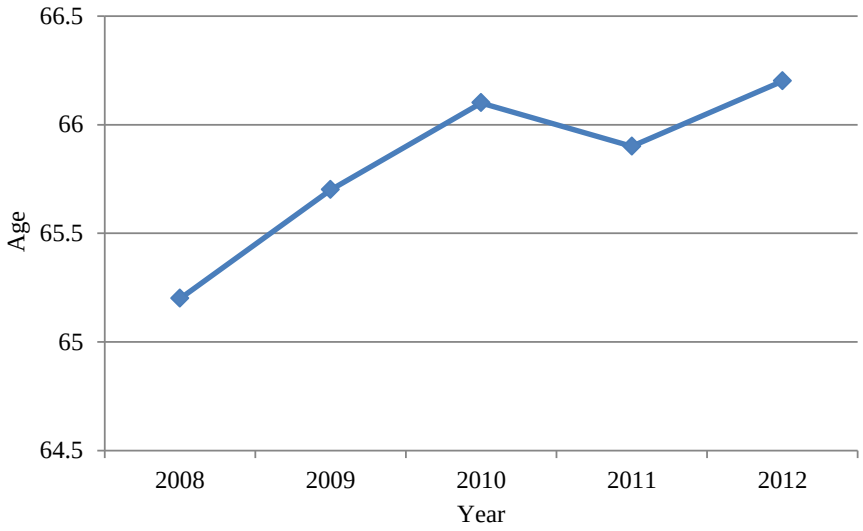

Figure 1-2 The age of agricultural population in Japan from 2008-2012

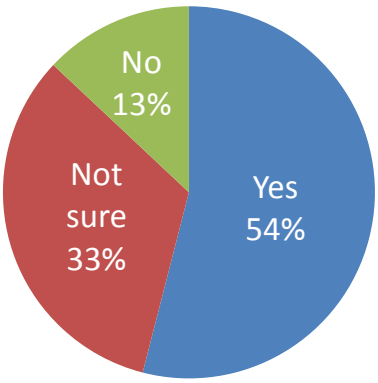

Figure 1-3 Response given by farmers in Hokkaido on agricultural robots (Northern Advancement Center for Science & Technology)

In order to solve the problems cause by the decreasing and aging of the agricultural population, the MAFF has been promoting the development of agricultural robots. A survey conducted to the farmers in Hokkaido, Japan showed that when asked whether they would like to try to use agricultural robots (robot tractors or so) in farm work, over 50% of the people responded with a positive answer. The result of the survey is shown in Figure 1-3.

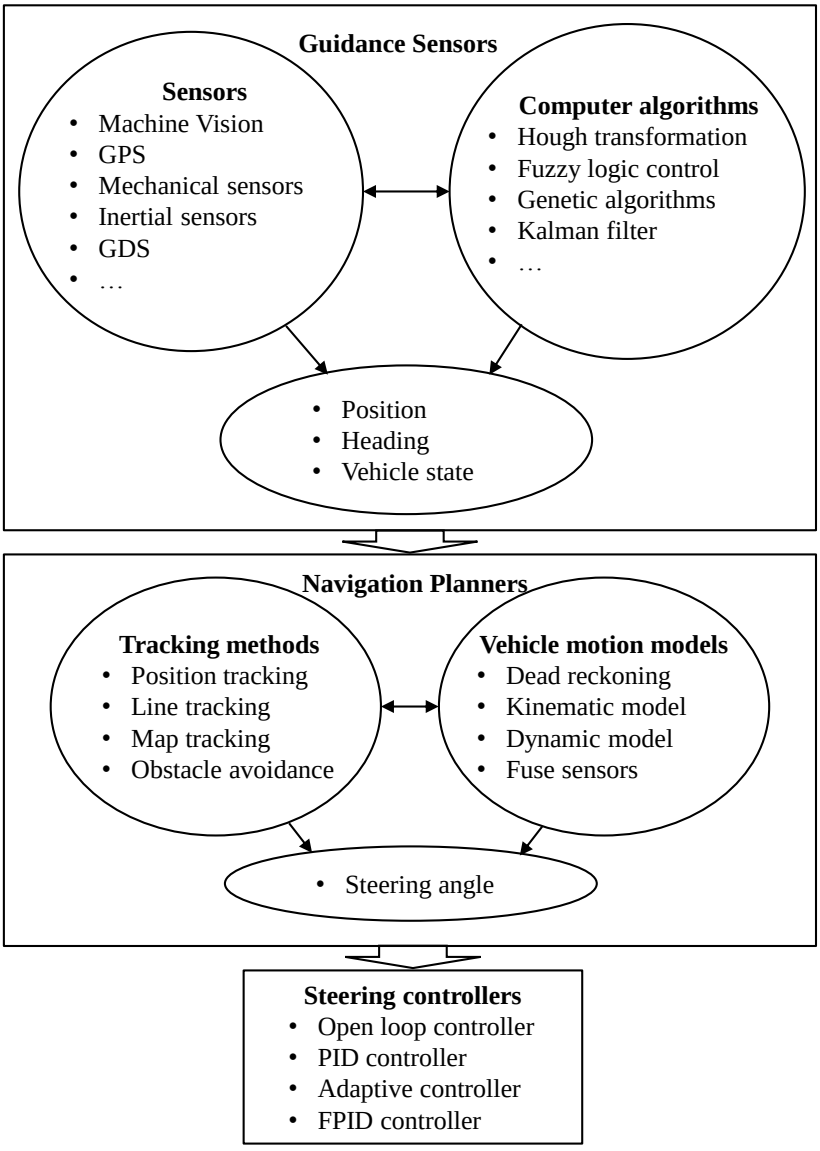

Figure 1-4 Framework of agricultural vehicle autonomous guidance system

As a result, the situation in Japan indicates that it is a trend to develop robot vehicles to replace human labor force in the field. At the same time, the government and the majority of the farmers are ready to accept agricultural vehicles in their farm work.

1.1.2 Autonomous navigation systems

Driving an agricultural vehicle requires the driver to be highly concentrated, for the vehicle should be driven either straight or parallel to a certain curve. At the same time, it is necessary for the driver to pay attention to the safety of driving. As a result, fatigue of the driver is likely to happen. However, if the driver can be replaced by an autonomous navigation vehicle, the problem can be solved, since a robot never fails to concentrate.

A framework of agricultural vehicle autonomous guidance system was presented by Ming Li *et al*. (2009) as shown in Figure 1-4. The key elements to it are guidance sensors, computational methods, navigation planners and steering controllers.

Figure 1-5 A robot tractor using a vision and a GDS sensor
(Ishii *et al*. 1994, 1995, 1998)

In term of navigation sensors, the most frequently used are Global Positioning System (GPS), inertial sensors, geomagnetic direction sensors (GDS), machine vision and laser sensors. Ishii *et al*. (1994, 1994, 1995, 1998) developed a robot tractor by

using a vision sensor and a GDS sensor, as shown in Figure 1-5. Tosaki *et al*. (1996, 1997, 1998) developed a unmanned sprayer by using induction cable. Noguchi *et al*. (1998) developed a guidance system by sensor fusion of an RTK-GPS, a GDS and machine vision. Tillet *et al*. (1998) developed a robot system for plant-scale husbandry by using a vision sensor, a wheel speed sensor, a GDS and an inclination sensor. Stombaugh *et al*. (1998) developed a kinematic differential GPS based autonomous navigation system by installing an automatic steering controller on a Case-IH Model 7220 tractor. Inoue *et al*. (1999) developed an automatic tractor by using Kalman-filter based sensor fusion. Nagasaka *et al*. (1999) fused an RTK-GPS and a FOG and developed a robot transplanting machine. Cho *et al*. (1999) developed a speed sprayer by using machine vision. It can even detect obstacles by an ultra-sonic sensor. Bell (2000) developed an automatic tractor by using carrier-phase differential GPS. Reid *et al.* (2000), developed automatic windrower by using vision system. Pinto *et al*. (2000), by using machine vision and principal component analysis, developed a vehicle guidance parameter determination system.

Figure 1-6 A robot tractor by using RTK-GPS and FOG
(Kise *et al.* 2001)

Benson *et al*. (2001) developed a steering system for combine harvester based on machine vision. Mizushima *et al*. (2001) developed an automatic guidance system by using sensor fusion of a GDS and a gyroscope. Kise *et al*. (2001, 2003) developed a robot tractor by using RTK-GPS and FOG, as shown in Figure 1-6. Bevly (2001) realized implement control for autonomous tractors. Noguchi *et al.* (2004) developed a master-slave robot system. Nagasaka *et al*. (2004, 2009, 2013) used global positioning and gyroscopes and developed autonomous guidance for rice transplanting. Han *et al.* (2004) developed a method to evaluate auto guidance systems. Suguri *et al.* (2004) developed an autonomous crawler wagon based on RTK-GPS. Keskin *et al*. (2006) developed an automatic agricultural vehicle based on low cost GPS receiver. Subramanian *et al*. (2006) developed an autonomous navigation system for citrus grove by using machine vision and laser radar. Iida and Yamada (2006) developed a rice harvesting machine by using a GPS and FOG. Barawid *et al*. (2007) developed an autonomous vehicle that can be used in an orchard by using 2D laser scanner and Hough Transformation, as shown in Figure 1-7. Gan-Mor *et al.* (2007) implemented the accuracy of RTK-GPS tractor guidance. Vougioukas (2007) realized a non-linear model predictive control for robots. Kaizu and Imou (2008) developed a dual-spectral camera system for paddy rice seedling row detection. Coen *et al.* (2008) developed a robot combine harvester. Oksanen and Visala (2009) developed a coverage path plan for field agricultural machines. Takai *et al.* (2010) developed a crawler-type robot tractor based on GPS and IMU. Cariou *et al.* (2010) realized a path following system. Noguchi and Barawid (2011) developed a robot farming system with multi-tractors. Iida *et al,* (2011, 2013) developed a head-feeding robot combine harvester. Saito et al.(2012) developed rice combine harvester based on CAN bus system. Perez-Ruiz *et al*. (2012a, 2012b)

developed a weed control system for transplanted row crops based on RTK-GPS. Backman et al. (2012a, 2012b, 2013) developed a navigation system for agricultural machines and a compensation system for snow ploughing. Kataoka *et al.* (2013) introduced an autonomous agriculture vehicle.

Figure 1-7 An autonomous vehicle using a 2D laser scanner
(Barawid *et al.* 2007)

1.2 Objectives

From the studies listed above, it can be concluded that the advantages to use the GPS systems are:

1. Absolute coordinate can be measured. Sometimes for a certain field, the farm use it for the same purpose every year, as a result, by measuring the absolute coordinate, it is possible to use it once and once again. Besides, it is easy to share the route among different robots, such as tractor, rice transplanting machine and combine harvester.

2. There is no error accumulation. Even if the GPS data might be inaccurate at one point, it does not affect other points.

3. Even if the predetermined route of the robot vehicle is a curve, the robot vehicle can still follow it easily if properly programed.

However, there are also some disadvantages to use GPS systems. One is that the signal of GPS satellites can be easily blocked by buildings and trees. As a result, GPS systems cannot be used as a navigation sensor in an orchard with trees taller than the GPS receiver. Moreover, there is inherent time delay in the GPS system.

For machine vision systems, there are both advantages and disadvantages and they are discussed as below. The vision systems can be used in the microwave shielded areas, such as in the orchard. The cost of machine vision systems is finally lower than the GPS systems. However, they can only measure relative positions and the lateral error often accumulates. For example, if a robot combine harvester harvests the crops with machine vision systems, the level of accuracy in current path usually depends on the previous path and the error may be greater as the number of path increases. Another disadvantage of machine vision system should be that it can be affected severely by weather condition and the condition of the field. For example, the lodging of crops has an adverse impact on the machine vision system on a robot combine harvester and in a backlighting situation the accuracy of machine vision usually decreases sharply.

As for the situation of a robot combine harvester, there are seldom many trees around the crop field. On the other hand, in order to develop a robot combine harvester usable even in a field with lodging crops, GPS systems was chosen as the navigation sensor for the system.

There are several challenges in the development of robot vehicles for agricultural use.

Sometimes, robots are not reliable due to their unreliable control system. Wiring of the robot may also cost a long time. For example, the interface to ECU may not be well connected and too many wires in the system make it impossible to check. Moreover, it usually takes the developer of the robot vehicle quite long time to obtain optimal control parameters. Furthermore, current robot combine harvesters always use one path plan for all the crops. However, different crops or fields may require different path plans.

In order to solve the problems described above, the objectives of this study were set as follows:

1. To develop a robot combine harvester that can receive position and posture data from corresponding sensors, such as a GPS receiver and an IMU.
2. To apply an algorithm to the robot combine and to control the robot combine harvester by sending commands to the ECU reliably.
3. To monitor the robot combine harvester by receiving status data from the vehicle
4. To find an effective and universal way to optimize the control parameters of the robot vehicle and improve the efficiency in optimization.
5. To develop two path plans for different situations, such as a large field and a small field or for wheat and for paddy rice, etc.
6. To develop a robot combine harvester that can be used for wheat, paddy rice and soybean.
7. To conduct experiments in the field for wheat, paddy rice and soybean.

CHAPTER 2

RESEARCH PLATFORM AND MATERIALS

2.1 Research platform

This research was conducted on a Yanmar AG1100 combine harvester, this machine is designed for not only paddy and wheat harvesting, but also soybean harvesting. Due to the size limit (100m by 30m) in Honshu area of Japan, agricultural machines are usually not in a large size. This machine, however, is the largest combine harvester produced by the manufactures in Japan. Figure 2-1 gives the original look of the combine harvester with a general-purpose header, which has no navigation equipment on it.

Figure 2-1 Original look of Yanmar AG1100 combine harvester

The AG1100 has 110 horsepower or 80.9 kW output and the rotation speed of the engine is 2500rpm. In order to prolong its working time, a 110-liter diesel tank is equipped, with which the combine can be expected to work continuously for a whole day.

This machine is designed to mainly conduct wheat and paddy rice harvesting work with a general-purpose header. If changed to row crop header, the combine harvester can also conduct soybean and other crops' harvesting. A more detailed specification is given in Table 2-1.

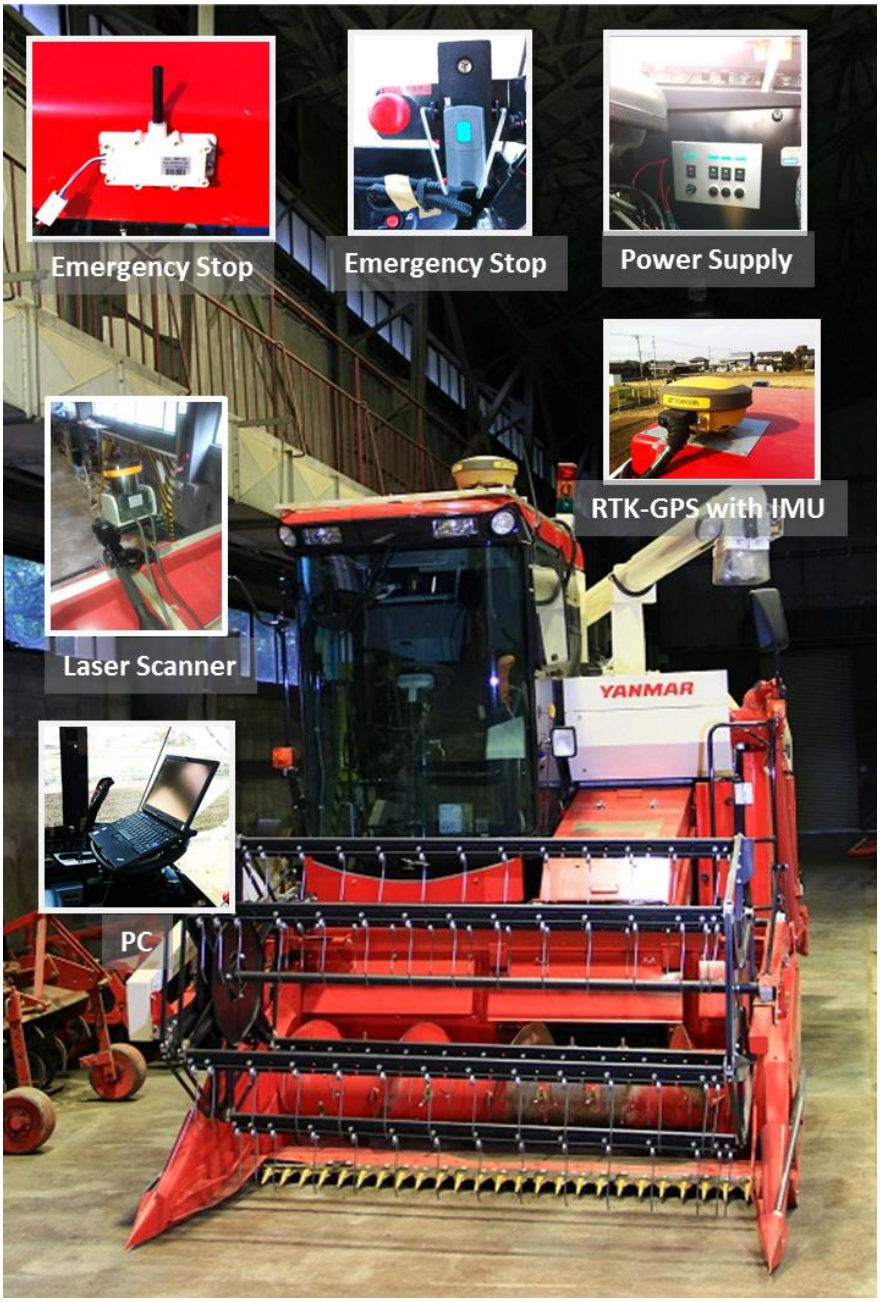

Figure 2-2 Robot combine harvester with necessary devices

Table 2-1 Combine Harvester Specifications

Dimensions:	
Overall Length:	6,150 mm
Overall Width:	2,350 mm
Overall Height:	2,760 mm
Weight:	4,610 kg
Engine:	
Volume:	3.053 L
Max Output:	80.9 kW
Max Rotation:	2,500 rpm
Fuel Type:	Diesel
Fuel Tank Volume:	110 L
Crawlers:	
Overall Length:	1,780 mm
Overall Width (Each):	500 mm
Distance:	1,185 mm
Transmission:	Full Time Drive System
Travelling Speed:	-2 m/s ~ 2m/s
Header:	
Divider Width:	2,060 mm
Cutter Width:	1,976 mm
Cutting Range (Height):	-100 mm ~ 1,000 mm
Reel Radius × Width:	1,000 mm × 1,915 mm
Rotation Speed:	Synchronized with Crawler
Grain Tank:	
Volume:	1,900 L
Unloading Height:	5,100 mm

In order to modify the combine harvester into a robot, several sensors and safety devices were also integrated to it, such as an RTK-GPS, a computer, a laser scanner and a set of emergency stop controllers. Figure 2-2 shows an illustration of this robot combine harvester with the devices described above.

2.1.1 Control system

This combine harvester is fully control by a CAN bus and it follows the ISO11783 standard. The standard was developed to facilitate the communications within the agricultural machines, such as between the robot combine harvester and its implements. It can also be used to monitor the status of each part of the vehicle.

Specifically, structure of the control system is given in Figure 2-3. The computer is connected to the CAN bus with a communication interface. Through this interface, the computer can send commands to or receive feedback from the combine harvester. The RTK-GPS is connected to the computer with an RS232 cable. The emergency stop controller, on the other hand, is connected directly to the combine harvester's control system. This enables an immediate stop of the machine in case of emergency, compared to the possible delay if connected to the computer.

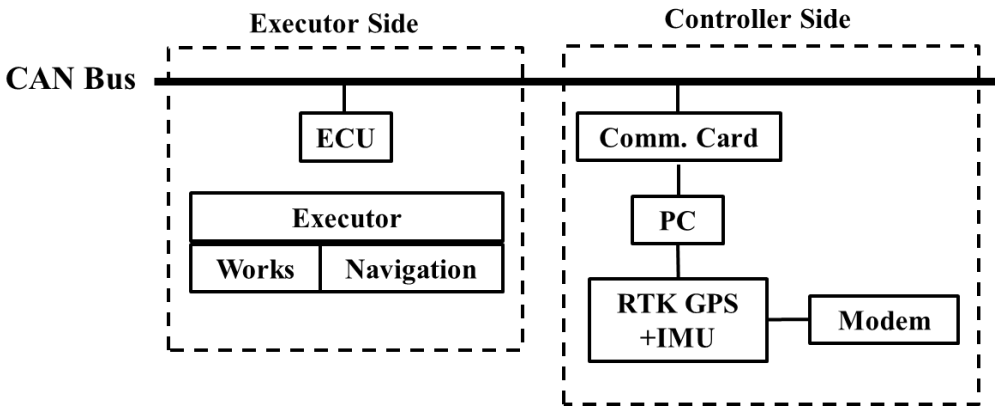

Figure 2-3 Structure of the control system

In addition, between the computer and the combine harvester's actuators, there is another ECU, serving as a guard to the machine, which can shield all wrong CAN messages and commands from the computer. It can also filter certain messages on the CAN bus. There are many messages on the bus all the time and if all the messages are delivered to the computer, it will be overloaded. To avoid this phenomenon, the filter ECU only transfers messages related to navigation and field work to the computer.

2.1.2 Steering system

With full-time drive system (FDS) derived from GC series of combine harvester, this combine harvester has an advantage in its movement, since during straight movement, e.g. forward movement and backward movement, the FDS system ensures that the crawlers of

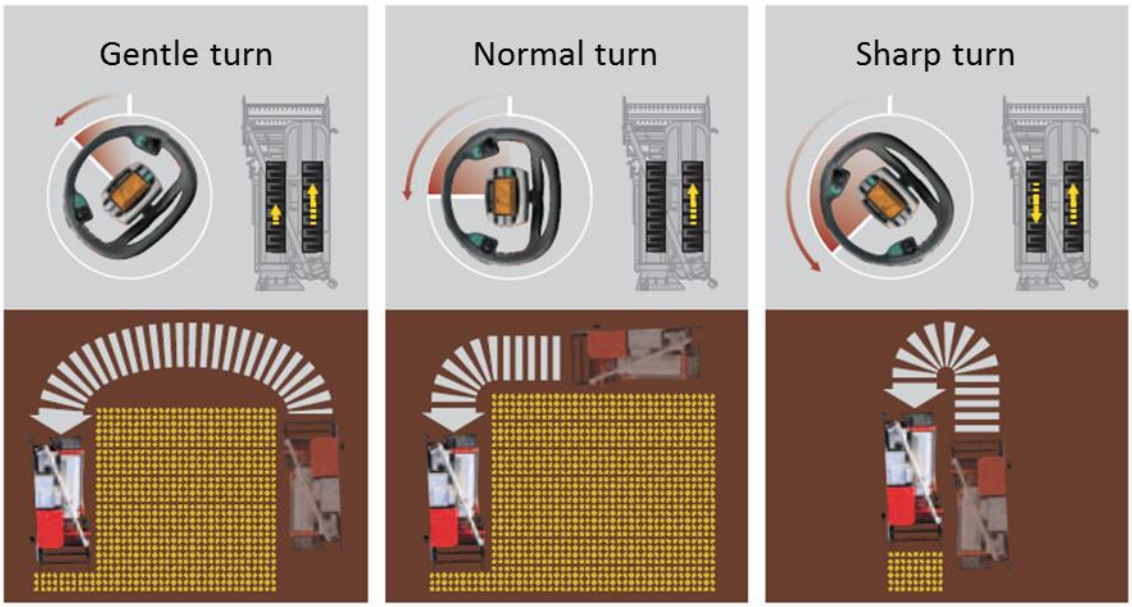

Figure 2-4 Steering system

the combine run in the same speed. And thus, if slipperiness of the ground is not obvious, the machine can run in a precise straight line. During turning, on the other hand, the FDS can perform in 3 different ways, as shown in Figure 2-4: in a gentle turning, the outside

crawler remains its speed and the inner crawler decreases its speed. As the steering angle increases, the inner crawler stops and turning radius decrease sharply. Finally, when steering angle reaches its maximal value, the inner crawler can even rotate in a reverse direction.

Besides, the FDS also enables an easier control of the combine – when steering angle of the combine remains the same, its turning radius also remains the same, which has no relation with the vehicle's speed.

2.1.3 Unloading system

This machine's unloading auger can be controlled easily by the unloading controller as well as by the computer. There are 6 preset positions, return position, right 1, right 2, right 3, back 1 and back 2, and they are shown in Figure 2-5. Respectively, they are the original position, with which the combine can run and work, and another 5 adjustable positions according to the position of the truck that receives the grain. When it is controlled by the unloading controller, with one touch of the button, the unloading auger will be set to the desired position. When it is controlled by the computer, on the other hand, it can be set to a certain position by sending just one command to the CAN bus.

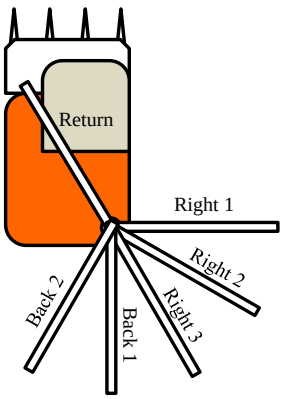

Figure 2-5 Available unloading auger positions

2.1.4 Other functions of the combine harvester

This combine harvester also has other functions that can ensure smooth work and control when in the field.

One of these functions is the automatic level control of the header. Sometimes the ground in the field is not level enough. In this case, the combine harvester may swing during harvesting. This may result in a yield loss since if the header swings with the vehicle. In this combine harvester, however, automatic level control function is available. When the vehicle swings, its header can remain level to the ground, as in Figure 2-6. This can also facilitate navigation of the robot, since the header control does not have to be included in the navigation program.

Figure 2-6 Automatic level control of the header

Another important function is header's height control. Sometimes the unevenness of the ground results in a swing in the machine's moving direction. This may result in a sudden decrease of the header's height and it may suffer from serious damage due to collision to the ground. The header height control solves this potential problem by adding 3 sensors to the bottom of the header and when any of them hit the ground, the header will

automatically lift slightly, and avoid damage to the header. Thus, during harvesting, no consideration of header's height is needed.

Combine harvester's engine load varies tremendously during harvesting work. It is closely related to crop density, vehicle speed and field condition. Traditionally when developing a robot combine harvester, the engine rotation speed should be set a relatively high value to prevent the vehicle's engine from flameout. In this way, a large amount of fuel is wasted due to the high rotation speed even when the vehicle is not working. This combine harvester can monitor working status and increase engine's rotation speed when it is working and decrease it otherwise. With this function, there is no need to monitor the engine load when the combine is working and running at a moderate speed.

In addition, the combine harvester is equipped with a "second mower". This is an important implement when it harvests paddy. When the machine harvests paddy, the engine load can be high. As a result, to harvest the paddy with a high speed, it should cut as little straw as possible. However, it is also important not to leave the straw in the field. In this case, the second mower is necessary, as in Figure 2-7. With this implement, crops

Figure 2-7 Second mower under the header

cut by the header are fed into the threshing part of the combine, and the straw cut by the second mower directly falls to the ground. This function is optional and usually it is only

used when harvesting paddy. It can increase working efficiency to a great extent by reducing the engine load.

Finally, when harvesting soybean, a special row crop header is introduced to the combine. A row crop header is shown in Figure 2-8. Since the distribution of the soybean seed is from the top to the bottom, the header has to be lowered to the surface of the ground to avoid any possible loss of the yield.

Figure 2-8 Row crop header for soybean

2.2 Navigation and safety sensors

In order to navigate a robot vehicle, usually two kinds of data should be precisely obtained – position data and posture data. Nowadays, frequently used devices to measure position data are GPS receivers, such as a DGPS (Differential GPS) receiver or an RTK-GPS (Real-Time Kinematic GPS) receiver. The posture data are usually measured by inertial sensors like a FOG (Fiber Optical Gyroscope) or an IMU (Inertial Measurement Unit). In this study, an RTK-GPS receiver with an IMU embedded in was used, for the reason that it can output position data and posture data of the robot at the

same time.

2.2.1 RTK-GPS

The Global Positioning System (GPS) is a space-based satellite navigation system that provides location and time information in all weather conditions, anywhere on or near the Earth where there is an unobstructed line of sight to four or more GPS satellites. This project was developed in 1973 to overcome the limitations of previous navigation systems (National Academy of Public Administration of U.S.A., 1995). The original GPS design included 24 orbiting satellites, and there are 6 orbital planes with 4 satellites in each (Daly, P., 1993), as shown in Figure 2-9 (Dana, Peter H., 1996).

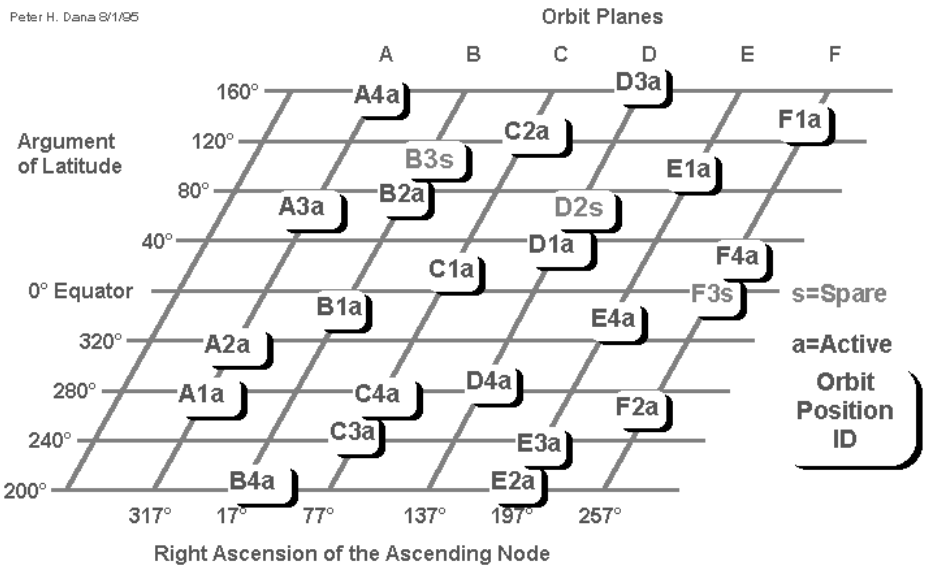

Figure 2-9 Simplified representation of nominal GPS constellation

Although, in the early years, the U.S. government intentionally degraded the accuracy for civilian use in the interest of national security, in 2000, its accuracy for civilian use has been improved from 100 m to 20 m. This action allowed up to 10 times improved accuracy for civilian GPS receivers, including agriculture (Buick, 2006).

By using the real-time kinematic (RTK) method, the accuracy level of GPS receivers

can be improved to a few centimeters. For an RTK-GPS, a base station and a rover receiver are required. The base station can be set up either by the user or by some carrier company. In the case of set up by the user, usually two GPS receivers are needed. One of them is used as the rover station and the other is used as the base station. A disadvantage of this method might be that when there is a building or trees between the rover station and base station, the communications may not be stable. The communication may not be reliable either when the rover is a long distance away from the base station. By using the VRS-RTK, the problem can be easily solved, although the cost increases slightly. However, Global Navigation Satellite System (GNSS) including GPS can become a low cost and high precise position sensor in the near future (Takasu and yasuda, 2009).

In this study, a Topcon AGI-3 RTK-GPS receiver was used. This GPS receiver also included an IMU and can output corrected IMU data. A PDA was used to receive correction signal from the VRS and send it to the GPS receiver.

2.2.2 2D laser scanner

Figure 2-10 2D laser scanner (UTM-30LX)

In this study, a 2D laser scanner was used as the safety device. The laser scanner is produced by Hokuyo automatic Co., Ltd., Japan. Figure 2-10 shows the appearance of the laser scanner. Table 2-2 is the specifications of the laser scanner.

Table 2-2 Specifications of a 2D laser scanner (UTM-30LX).

Power source	Voltage: 12 VDC±10% Current: Max:1A, Normal: 0.7 A
Light source	Semiconductor laser diode (λ=905nm) Laser safety Class 1 (FDA)
Detection Range	0.1 to 30m (White Square Kent Sheet 500 mm or more) Max.60 m (<30 m guaranteed)
Scan angle	270°
Accuracy	0.1 to 10 m: ±30 mm 10 to 30 m: ±50 mm
Angular Resolution	0.25°(360°/1,440 steps)
Scan Time	25 ms/scan (40 Hz)
Sound level	Less than 25dB
Interface	USB2.0 (Full Speed)
Synchronous output	NPN open collector
Command system	Exclusively designed command SCIP Ver.2.0
Connection	Power and Synchronous output: 2 m flying lead wire USB: 2m cable with type-A connector
Ambient (Temperature/Humidity)	-10 to +50 degrees C less than 85% RH (without dew and frost)
Vibration Resistance	Double amplitude 1.5 mm 10 to 55 Hz, 2 hours each in X, Y and Z direction
Impact Resistance	196 m/s^2, 10 times in X, Y and Z direction
Weight	Approx. 370g (with cable attachment)

CHAPTER 3

NAVIGATION ALGORITHMS OF THE ROBOT COMBINE HARVESTER

3.1 Introduction

The objective of this chapter is to develop a navigation-map-based robot combine harvester. At first, composition of navigation map is introduced in details, including navigation coordinate and navigation code. There is also introduction about how should the robot perform when it uses such a navigation map. This includes vehicle speed control, implement height control, steering angle control and so forth.

In addition, since the combine harvester's implement is in front of the vehicle, its position different from that of the GPS receiver (usually the center of gravity). And this shift of position can be several meters. In field work, it is important that this difference should be considered so as to avoid damaging crops. This chapter also introduces two methods to compensate this difference.

Contents in this chapter are also the bases for the robot combine harvester's navigation.

3.2 Navigation Map and Control Algorithm

3.2.1 Navigation map and task planning

The navigation map can usually be described in two ways: it can either be described by a straight line/a curve or it can be described by a series of points. In this study, the navigation map is described by the second method and in the map the series of points

are called navigation points.

The navigation map is a Euclidian three-dimensional space E^3 that consisted of navigation points including navigation information in each of them. That is, the set Ω of navigation points forms the navigation map as represented by equation Eq. (3-1).

$$\Omega = \{\omega_i | \omega_i \in E^3, 0 < i < N\}, \tag{3-1}$$

where $\omega_i = (Lat_i, Lon_i, Code_i)$ contains a navigation point that contains values of a latitude, a longitude and a navigation code as shown in Figure 3-1. And *N* is the number of all the navigation points in a map.

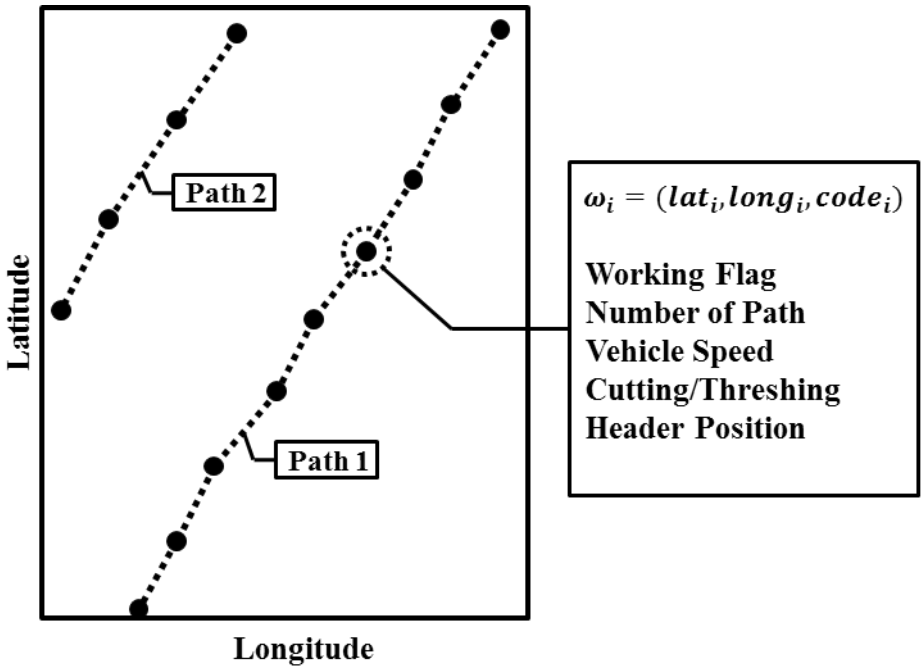

Figure 3-1 Navigation map for robot combine harvester

Originally in the navigation code, as introduced by Kise *et al.* (2001), there are six sections designating the performance of a robot tractor at a navigation point. In the case of a combine harvester, however, there are 5 sections containing the information in Table 3-1. Specifically, in the Cutter/Threshing section, 0 means neither the cutter nor

the threshing drum clutch works. 1 means only threshing drum clutch works and 2 means both of them work.

Table 3-1 Details of the navigation code

Section	Function
Working Flag	Operation conditions (Working, Turning or Stop.)
Number of Path	Current path number
Vehicle Speed	1 to 8
Cutter/Threshing	0 to 2
Header Position	Up or Down

3.2.2 Steering controller

In order to control a robot vehicle in a field, it is important to calculate the vehicle's steering angle based on its lateral error and heading/yaw error (Noguchi *et al*, 1998). This research also uses this method and the robot's steering angle is calculated by PI control based on its lateral error d and heading error $\Delta\phi$. Specifically, steering angle of the robot is calculated based on the following method.

A sub set of Ω, with the name Ω^*, was extracted to generate a new local navigation map in a Euclidian two-dimensional space E^2, which can be expressed by Eq. (3-2).

$$\Omega^* = \{\omega_i^* | \omega_i^* \in E^2, 0 < i < N^*\} \tag{3-2}$$

Navigation points in this subset can be described as $\omega_i{}^* = (Lat, Lon)$.

Figure 3-2 shows the method to calculate lateral error d and heading error $\Delta\phi$.

As shown in Figure 3-2, the robot vehicle is located in the UTM coordinate, with the

horizontal axis indicating easting, and vertical axis indicating northing. In addition, ϕ is the vehicle direction, ϕ_d is the target direction. And η is the vehicle's position, $\eta \in E^2$.

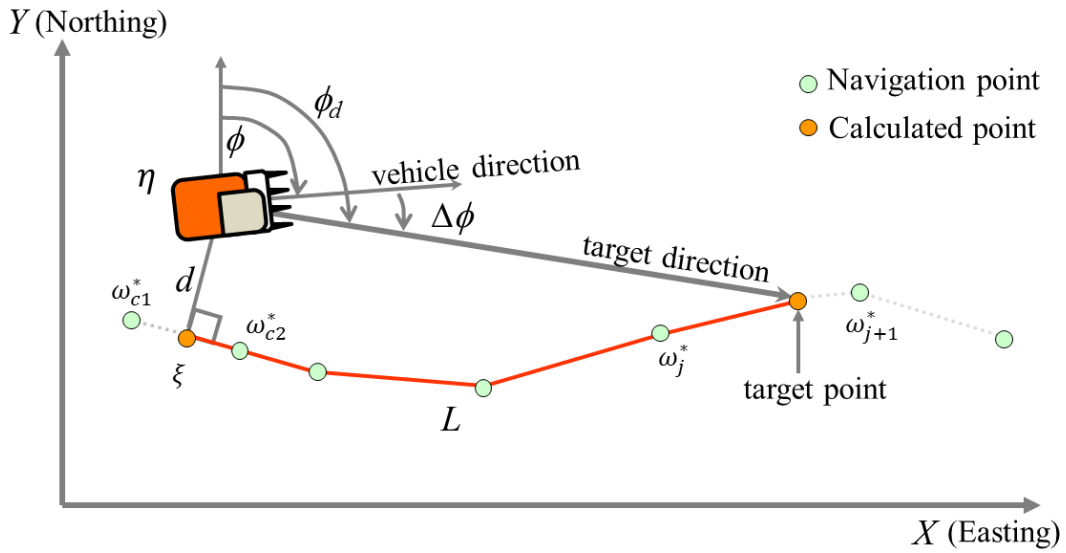

Figure 3-2 Determining d and $\Delta\phi$ on a navigation map

To calculate the vehicle's lateral error d, the closest navigation point and the second closest point should be calculated in the following method, as given respectively by Eq. (3-3) and (3-4).

$$\omega_{c1}^* = \{\omega_i^* | min_{i=1}^N(\|\omega_i^* - \eta\|),\ \omega_i^* \in \Omega^*\} \tag{3-3}$$

$$\omega_{c2}^* = \{\omega_i^* | min_{i=1}^N(\|\omega_i^* - \eta\|),\ \omega_i^* \in \Omega^*,\ \omega_i^* \neq \omega_{c1}^*\} \tag{3-4}$$

In these two equations, $\|\cdot\|$ are the norms of the vectors. And all the vectors on the closed interval can be expressed by Eq. (3-5)

$$[\omega_{c1}^*, \omega_{c2}^*] = \{\xi | \xi = \lambda\omega_{c1}^* + (1-\lambda)\omega_{c2}^*, 0 \leq \lambda \leq 1, \xi \epsilon E^2\} \tag{3-5}$$

Thereby, the lateral error d can be calculated by Eq. (3-6).

$$d = \min_{[\omega_{c1}^*, \omega_{c2}^*]} \|\xi - \eta\| \tag{3-6}$$

And to calculate the vehicle's heading error, target direction of the vehicle should be determined. In this study, a control parameter named look-ahead distance, *L*, is used. This parameter is defined as the length of the polygonal line from the closest point $\xi_{closest}$ to the ξ_t within the range of $[\omega_j^*, \omega_{j+1}^*]$. And the target point can be found in Ω^* by Eq. (3-7) and (3-8).

$$\|\omega_{c2}^* - \xi_{closest}\| + \sum_{i=c2+1}^{j} \|\omega_j^* - \omega_{j-1}^*\| \leq L \tag{3-7}$$

$$\|\omega_{c2}^* - \xi_{closest}\| + \sum_{i=c2+1}^{j+1} \|\omega_j^* - \omega_{j-1}^*\| \geq L \tag{3-8}$$

Since ξ_t is on the vector $[\omega_j^*, \omega_{j+1}^*]$, it can be expressed by Eq. (3-9).

$$\xi_t = \{\xi_t | \xi_t = \lambda\omega_j^* + (1-\lambda)\omega_{j+1}^*, 0 \leq \lambda \leq 1, \xi_t \epsilon E^2\} \tag{3-9}$$

Then the target direction ϕ_d can be calculated by Eq. (3-10).

$$\phi_d = \cos^{-1}\left(\frac{\xi_t - \eta}{\|\xi_t - \eta\|} \cdot d_N\right), \tag{3-10}$$

where d_N is the vector pointing at north or the direction of vertical axis. Finally, the heading/yaw error of the robot can be calculated by Eq. (3-11).

$$\Delta\phi = \phi - \phi_d \tag{3-11}$$

With lateral error d and heading error $\Delta\phi$, steering angle of the combine harvester can be calculated by Eq. (3-12).

$$\delta = g_l d + g_h \Delta\phi \tag{3-12}$$

From Eq. (3-12), it is obvious that steering angle of the robot vehicle is based on lateral error d and heading error $\Delta\phi$. And since they are closely related to the

look-ahead distance L, a proper look-ahead distance can result in a smooth control of the vehicle. On the other hand, since control parameters g_l and g_h can be modified in a wide range, they are the main factors that determine the accuracy of navigation. Usually, a proper choice of g_l and g_h not only ensures that the vehicle can follow the target path with a high accuracy, but also guarantee a quick correction of the position when the vehicle enters the next path. In this study, g_l and g_h are also named lateral gain and heading gain, respectively.

3.3 Combine position correction

In field navigation, a robot combine harvester is different from a robot tractor mainly in that the implement of a combine is in the front and that of a tractor is at the back. And since the GPS receiver is usually mounted on the center of the crawlers or on the cabin of the vehicle, it cannot represent the real position of the implement. As a result, when navigating in the field, the header of the combine harvester enters the navigation path much earlier than the GPS receiver, as shown in Figure 3-3.

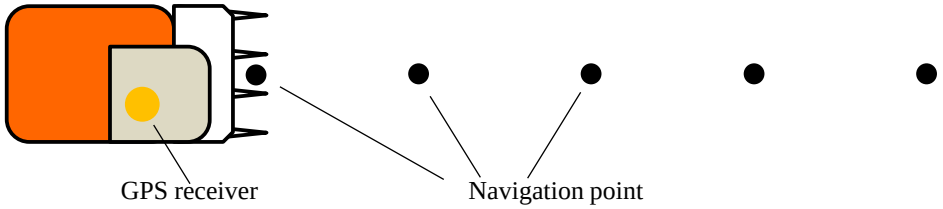

a) Header entering navigation path

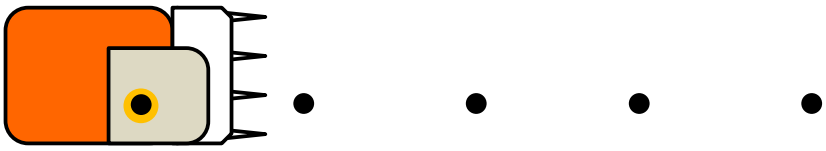

b) GPS receiver entering navigation path

Figure 3-3 Entering a navigation path

In Figure 3-3-a), the combine harvester's header is at the first navigation point, which means that it has already entered the navigation path. However, according to the GPS position, there is still some distance before entering the path. On the other hand, in Figure 3-3-b), the GPS receiver has just arrived at the first point of the navigation path, yet the header has already entered the path for a certain distance. As is known to all, the combine harvester should lower the header as soon as the header enters the path. However, if the combine position is judged by the GPS receiver, it is entirely possible that the robot may run over some crops in the field.

As a result, to avoid running over crops, corrections to the navigation map and/or correction to the combine harvester's positions were necessary in this research.

3.3.1 Correction to combine harvester's position

Combine harvester's position can be corrected by measuring the relative position between the GPS receiver and the center of the combine harvester's header, as shown in Figure 3-4.

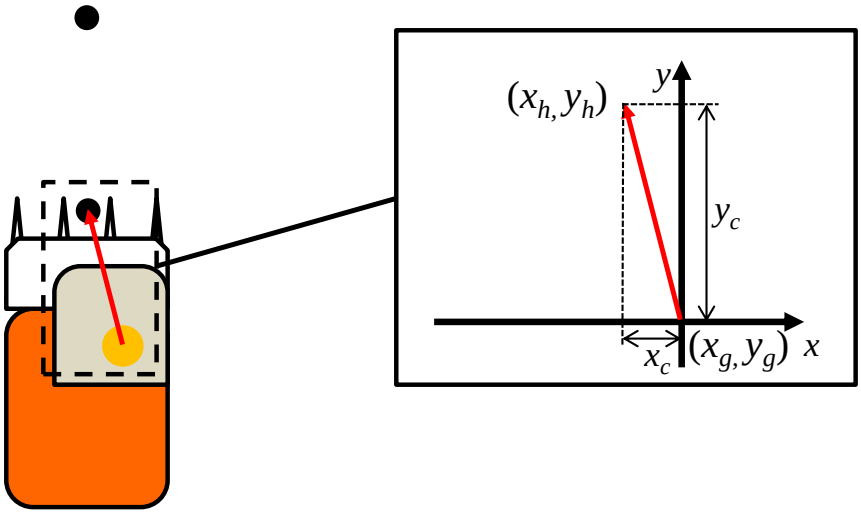

Figure 3-4 Combine harvester's header position

Assume that when the combine harvester facing north its heading angle is 0, the vector that describes the relative position can be written as (x_c, y_c). When the combine harvester is in a position (x_g, y_g) by the GPS receiver, with a certain heading ϕ, as shown in Figure 3-5, its header's position can be calculated by Eq. (3-13)

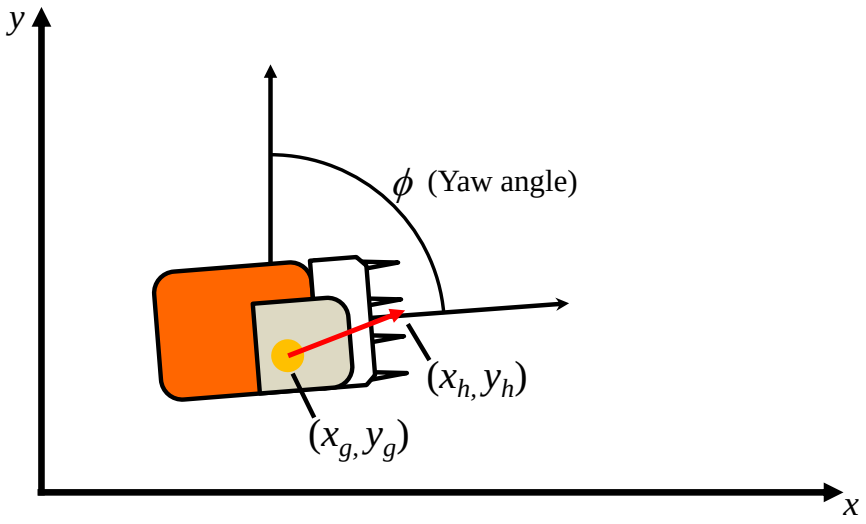

Figure 3-5 Header position with a certain heading

$$\begin{cases} x_h = x_g - x_c \cos\phi + y_c \sin\phi \\ y_h = y_g - x_c \cos\phi - y_c \sin\phi \end{cases} \tag{3-13}$$

where (x_h, y_h) is the position of the robot combine harvester's header.

3.3.2 Correction to the navigation map

Apart from the correction to the combine harvester's position, it is also possible to correct the coordinates of the navigation map. Usually, this correction is conducted when the navigation map is in a straight line or almost in a straight line. Figure 3-6 shows the method that is used to correct navigation map.

Accordingly, corrections of the navigation map can be conducted by applying Eq. (3-14).

$$\begin{cases} x_g = x_h + x_c \cos\phi - y_c \sin\phi \\ y_g = y_h + x_c \cos\phi + y_c \sin\phi \end{cases} \quad (3\text{-}14)$$

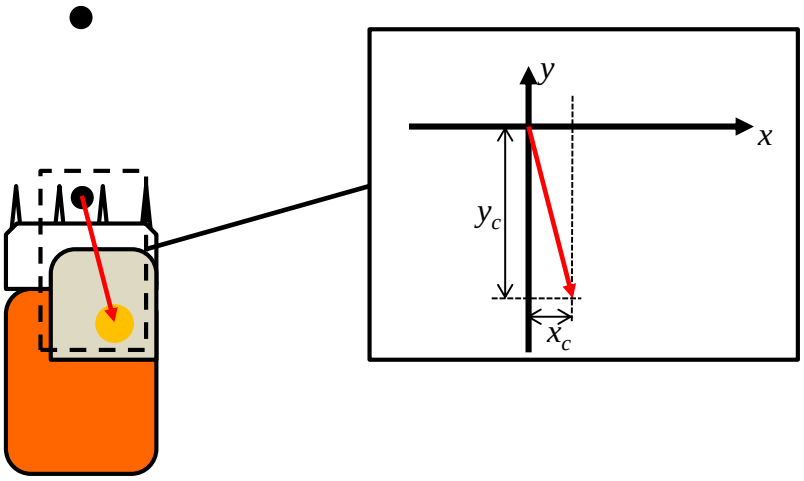

Figure 3-6 Correction of the coordinates of navigation map

3.4 Results and discussion

By the method discussed in this chapter, a navigation map with task planning code was made. The navigation map was made by two points recorded in the experimental field of Hokkaido University, as shown in Figure 3-7.

The coordinates of the starting point is (527425.413E, 4769126.354N, 54T) and the ending point is (527389.357, 4769185.067, 54T). In the map, there are four paths in total, which are parallel to each other. In the four paths, the first path is the basic path, which was made by the starting point and the ending point. The other three paths were made based on the first path, and the distance between adjacent paths was 2.0 m, since the width of the combine harvester's header is 2.0 m. Figure 3-7 also shows the detail of the navigation code as "1-10-1000-1-1-0000001-1". Respectively, the numbers separated by the hyphens mean header position being low, threshing and cutting clutches being both on, combine harvester going by the lever angle, combine harvester moving forward, path number being one and combine harvester being working.

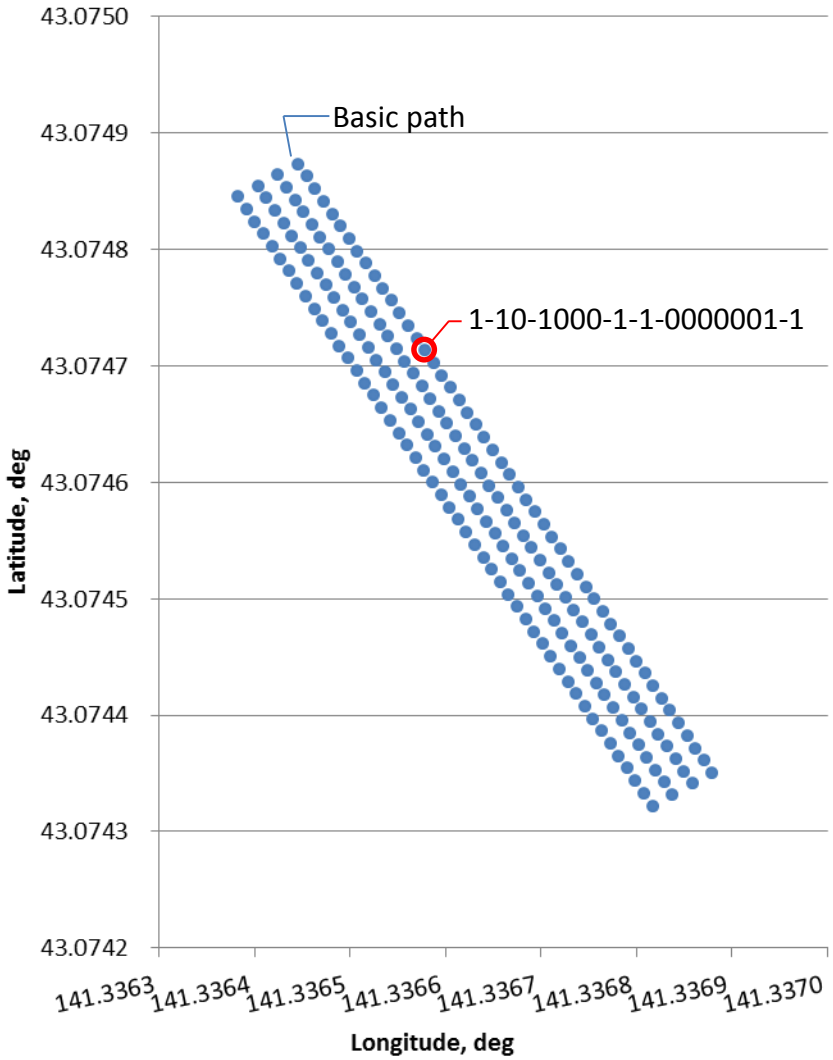

Figure 3-7 A navigation map for experiment in Hokkaido University

After the navigation map was made, the combine harvester was put into the field and two tests were conducted with different lateral gains and heading gains. In these two tests, the combine harvester only navigated in the basic path, so as to test its ability to follow a straight line, especially its performance with various gain pairs.

In the first test, the heading gain and lateral gain were set to 0.3 and 5 respectively, and the results of the test are as follows.

Figure 3-8 shows the result of the robot combine harvester traversing the navigation

path. It is obvious that the combine harvester is following the predetermined path although there is some oscillation.

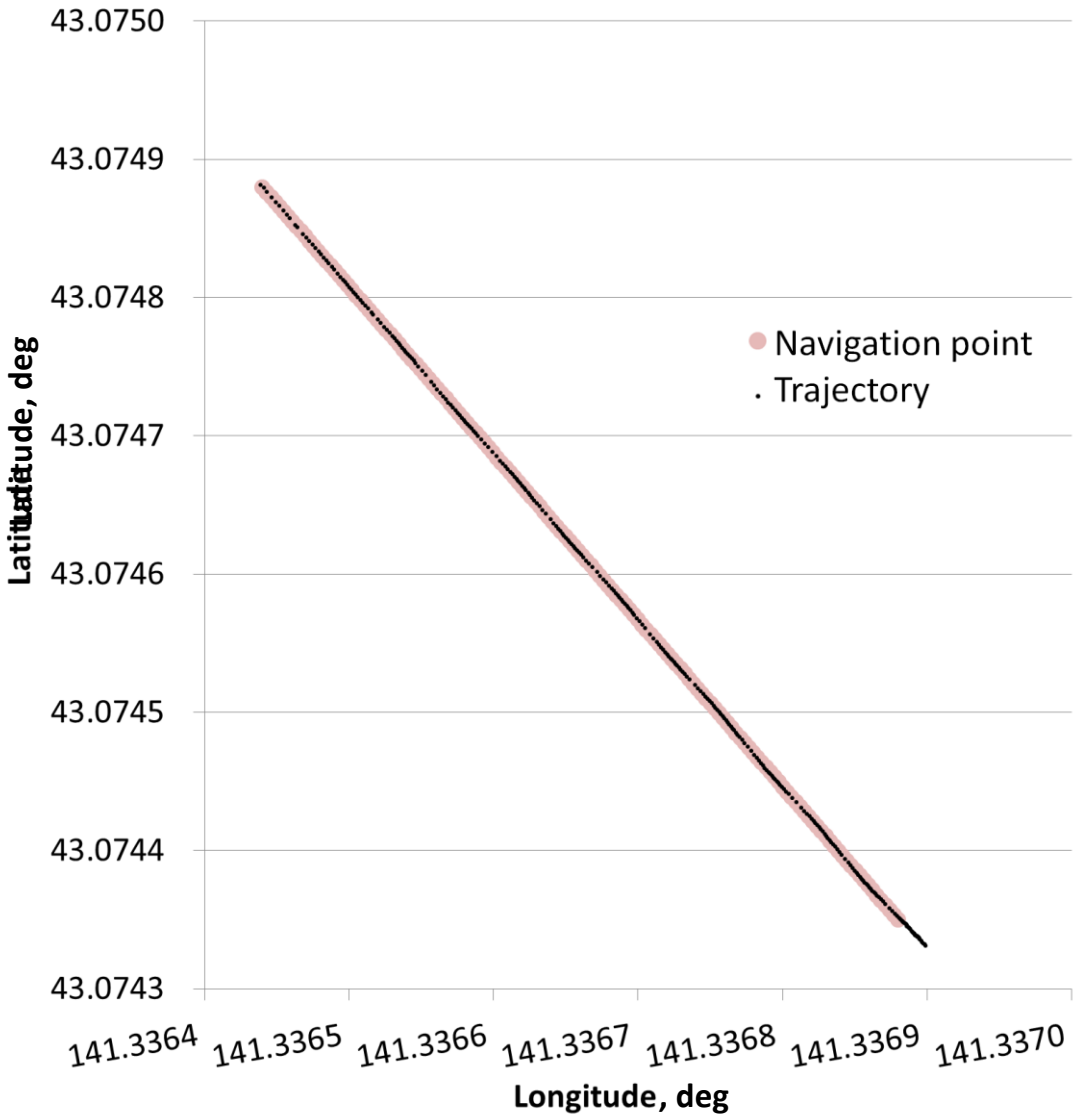

Figure 3-8 Map and trajectory of Field Test-1

As shown in Figure 3-9, the initial lateral error of this test was about 0.25 m, after this the combine harvester went closer to its target path. There was certain oscillation, but the vehicle always traveled within a 0.15 m range. The RMS value of the lateral error was 0.092 m. This accuracy for lateral error was acceptable on the operation of a

combine harvester. Figure 3-10 shows the heading error of the same test. The initial heading error of the test was about 2.6 deg. When running along the target path, the heading error ranged from -3 to 3 deg. The RMS value of the heading error was 2.81 deg.

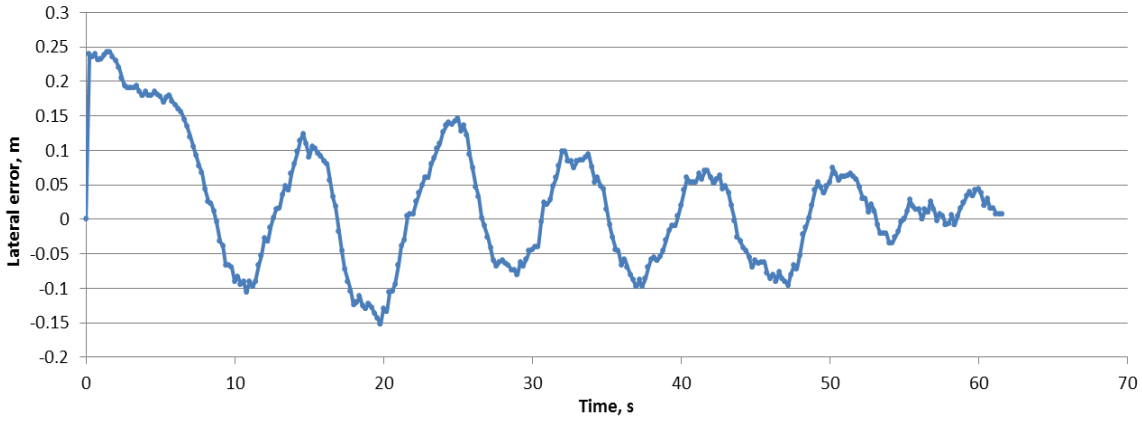

Figure 3-9 Lateral error in Field Test-1

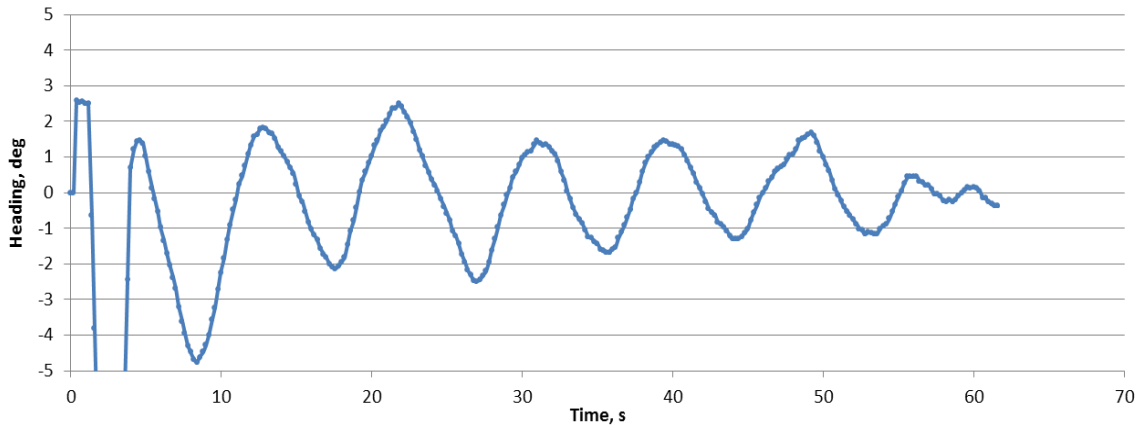

Figure 3-10 Heading error in Field Test-1

Thereby, another experiment was conducted, with the heading gain and lateral gain set to 0.8 and 8, respectively.

Figure 3-11 shows the result of the second field test. This time, however, the combine harvester was oscillating obviously, although generally it is still following the

predetermined path. The cause of this oscillation was considered to be the large value of lateral gain and heading gain.

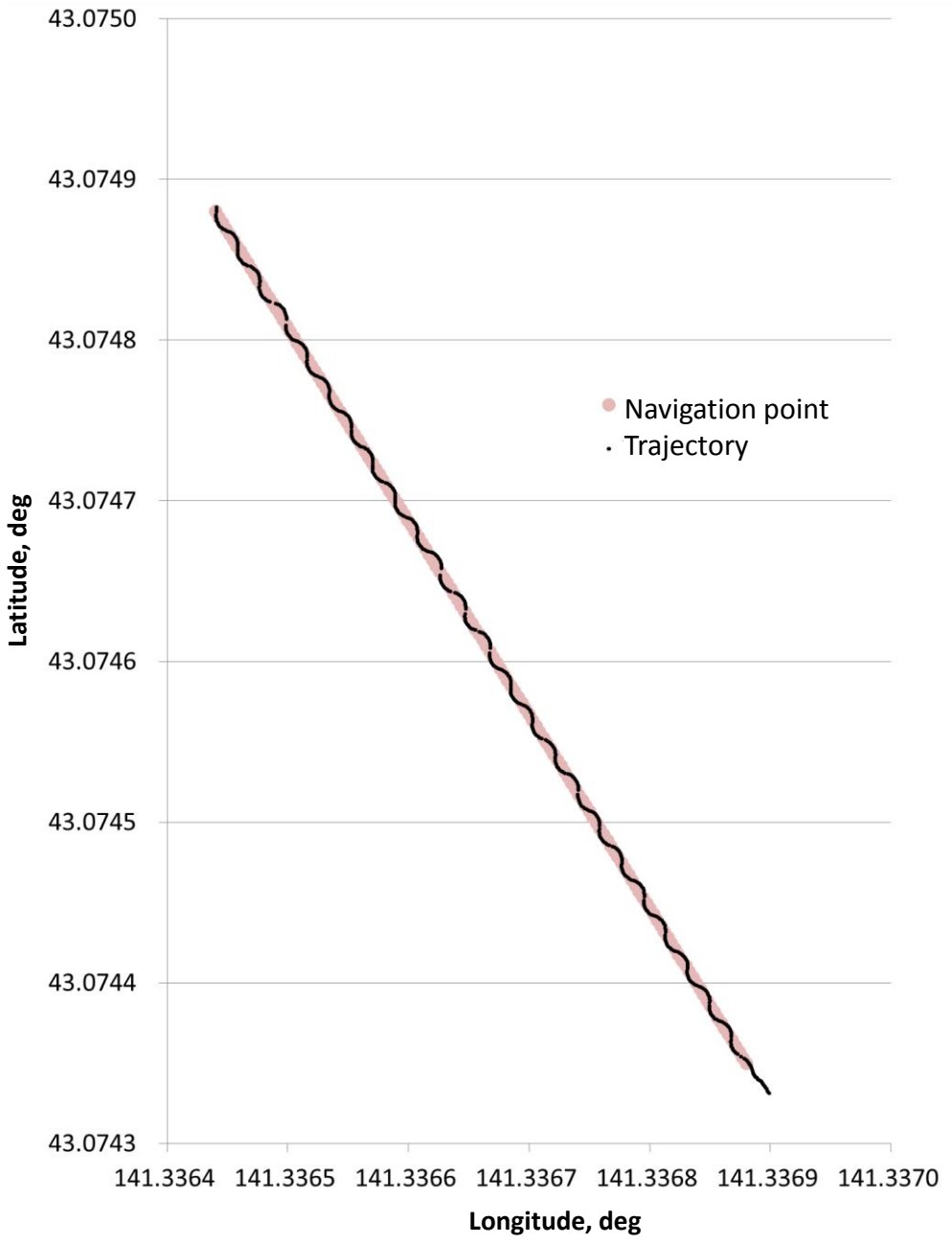

Figure 3-11 Map and trajectory of Field Test-2

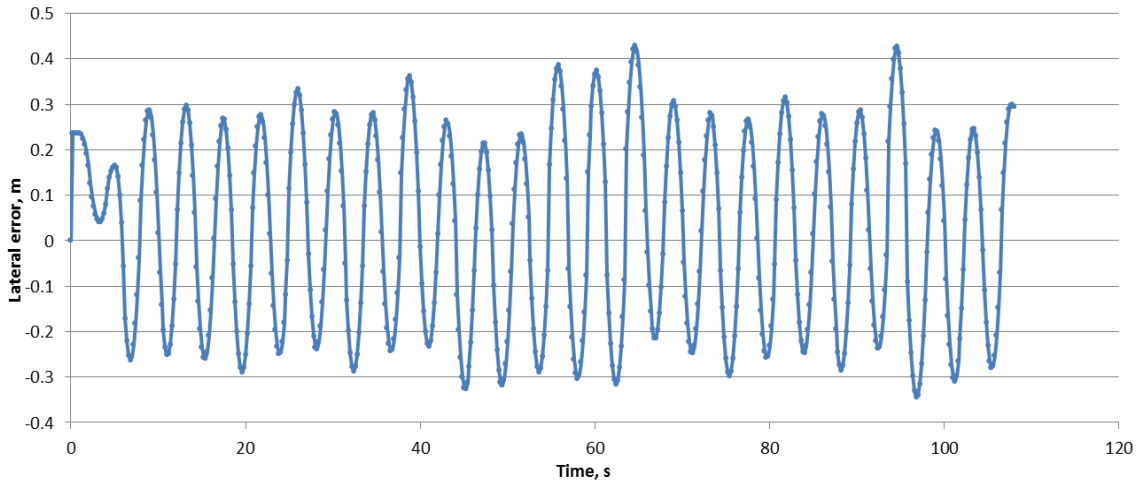

Figure 3-12 Lateral error in Field Test-2

As shown in Figure 3-12, the initial lateral error of the field test was about 0.25 m, after the test started, the combine harvester oscillated from -0.3 m to 0.4 m, and it could not settle down.

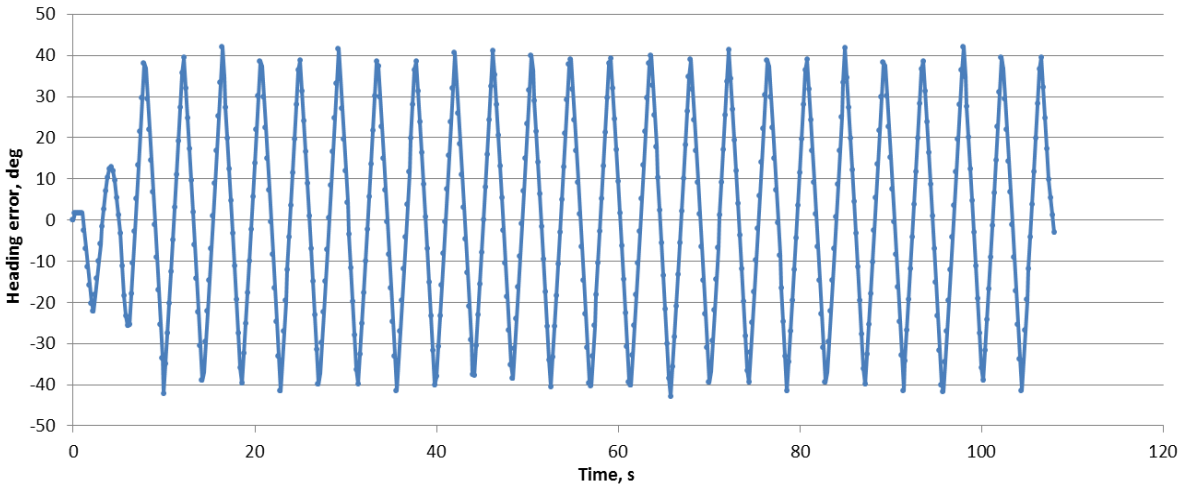

Figure 3-13 Heading error in Field Test-2

As shown in Figure 3-13, the combine harvester's heading angle oscillated from -40 deg to 40 deg throughout the whole test, and the amplitude of the oscillation is nearly the same. This indicated that the heading gain dominated the calculation of the steering

angle, and a heading gain of 0.8 with a lateral gain of 8 is too large for the robot combine harvester's control.

In addition, the correction to the navigation map explained in section 3.3.2 was also tested. And the result is shown in Figure 3-14. The robot combine harvester should start at the place pointed out by the red arrow. It should enter the next path and navigates in the opposite direction. Since there is also a lateral shift, the distances between adjacent paths are not equal.

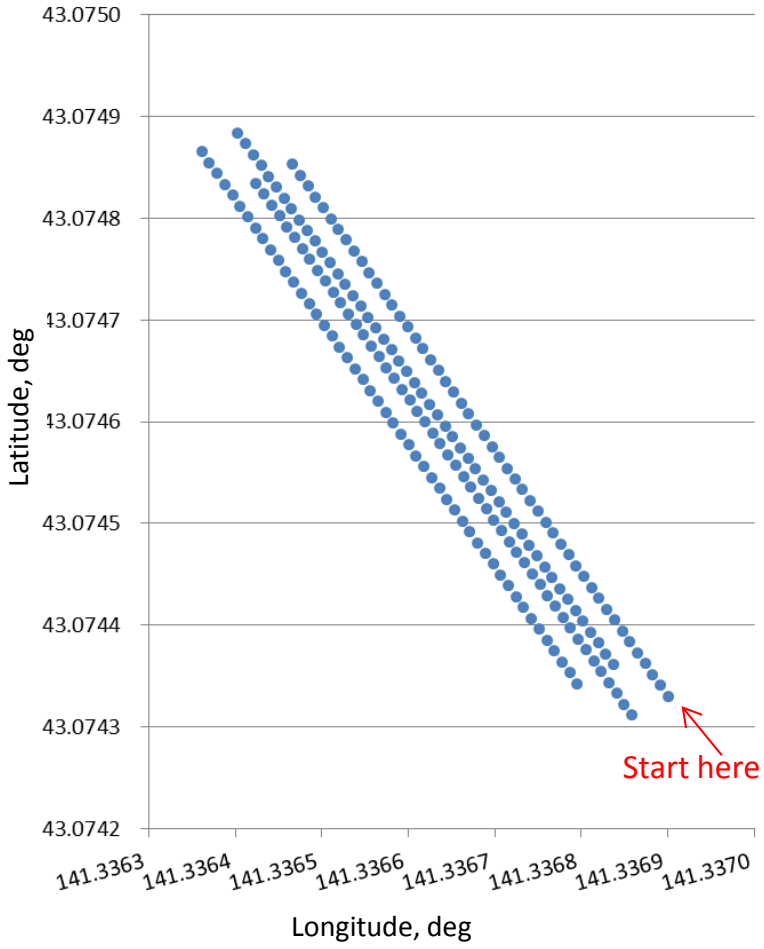

Figure 3-14 Corrected navigation map

CHAPTER 4

OPTIMIZATION OF PERFORMANCE BASED ON KINEMATIC MODEL

4.1 Introduction

The aim of this chapter was to develop a kinematic model for the robot combine harvester and to use the model to improve the performance of the robot. It was expected that with this study, the robot combine would be able to run along a straight line with the least oscillation and smallest lateral error. To achieve this goal, various data were recorded in the field and the kinematic model was built. An experiment was also conducted to test the accuracy of the model. Based on the kinematic model, optimizations of a steering controller were conducted, so as to obtain the optimized control parameters. The optimized control parameters exist and they were verified by field experiments. In a stable state, the RMS value of lateral error was 0.025 m, with a maximum of 0.066 m. Thus, the optimization method for control parameters of the robot combine harvester was acceptable.

4.2 Materials and methods

4.2.1 Modeling of the combine harvester

The combine harvester is controlled by a lever and a steering wheel. The lever controls the linear velocity of the vehicle and the steering wheel controls yaw angular velocity of the vehicle. Thus, it is crucial to find out the relation among linear velocity, yaw angular velocity, lever angle and steering angle. In order to optimize control

parameters for steering the combine harvester, it is necessary to build a kinematic model for it.

In the first step, when the combine harvester runs in a straight line, the relation between lever angle and speed of the crawlers was measured, as shown in Figure 4-1.

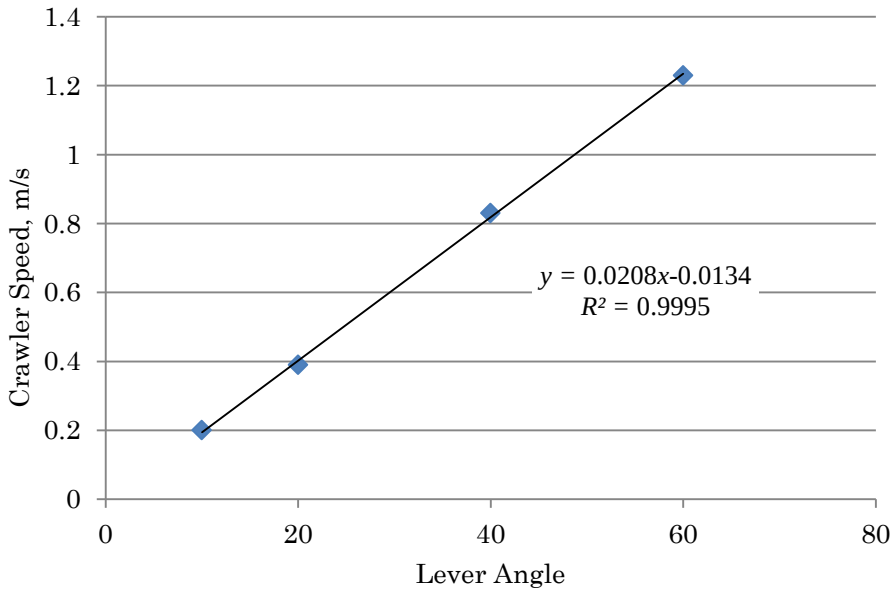

Figure 4-1 Relation between speed and lever angle in straight movement

Thus, when the combine harvester travels in a straight line, its speed can be calculated by Eq. (4-1).

$$v_s = 0.0208l - 0.0134, \tag{4-1}$$

where v_s stands for velocity of the vehicle (m/s) in a straight movement, and l is the lever angle of the vehicle, whose range is from -100 to 100, with no unit.

In addition, since one of the characteristics of the combine harvester is that the turning radius is solely determined by its steering angle regardless of the vehicle speed, relation between steering angle and turning radius was measured. The relation is shown in Figure 4-2.

Therefore, the turning radius of the combine harvester can be calculated by Eq. (4-2).

$$R = 450.5(|\delta|)^{-1.318}, \tag{4-2}$$

where R is the turning radius (m), and δ is the steering angle of the vehicle, whose range is also from -100 to 100 and it has no unit.

Moreover, when the combine harvester turns, the outer crawler's speed remains the same, while the inner crawler's speed decreases. Given that the distance between the crawlers is 1.185 m, when the combine harvester turns, its speed (speed of the center of crawlers) can be calculated by Eq. (4-3).

$$v_t = v_s \left(\frac{R}{R+0.5925}\right), \tag{4-3}$$

where v_t is the vehicle's (center of the crawlers) speed (m/s) during turning; v_s is the vehicle's speed (m/s) in a straight movement (outer crawler's speed); and R is the turning radius (m) calculated by Eq. (4-2).

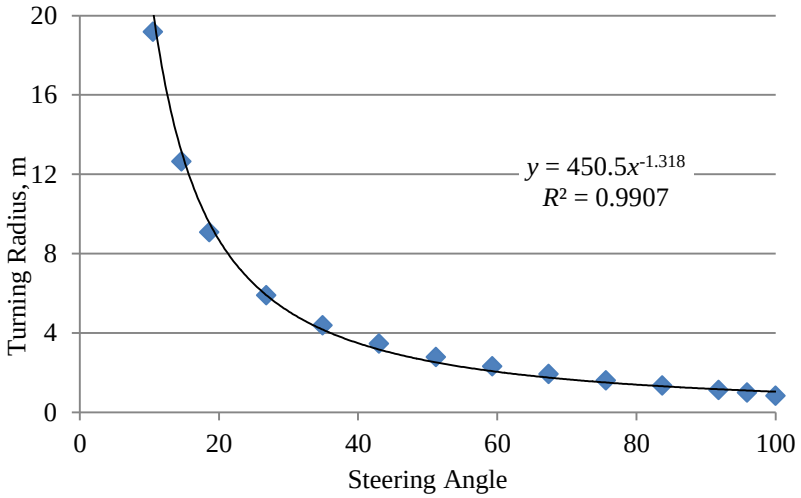

Figure 4-2 Relation between turning radius and steering angle

In the simulation program, the combine harvester's position and heading angle were calculated by the following method.

When the combine harvester is turning, it moves in an arc, and the method in Figure 4-3 was used.

Assume that combine's current coordinate is (x_0, y_0), with a heading angle of ϕ_0, and its yaw angular velocity is ω; after a short period of time Δt, the combine's coordinate (x_t, y_t) and heading angle ϕ_t can be calculated by Eq. (4-4) and Eq. (4-5).

$$\begin{pmatrix} y_t \\ x_t \end{pmatrix} = \begin{pmatrix} y_0 \\ x_0 \end{pmatrix} + \frac{\delta R}{|\delta|} \begin{pmatrix} \cos\phi_0 & \sin\phi_0 \\ -\sin\phi_0 & \cos\phi_0 \end{pmatrix} \begin{pmatrix} \sin\Delta\phi \\ 1-\cos\Delta\phi \end{pmatrix}, \quad (4\text{-}4)$$

$$\Delta\phi = \phi_t - \phi_0 = \omega \times \Delta t, \quad (4\text{-}5)$$

where, according to Eq. (4-1), Eq. (4-2) and Eq. (4-3), yaw angular velocity ω can be calculated by Eq. (4-6):

$$\omega = \frac{v_t}{\mathrm{R}} = \frac{(0.0208\mathrm{l} - 0.0134)}{450.5(\delta)^{-1.318} + 0.5925}. \quad (4\text{-}6)$$

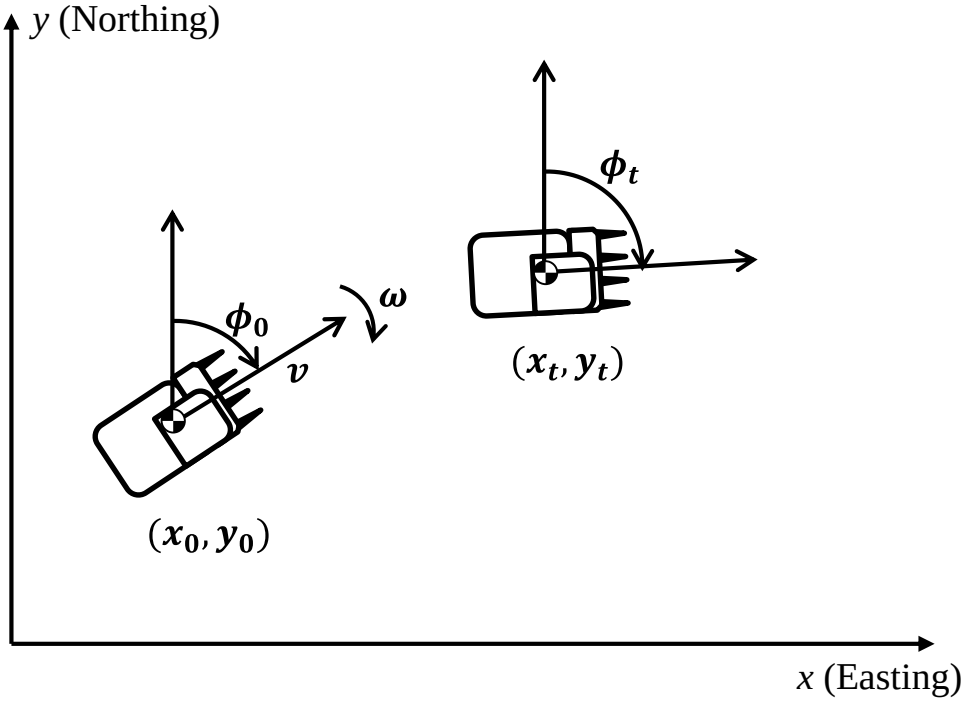

Figure 4-3 Calculation of position and heading angle

In addition, when the robot combine harvester travels in a straight line, its position can be calculated by Eq. (4-7)， Eq. (4-8) and Eq. (4-9).

$$x_t = x_0 + \sin\phi_0 \times (0.0208l - 0.0134) \times \Delta t \tag{4-7}$$

$$y_t = y_0 + \cos\phi_0 \times (0.0208l - 0.0134) \times \Delta t \tag{4-8}$$

$$\phi_t = \phi_0 \tag{4-9}$$

4.2.2 Verification of the kinematic model

Keyhole turning is an important turning method for crawler-type agricultural vehicles, for it can effectively prevent the vehicle from causing damage to the field. As shown in Figure 4-4, there are three steps in the keyhole turning. From point A to point B, the vehicle turns 45 deg and its trajectory forms an arc. From point B to point C, the vehicle turns -225 deg and at point C it is in the same direction as the next path. After point C, the vehicle generates a path from point C to point D. In the field verification, the path from point A to point C was tested.

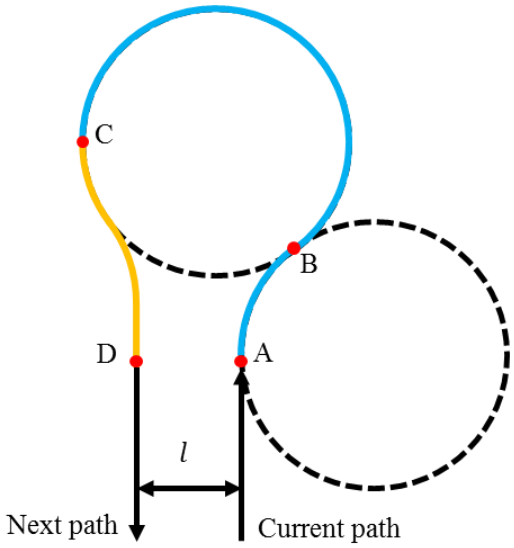

Figure 4-4 Keyhole turning

The result of the field verification is shown in Figure 4-5. In the test, robot combine harvester's trajectory was recorded in the field. The vehicle started to turn at the point (527435.237E, 4768963.244N, 54T), with its heading being -101.6 deg. As a result, in the simulation, the model was set to the same point with the same heading. The result of the keyhole turning showed that with the same position and heading at point A, there was some bias at point C. This was considered to be caused by the difference in the surface of the ground. The model was made by using data recorded in a field, and the verification experiment was conducted on an asphalt ground.

From the field verification, conclusion can be drawn that the model can be used in the optimization of the robot combine harvester's performance, since it has a satisfactory accuracy.

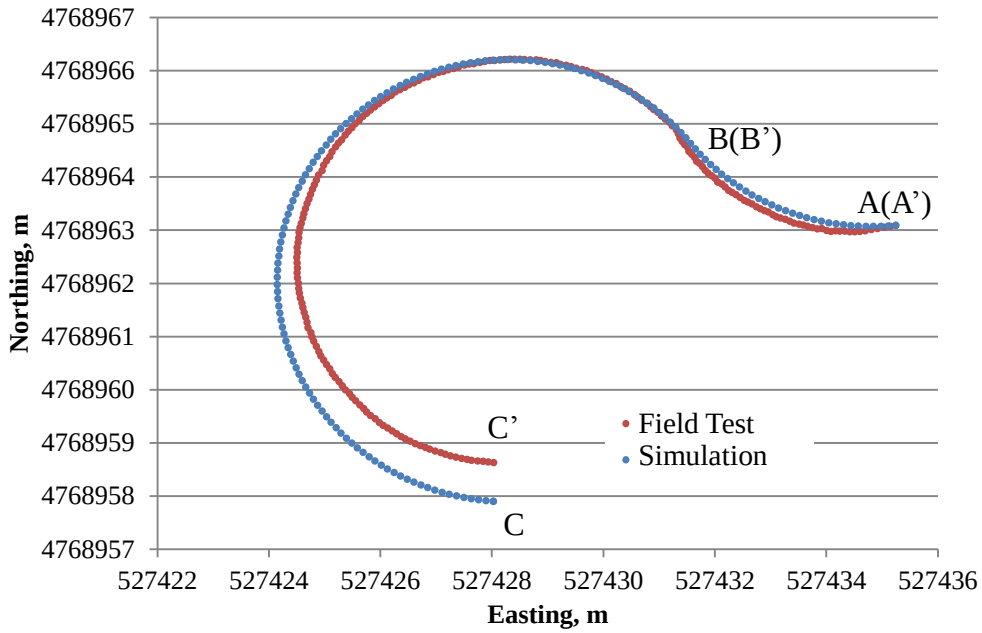

Figure 4-5 Result of model verification test

4.2.3 Optimization algorithms

There are two states when the robot runs along a target path – "Approaching state"

and “Stable state”. When vehicle enters a range with a lateral error of no more than $\pm$0.05 m and heading error of $\pm$3 deg, then it is considered that the vehicle has entered a stable state. Otherwise, it is considered to be running in an approaching state. Usually, good performance can be judged by two criteria: firstly, it should approach the target path as soon as possible; and secondly, it should follow the target line with a high accuracy and least oscillation, as shown in Figure 4-6.

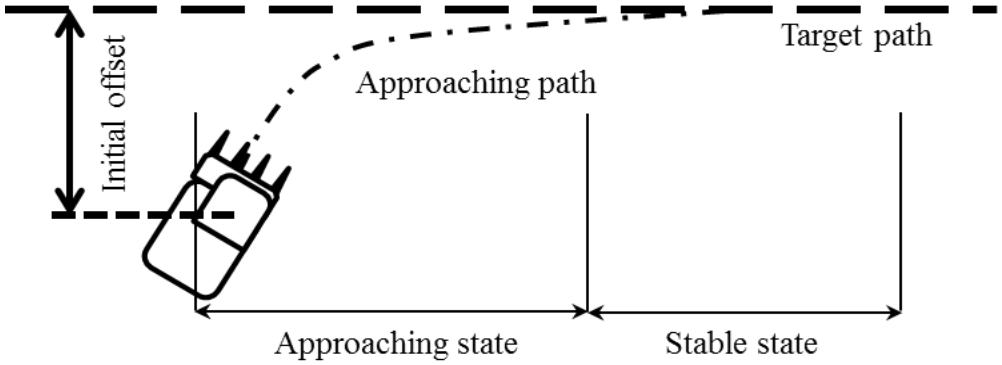

Figure 4-6 Approaching path for robot combine harvester

4.2.3.1 Optimization of control parameters in “stable state”

By precedent field experiment, it has been verified that, running under a vehicle speed of 1.2 m/s, when lateral gain is greater than 10 or when heading gain is greater than 1, the vehicle obviously oscillate and cannot follow a target line smoothly. Thus, simulations with lateral gain smaller than 10 and heading gain smaller than 1 were conducted, with a lateral gain step of 1 and heading gain step of 0.1. Thus, with all these gain pairs, the simulation was conducted 100 times. After this iteration, the gain pair of interest $\{g_l', g_h'\}$ was selected and iterations were conducted again within the following range:

$$g_l \in (g_l' - 0.5, g_l' + 0.5]$$

$$g_h \in (\mathrm{g_h}' - 0.05, g_h' + 0.05]$$

and iterations in this step were conducted with a smaller gain step, 0.1 for lateral gain and 0.01 for heading gain, for 100 times as well. After the iterations, the optimized gain pair $\{g_{lo}, g_{ho}\}$ was found.

4.2.3.2 Optimization of control parameters in "approaching state"

For the approaching state, simulations were conducted with Golden Section Search algorithm to find out a pair of optimized control parameters, by using which the combine harvester can approach the target path in the shortest time. At this stage, the relation between control parameters and initial lateral error was tested.

To find out a pair of optimized control parameters, optimization was conducted twice. On the first time, the heading gain of the robot was fixed to a proper value, for the reason that a large heading gain may lock the vehicle to its target heading angle and prevent the vehicle from going into its target path or it can make the vehicle oscillate. During this optimization, the relation between the initial lateral error and the optimized lateral gain was found. On the second time, the lateral gain was set according to the previously relation and the optimized heading gain was found.

Specifically, the process of this algorithm is shown in Figure 4-7. To find an optimized gain pair, the range $[a_1, b_1]$ should firstly be decided; in this case 0-10 for g_l, and 0-1 for g_h. Then a precision requirement ε should also be decided. After the iteration achieves this precision, it will stop. In this study, ε was set to 0.1 for lateral gain and 0.01 for heading gain. Then, by using corresponding equations, two candidate gains λ_1 and μ_1 should be calculated. Simulating with these two gains, the time when the vehicle enters a stable state can be calculated, and set step index *k* to 1. Comparing the two simulation results, the interval and two new gains λ_k and μ_k can be calculated

and a new iteration can be started. After the preset precision is achieved, the iteration will stop and print the optimized gain.

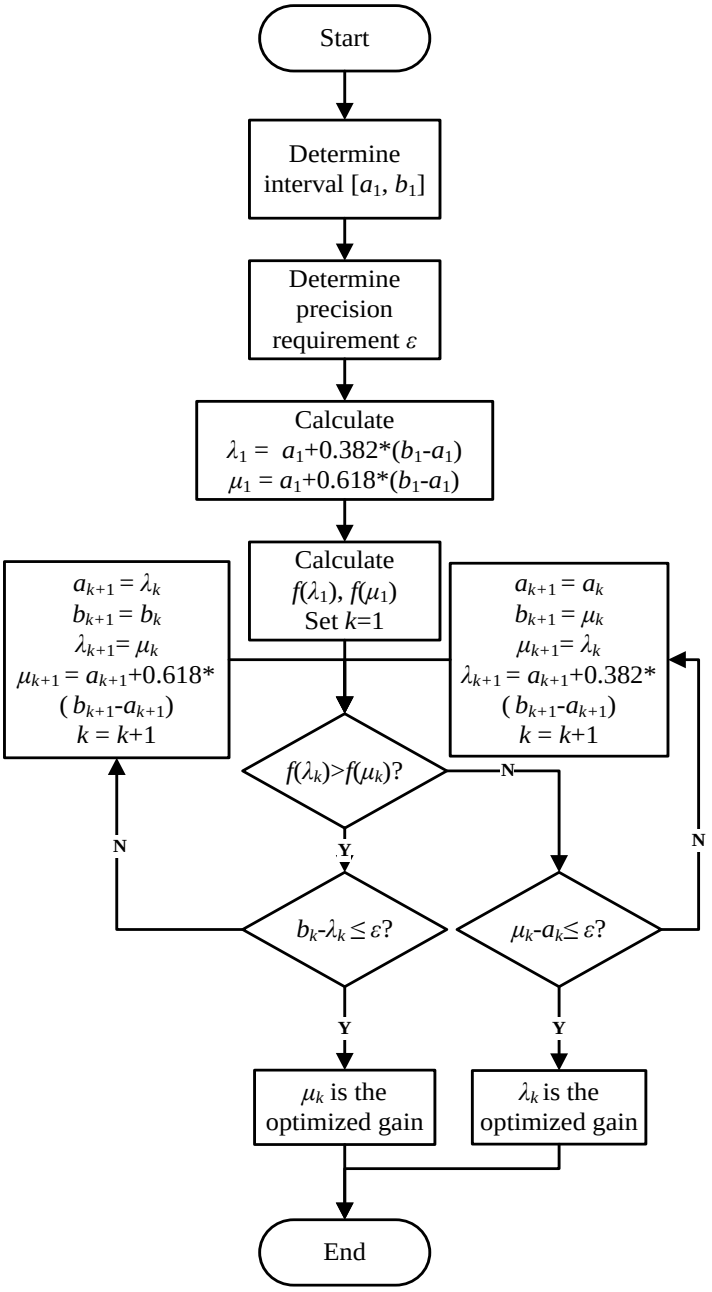

Figure 4-7 Process flow of the Golden Section Search

4.3 Results and discussion

4.3.1 Results of optimization for stable state

The objective of this optimization was to improve accuracy in stable state, so that the vehicle can follow a target path with the least oscillation. In the first iteration, the initial lateral error was set to -0.05 m, and heading error was set to a random value from -3 deg to 3 deg, that the vehicle was in a stable state. And simulations were conducted when lateral gain was in 0-10 and heading error was in 0-1.

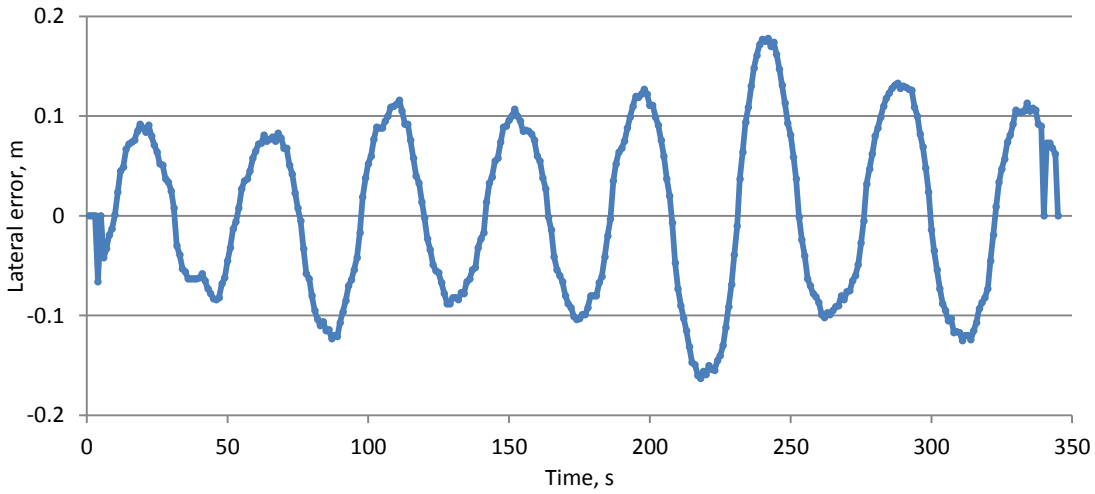

Figure 4-8 Simulation result when g_l=8, g_h=0.2

As shown in Figure 4-8, when the lateral gain is large and heading gain is small, the vehicle's steering was dominated by the lateral gain and heading gain has merely any effect on the vehicle's steering. The vehicle oscillated and could not settle.

On the other hand, when the vehicle's lateral gain is small and heading gain is large, the vehicle could not settle either. The result of the simulation when lateral error is 2 and heading gain is 0.9 is shown in Figure 4-9.

Thus, when either the lateral gain or heading gain is large, the vehicle could not

navigate with a high level of accuracy. When the vehicle's lateral gain and heading gain became moderate, the accuracy of the navigation had also improved. When the lateral gain was 6 and heading gain was 0.4, the navigation result was shown in Figure 4-10.

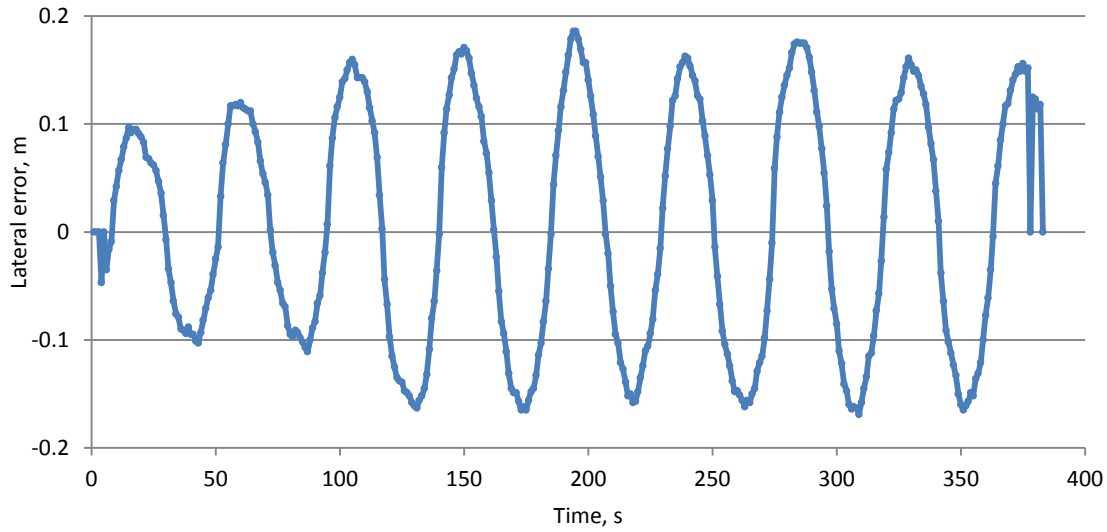

Figure 4-9 Simulation result when g_l=2, g_h=0.9

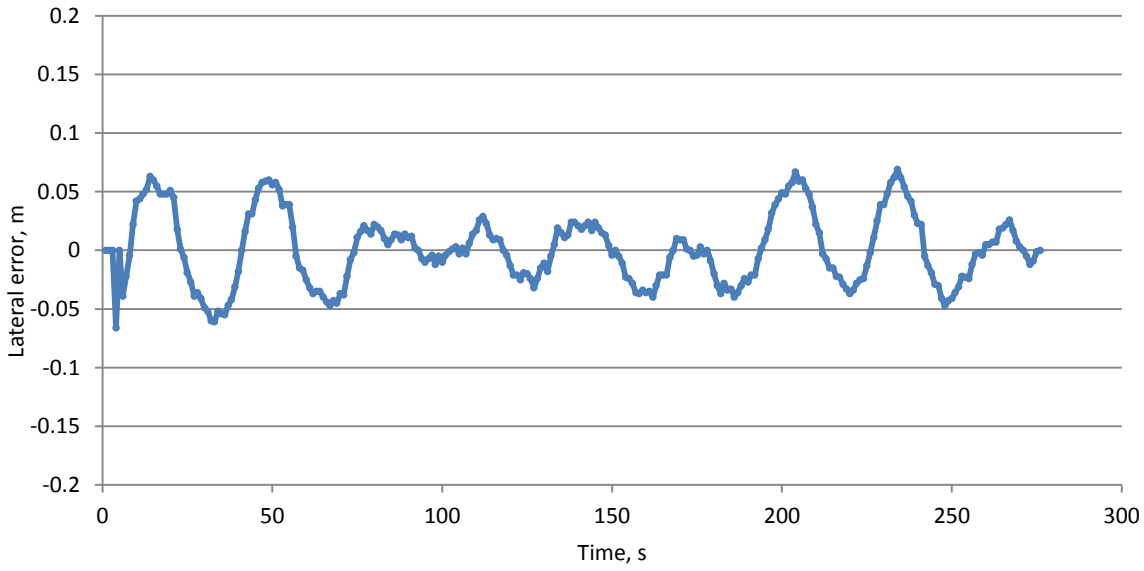

Figure 4-10 Simulation result when g_l=6, g_h=0.4

The simulation result was good in that most of the time its lateral error was in a

$\pm$0.05 m interval. However, one disadvantage of the performance is that the vehicle oscillates too much and it still needed to be improved.

Finally, after this iteration, a pair of g_l=4.0 and g_h=0.5 was found. The result of this simulation is shown in Figure 4-11. Specifically, the RMS value of lateral error is 0.022 m, with a maximum of 0.056 m. From the data, it is obvious that the accuracy of the navigation is relatively high and most importantly, the vehicle did not oscillate very much.

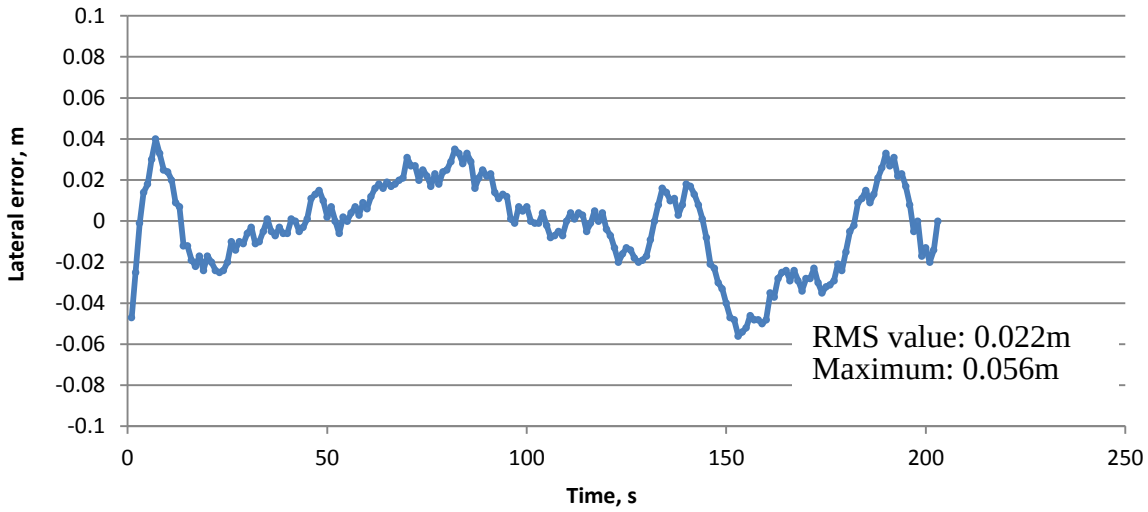

Figure 4-11 Optimized result of the first iteration for stable state

Although the simulation result in the first step seemed satisfactory, since the iteration step is a little big, this result can only indicate that the optimized gain pair is close to these values. And another iteration with smaller gain step is necessary, so as to find out a pair of better gains.

Thereby, based on the results of first iteration, a new iteration was conducted within the interval of $g_l \in (3.5, 4.5]$, with a step of 0.1 and $g_h \in (0.45, 0.55]$, with a step of 0.01. The initial condition of this iteration was the same.

Figure 4-12 shows the result when lateral gain was 3.5 and heading was 0.50. It can

be seen that the lateral error of the simulation was good and most of the time the vehicle ran within a ± 0.05 m range. Besides, the vehicle was not oscillating too much. However, the overshoot in the beginning of the simulation was not satisfactory. This also indicated that the heading gain of the robot shall be larger, since the heading gain can overcome the overshooting to some extent.

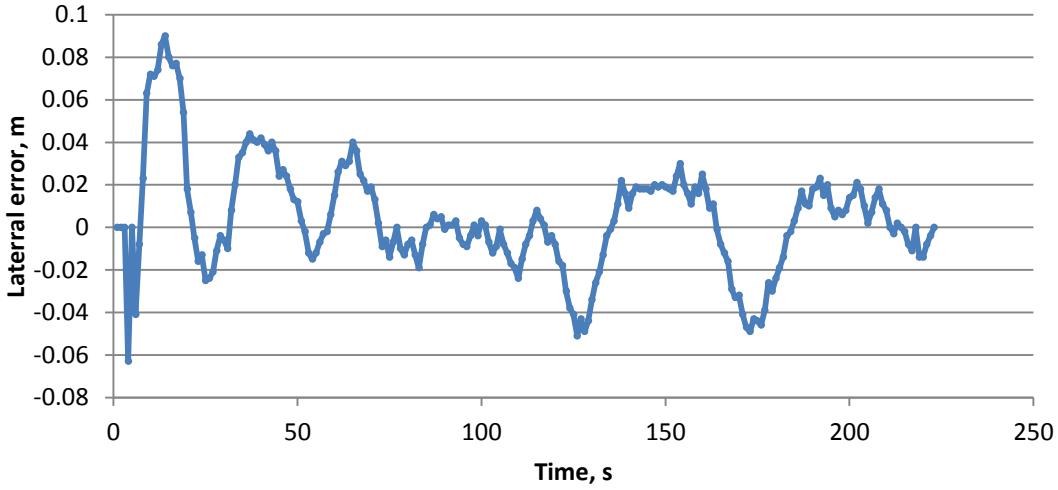

Figure 4-12 Simulation result when g_l=3.5, g_h=0.50

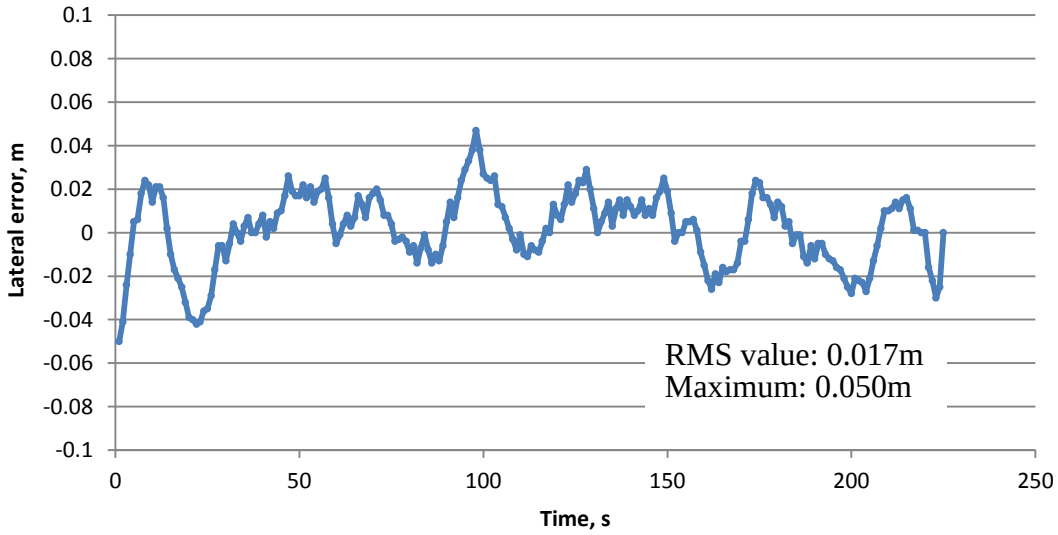

Figure 4-13 Optimized result of the second iteration for stable state

After the iteration, a pair of more precise control parameters was found – lateral gain

(g_l) =4.1 and heading gain (g_h) =0.55. The result of this simulation is shown in Figure 4-13. Specifically, the RMS value of lateral error is 0.017 m with a maximum of 0.050 m.

By comparing the optimization results in step 1 and step 2, it is obvious to all that when the lateral gain (g_l) is 4.1 and heading gain (g_h) is 0.55, the performance of the vehicle is better, for that it has a better navigation result, which can be told by the RMS value of the lateral error. Also, the overshoot of the control is moderate.

4.3.2 Results of optimization for approaching state

The objective of this optimization is to find out a pair of gains to ensure that the vehicle can reach stable state in the shortest time when it is trying to approach a target line. Usually, a field map is made up of several paths and when the vehicle turn from one path to another, there is inevitably some offset. In some other occasions, the field may not be flat enough that the robot is disturbed and it results in a large offset. In these occasions, a pair of new gains should be applied so that the vehicle can go back to the target path as quickly as possible.

As stated before, the optimization was conducted in two steps. In the first step, based on the iteration, heading gain was set to 0.55, just same as the optimization result in stable state optimization, and Golden Section Search was conducted, under the initial lateral error ranging from 0.15 m to 0.75 m. The result of optimization is shown in Figure 4-14.

Obvious as it is that there is hardly any relation between optimized lateral gain and initial lateral error, if any. Moreover, nearly all of these simulation results fell into an interval from 5.3 to 6.8, and by averaging these optimized gain, a mean of 6.26 was

obtained. In the second step, by setting the lateral gain to 6.26, the optimization was conducted when initial lateral error ranging from 0.15 m to 0.75 m, and the result is shown in Figure 4-15.

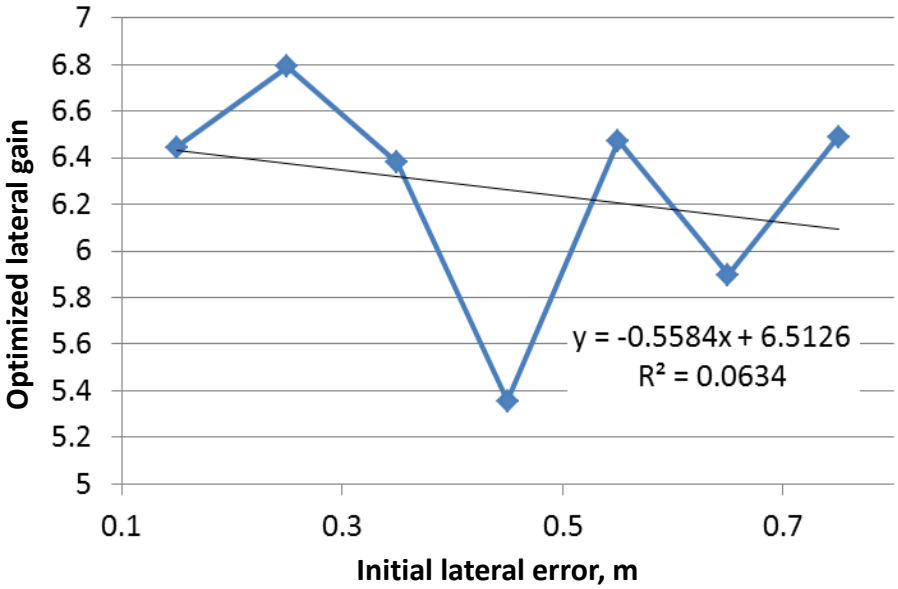

Figure 4-14 Optimized lateral gains in various initial offsets

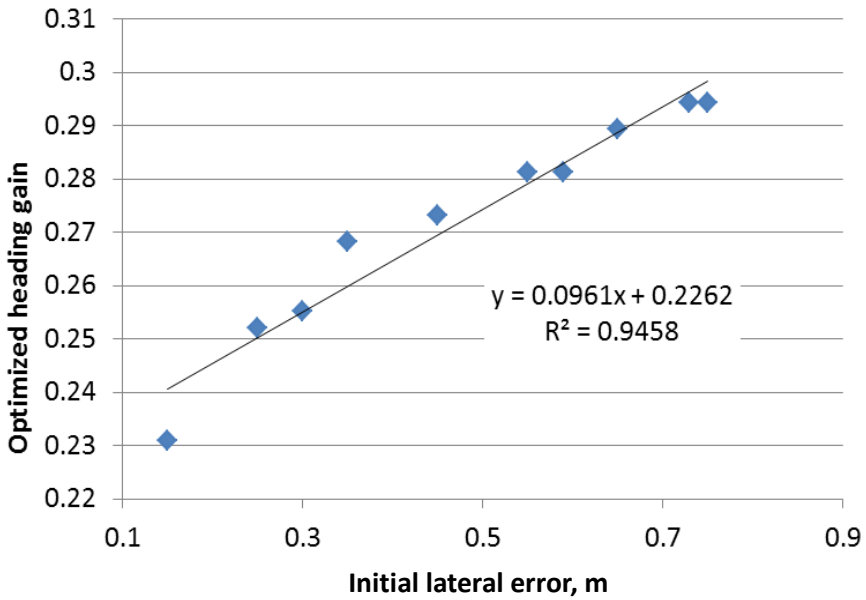

Figure 4-15 Optimized heading gains in various conditions

It is manifest that the relation between initial lateral error and optimized heading gain

is direct proportional, which can be calculated by Eq.(4-10)

$$g_h = 0.0961 d_0 + 0.2262 \tag{4-10}$$

where g_h is heading gain and d_0 is the initial lateral error. It can be used to calculate an appropriate heading gain before the vehicle enters a stable state.

4.3.3 Field verification

To verify the optimized results obtained in this research, control parameters of the vehicle was set up as follows: Before the vehicle enters a stable state, lateral gain was set to 6.26 and heading gain was set according to Eq.(3-10); after the vehicle enters a stable state, the lateral gain was set to 4.1 and the heading gain was set to 0.55 same as the optimized gains obtained from the simulations. Moreover, the initial lateral error was set to 0.15m, 0.3m and 0.7 m, so as to test the performance of the vehicle under different initial conditions. Heading of the robot was set generally parallel to the path, so as to be similar to the real condition after turning from one path to the next. Results of the field tests are shown in Figure 4-16, Figure 4-17, and Figure 4-18.

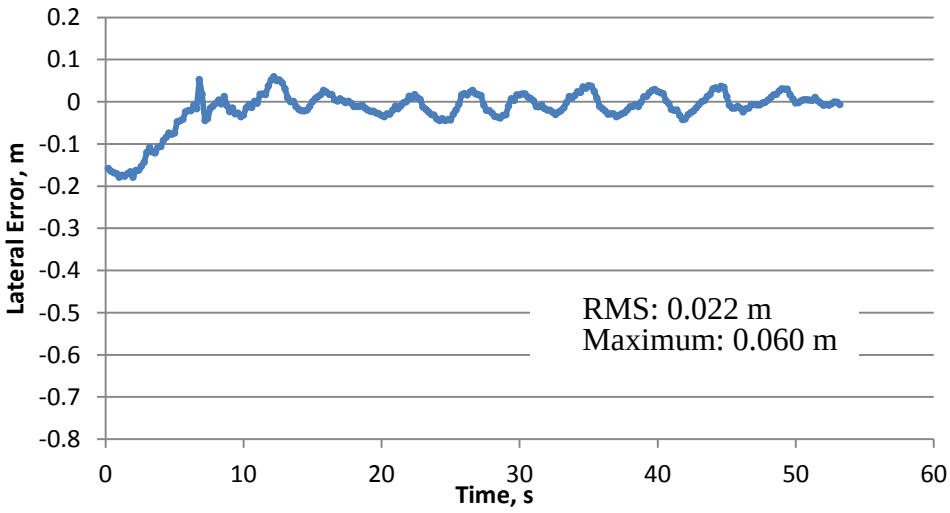

Figure 4-16 Field verification with 0.15 m of initial offset

As shown in Figure 4-16, when the initial lateral error was about -0.15 m, it took the vehicle nearly 7 s to enter a stable state. In the stable state, the RMS lateral error was about 0.022 m, with a maximum of 0.060m. The overshoot during this was 0.05 m and this was acceptable because the vehicle still stayed in a stable state.

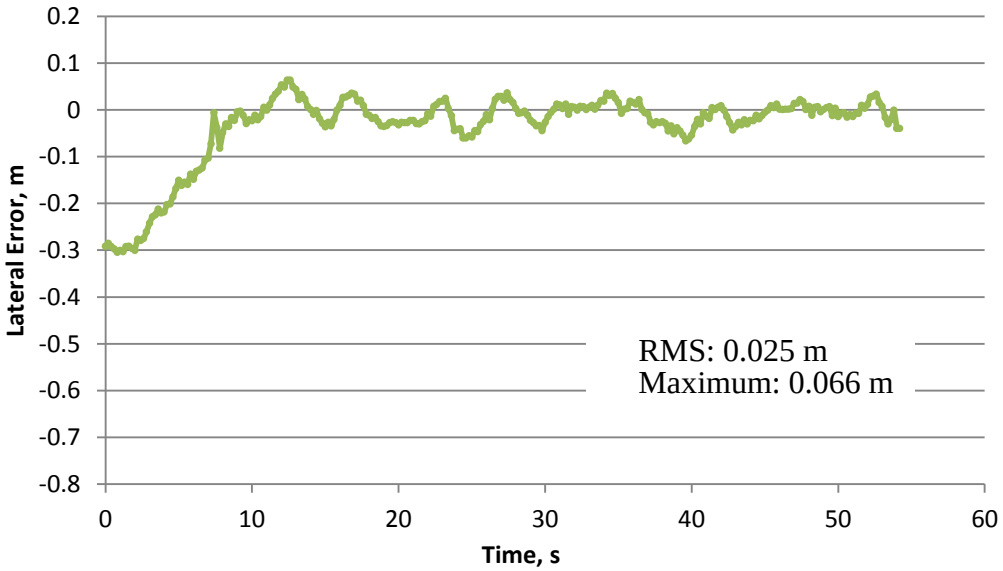

Figure 4-17 Field verification with 0.30 m of initial offset

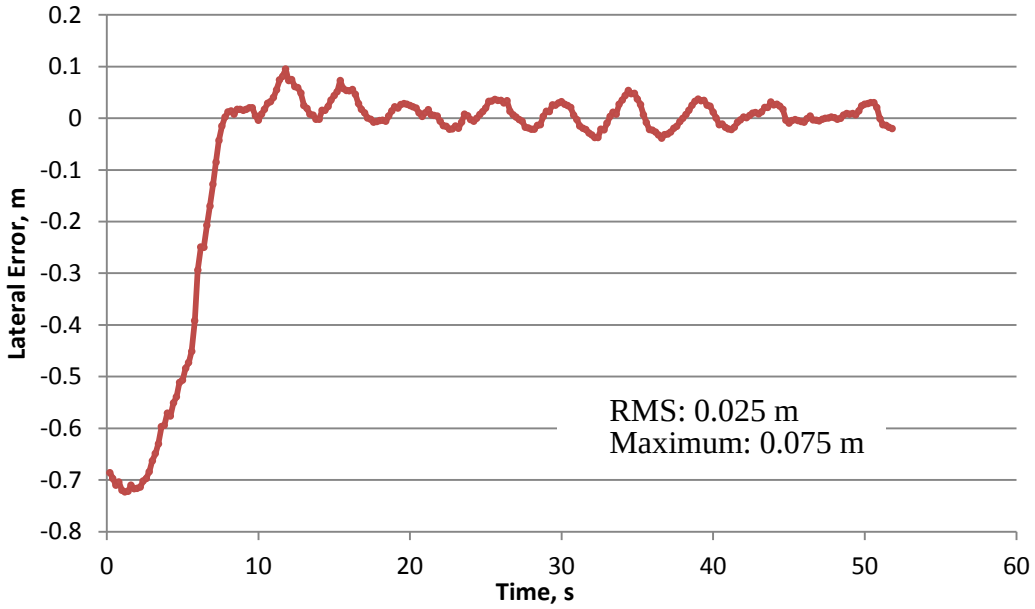

Figure 4-18 Field verification with 0.70 m of initial offset

Moreover, as shown in Figure 4-17, when initial lateral error was about 0.3 m, it took the vehicle nearly 7 s to enter a stable state. In the stable state, the RMS lateral error was about 0.025 m, with a maximum of 0.066 m. The overshoot was about 0.05m.

Finally, when the initial lateral error was about -0.7 m, as shown in Figure 4-18, it took the vehicle nearly 10 s to enter a stable state and in the stable state, the RMS lateral error was about 0.025 m, with a maximum of 0.075 m. Based on the data above, Table 4-1 was summarized.

Table 4-1 Summary of field experiment results

Initial lateral error (m)	0.15	0.3	0.7
Settling time (s)	7.0	7.0	10.0
RMS lateral error (m)	0.022	0.025	0.025
Max. of lateral error(m)	0.060	0.066	0.075

4.4 Conclusions

Tuning control parameters of a robot vehicle is tedious work. It can sometimes take a developer several days. This research, however, proposed and studied an efficient way to tune vehicle control parameters. In the study, a kinematic model for a robot combine harvester was developed and this model was used in the control parameters optimization. The optimization includes two steps: iterations for vehicle in a stable state and Golden Section Search for an approaching state. The whole optimization process took no more than an hour – highly efficient compared with traditional tuning method. Finally, the optimized control parameters were tested in the field and results showed that by using

the optimized control parameters, it took the combine harvester about 10 s to enter a stable state and after entering the stable state; the robot combine harvester can run in the field with the error of 0.025 m at the speed of 1.2 m/s. Consequently, it can be concluded that the optimization method is acceptable.

CHAPTER 5

PATH PLANS OF THE ROBOT COMBINE HARVESTER

5.1 Introduction

The objective of this chapter was to develop suitable path plans for the robot combine harvester. Basically, the navigation algorithm used in this chapter has been introduced in Chapter 3. This chapter focused mainly on the method with which the combine harvester could complete a whole crop field. In this chapter, two navigation path plans were proposed and tested. By using the navigation map correction method introduced in Chapter 3, they were also corrected so that damage to the crops could be avoided.

Specifically, the two path plans are called the human-like path plan and the high-efficiency path plan. In the human-like path plan, the robot combine harvester harvests from the perimeter of the field to the center of it, while in the high-efficiency path plan the robot harvests in a method that human beings, even a highly proficient farmer, cannot perform. Since the vehicle does not harvest the field line by line and it is almost impossible to determine where to enter the field without the help of the GNSS.

Tests were conducted in the experimental field of Hokkaido University and an experimental field in Memuro Town, Hokkaido, where the ground was even and easy for the robot to navigate. Data were recorded to check the accuracy of the vehicle. Lateral error and heading error were studied. Results of the tests showed that the robot combine harvester was able to fulfill the two path plans proposed. It is indicated that with certain compensation method and some safety device, the robot vehicle can be tested in the real field where the ground is uneven and more challenging for navigation.

5.2 Materials and methods

5.2.1 Human-like path plan

In this study, the robot combine harvester was designed to harvest from the perimeter of the field to the center, just like what farmers do in the field; and this path-plan is called human-like path plan. The illustration of this path-plan is shown in Figure 5-1. In this figure, the numbers are the order of paths, and the arrows show where the robot combine should start a path and in which direction should the robot start.

This path-plan was applied mainly because that when the combine harvester uses the standard 2-meter-wide header, the wheat or paddy is sometimes run over by the right crawler. In this path-plan, however, the right crawler is always running on the harvested area and can avoid running over the crop. And this path plan can also be used for wheat harvesting with a 2.5-meter-wide header, although there is no risk of running over the crop.

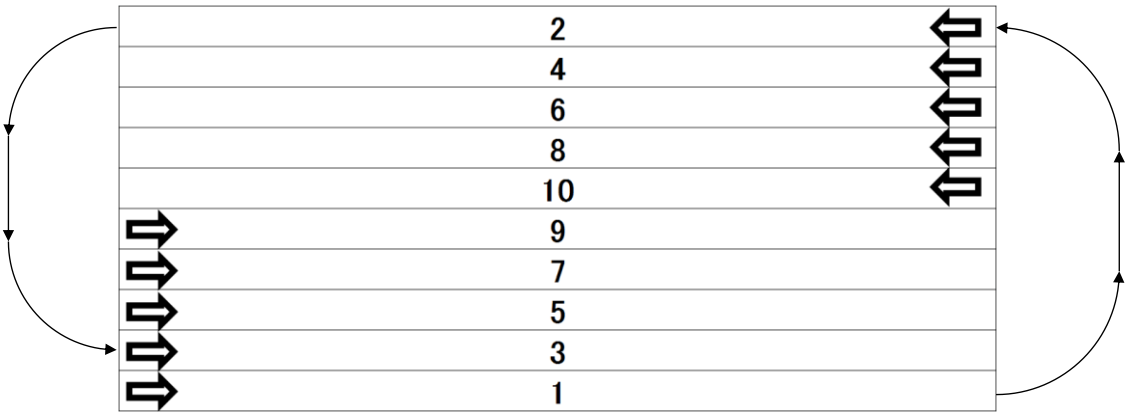

Figure 5-1 Human-like path plan

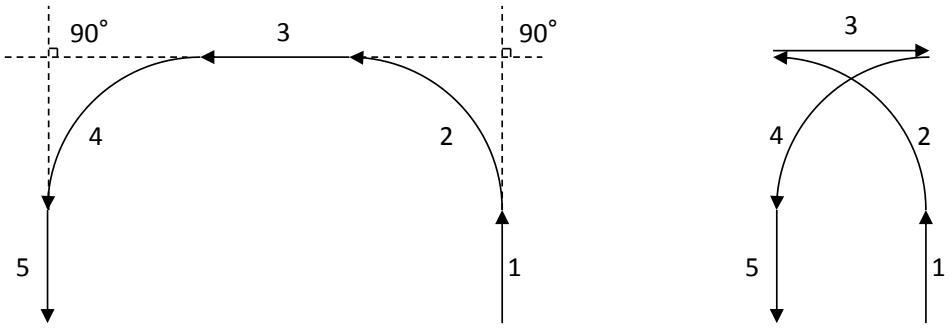

(1) Turning with forward movement (2) Turning with backward movement

Figure 5-2 Turning of human-like path plan

At the end of each path, the combine harvester should turn to the next path. Two turning methods were designed for the robot. They are turning with forward movement and turning with backward movement, which are shown in Figure 5-2. The turning includes 5 steps. Since the cutter of a combine is in front of the vehicle, turning of a combine harvester requires a large space. Thus, the first step of turning is to go forward to ensure that there is enough space to turn. The second step is to turn 90 deg left. And the third step is to go to a proper spot for entering the next path. It is possible for the combine harvester to go either forward or backward. The next step is to turn another 90 deg left, so that the vehicle's heading is the same to the heading of next path. Finally the robot looks for the entrance of next path and finishes step 5.

5.2.2 High-efficiency path plan

There is another path-plan for the robot combine harvester and its illustration is shown in Figure 5-3. There are 18 paths in total in this high-efficiency path-plan. And the paths can be divided into two groups – 9 paths in each group. In these two groups, only turning directions are different (in the first 9 paths, the robot turns left and in the next 9 paths, the robot turns right.)

This path-plan is created for a higher efficiency of harvesting and the difference mainly lies in turning. In the human-like path-plan, there is a straight movement either forward or backward. This straight movement can cost a long time when current path is a long distance away from the next. In this path planning, however, there are no straight movements when the combine harvester turns at the end of each path – it should either skip 4 paths (as turning from path 1 to path 2) or skip 3 paths (as turning from path 2 to path 3). The turning is shown in Figure 5-4. This is possible based on the fact that when turning parameters of the robot are properly set, the turning diameter can perfectly be equal to the distance between current and next path.

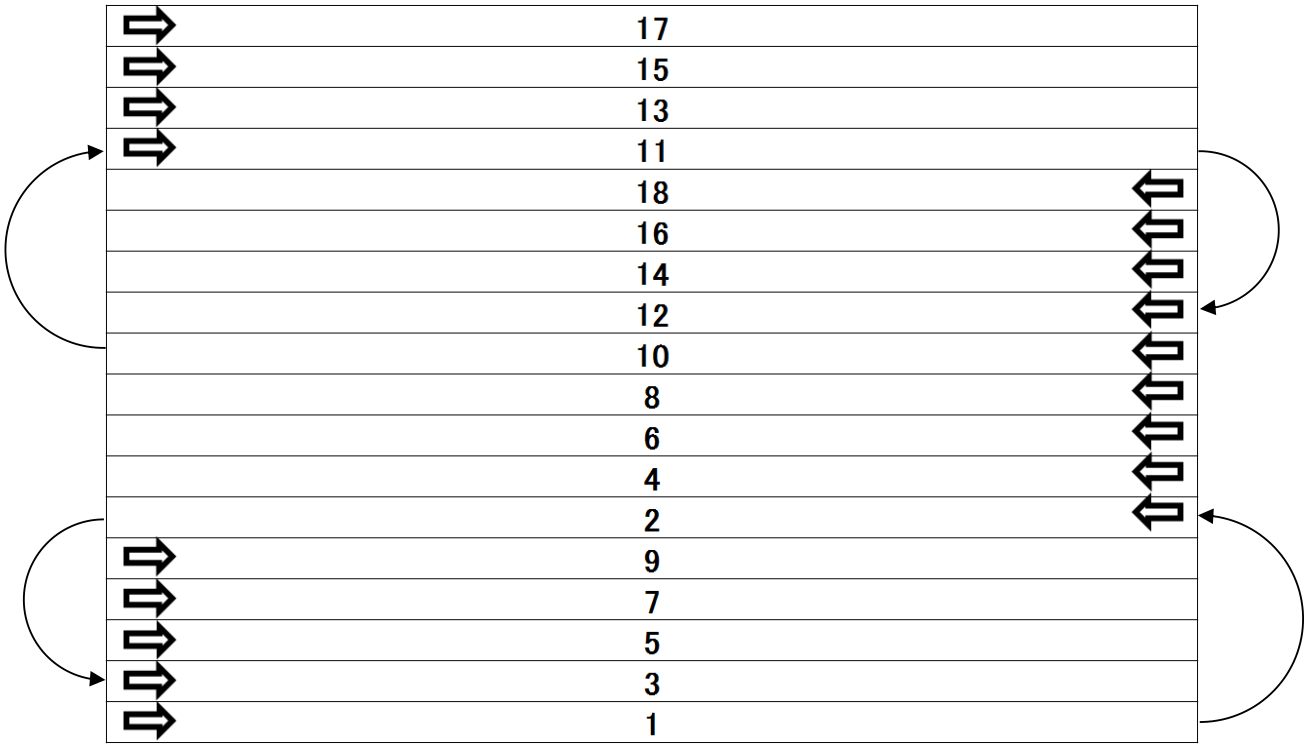

Figure 5-3 High-efficiency path-plan

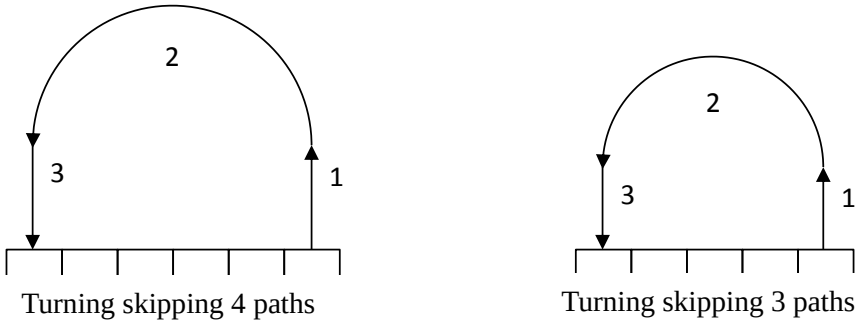

Figure 5-4 Turning for high-efficiency path-plan

By using this path plan, efficiency of harvesting can be improved. When the combine harvester runs with a 2-meter-wide header and the running speed is 1m/s, this change can save up to 5 minutes time when the robot harvests a field with 18 paths. Given that the size of farm in Honshu area of Japan is small, turning of at the head land of field accounts for a higher ratio of all harvesting time. Thus, this method can increase efficiency of harvesting to a great extent.

In addition, this turning method can only be done by a robot with GPS receivers, since it is impossible for a human being to determine the entrance point of next path in the field when the crop is not harvested line by line.

5.3 Results and discussion

5.3.1 Experiments of human-like path plan

Before real field experiments, the human-like path plan was tested in the experimental field in Hokkaido University. The objective of this experiment was to test whether the robot combine harvester can perform the field work by using human-like path plan. Due to the limitation of the size of the field, a map with 4 paths was made. However, by using this field, all kinds of tests can be conducted, including correction of the navigation map, turning of the vehicle, etc. The accuracy of the robot combine

harvester was also tested in the experiment.

Navigation map of the experiment included 4 paths. The order of the paths is shown in Figure 5-5.

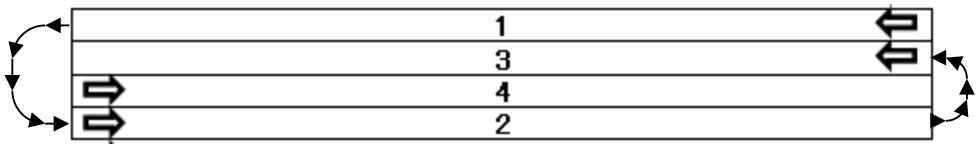

Figure 5-5 Order of paths in Hokkaido University field test

By using the method discussed in Chapter 3, the map was made. It is shown in Figure 5-6. The combine harvester was supposed to start at the place of the red arrow. The distance between adjacent paths is 2.3 meters. The combine harvester shall perform a turning with forward movement between path 1 and path 2. From path 3 to path 4, the combine harvester shall perform a turning with backward movement.

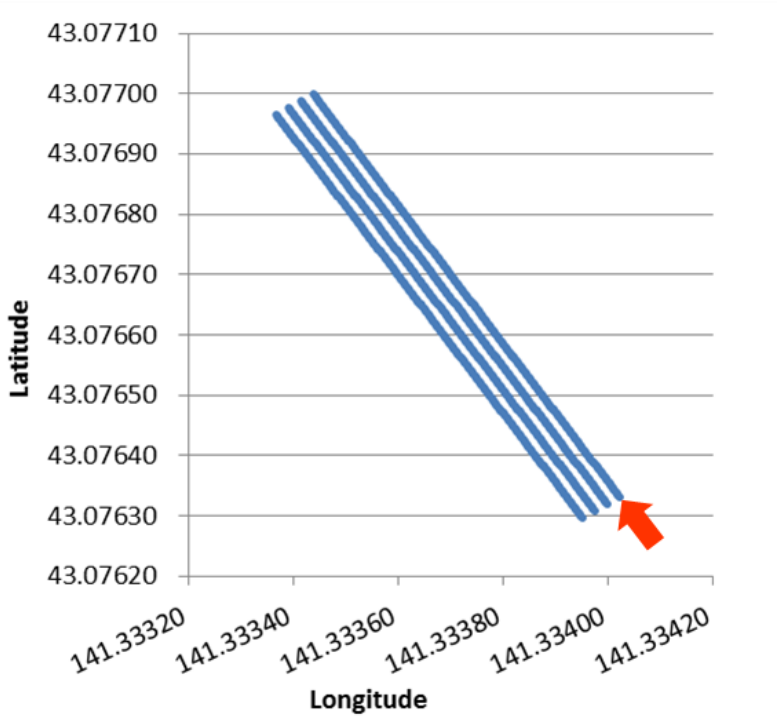

Figure 5-6 Navigation map of Hokkaido University field test

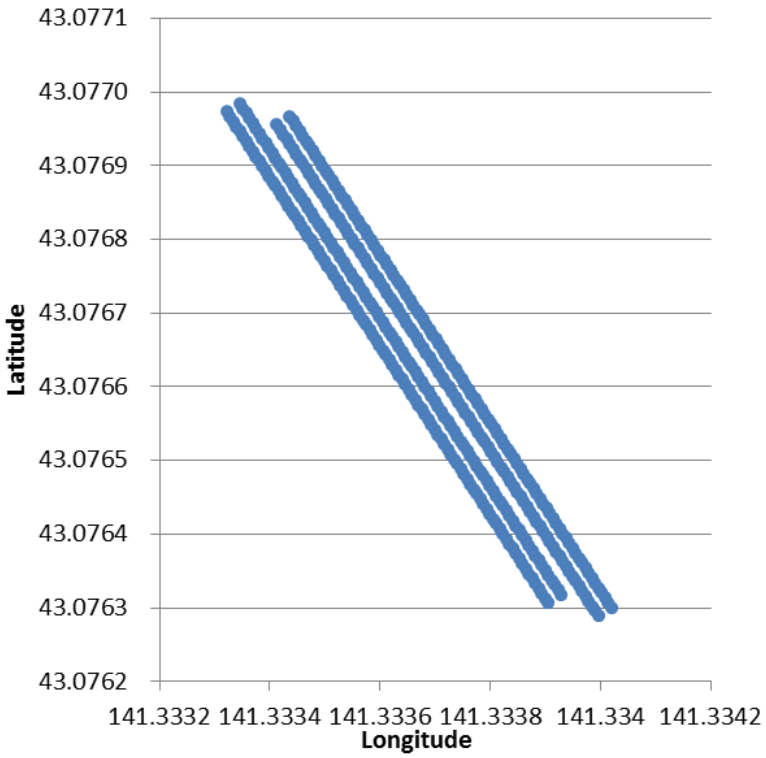

Figure 5-7 Corrected navigation map of Hokkaido University field test

After the navigation map was made, it was corrected by using the method discussed in Chapter 3. The corrected map for the field test is shown in Figure 5-7. Notice that correction to this map is different from that shown in Figure 3-14, for the robot vehicle was supposed to complete the field with human-like path plan, not line by line.

Result of the field test is shown in Figure 5-8. In this test, the combine harvester followed the navigation paths in a high level of accuracy. Specifically, the lateral error and heading error of this field test are shown in Figure 5-9 and Figure 5-10.

Figure 5-9 shows that the vehicle started with a lateral error of -0.2 m. After initialization, the vehicle went into a stable state. Most of time, it was running within a $\pm$0.06 m interval. After turning, the lateral error had its maximum, which was 0.15 m. However, the vehicle could approach the target path within 10 s. After approaching the target path, it could stably run in a $\pm$0.06 m interval. The RMS value of the lateral error

was 0.043 m.

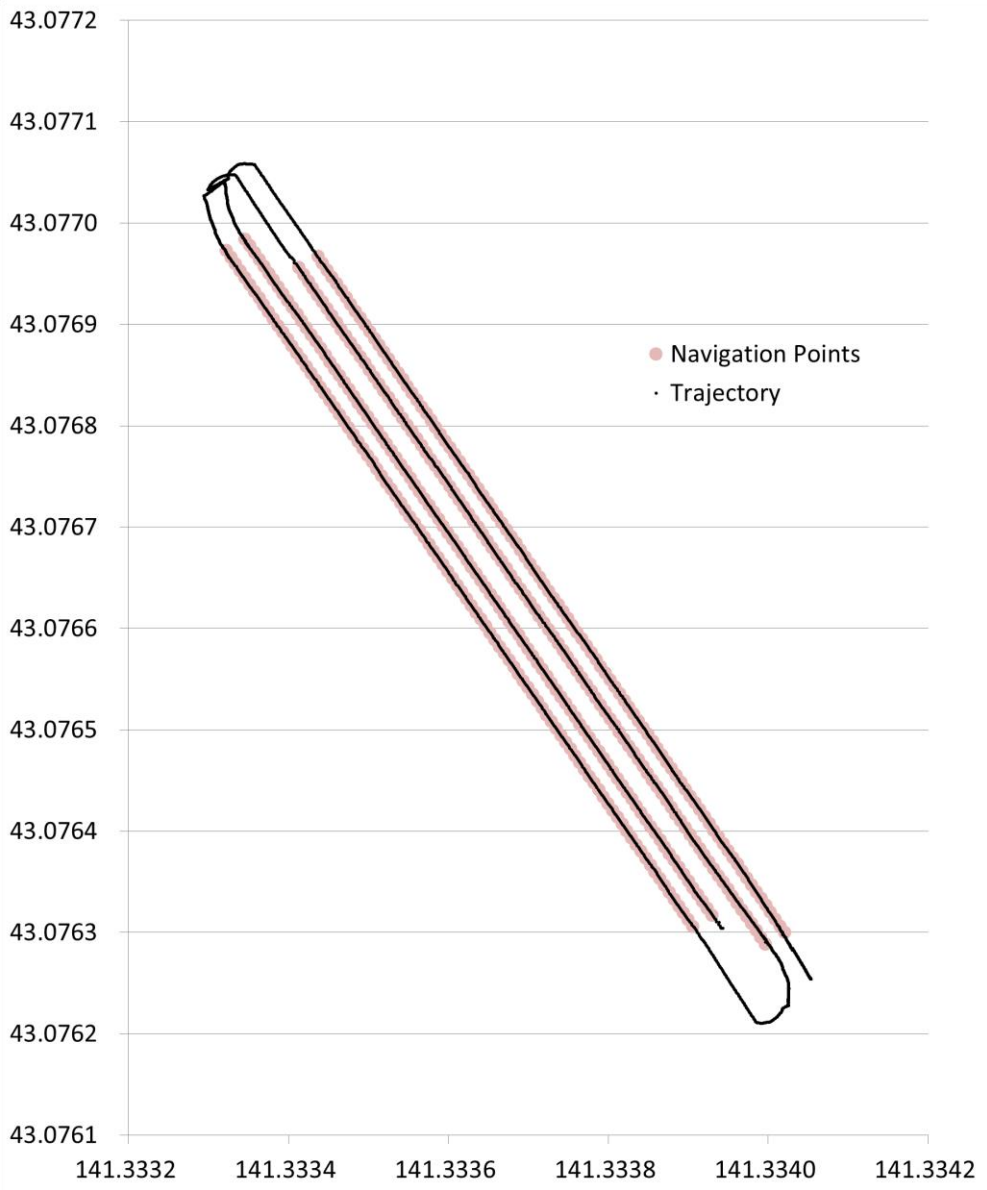

Figure 5-8 Results of Hokkaido University field test

Figure 5-10 shows that most of the time, the robot vehicle ran with a heading error no more than ± 2 deg, except when the vehicle was trying to enter a new path. After the vehicle entered a new path, it returned to a small heading error at once. The RMS value of the heading error was 0.896 deg.

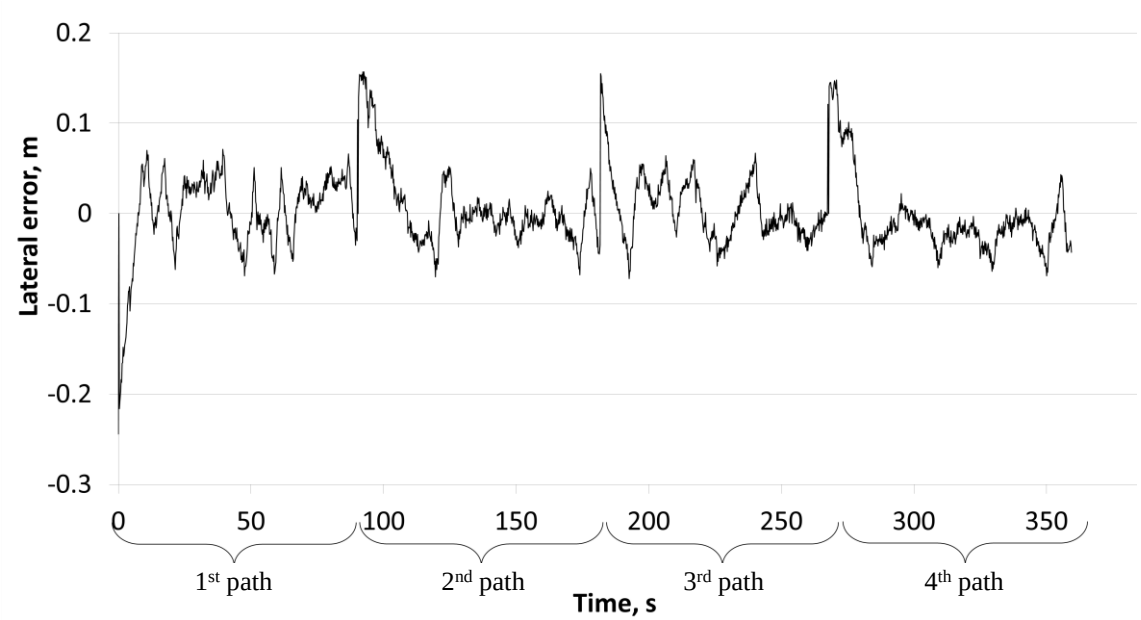

Figure 5-9 Lateral error of Hokkaido University field test

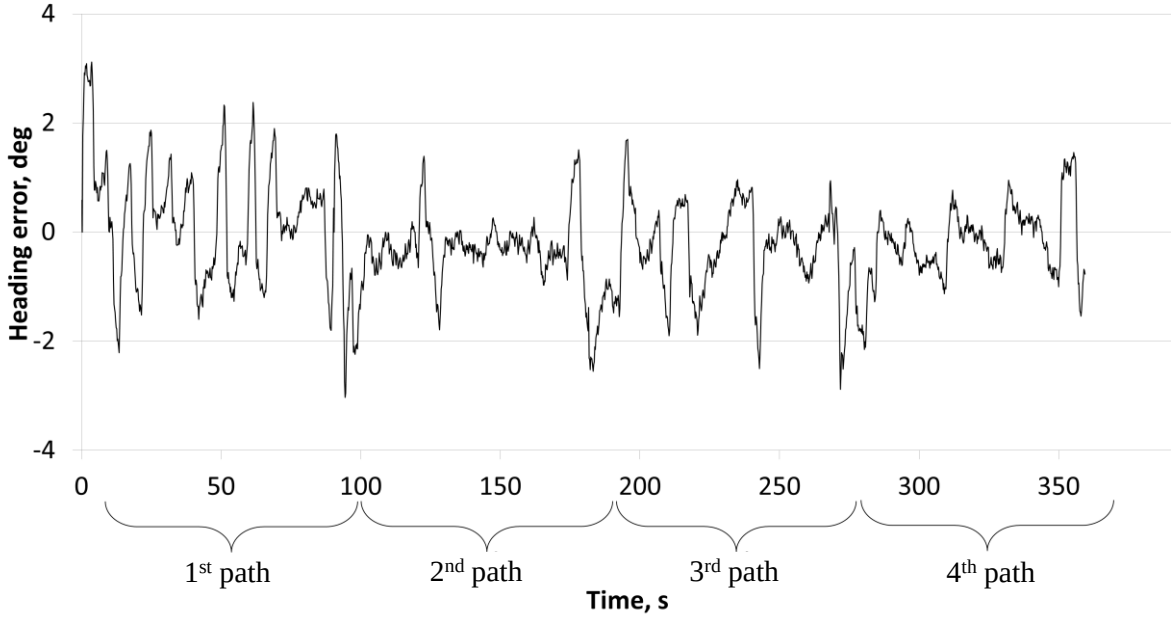

Figure 5-10 Heading error of Hokkaido University field test

Turnings of the human-like path plan were also tested. Turning with forward movement was tested when the robot combine harvester turned from path 1 to path 2. Data recorded are shown in Figure 5-11.

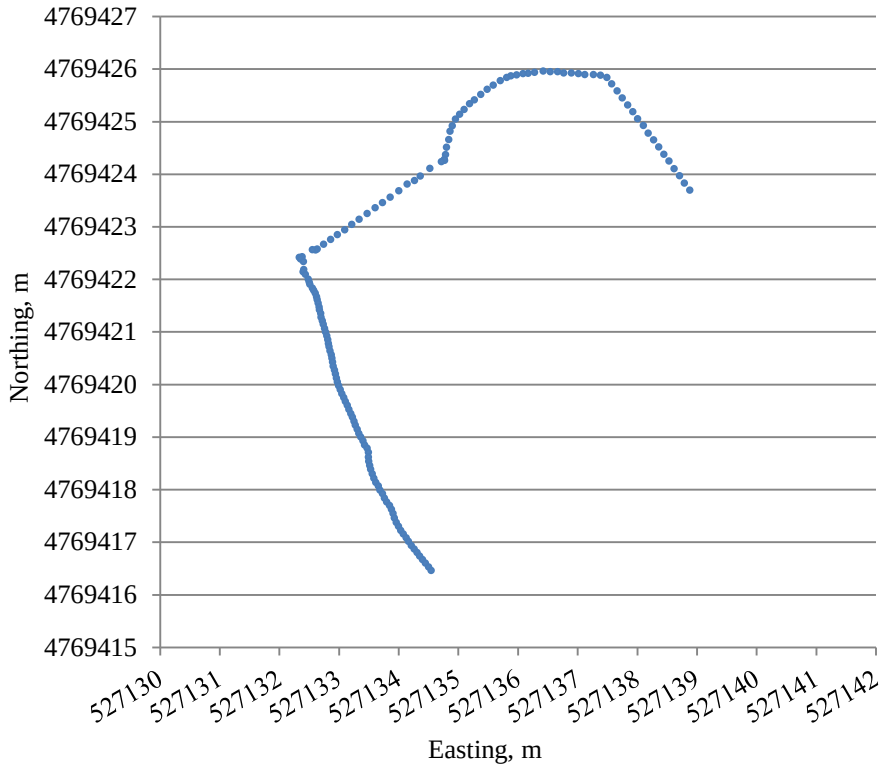

Figure 5-11 Data of turning with forward movement

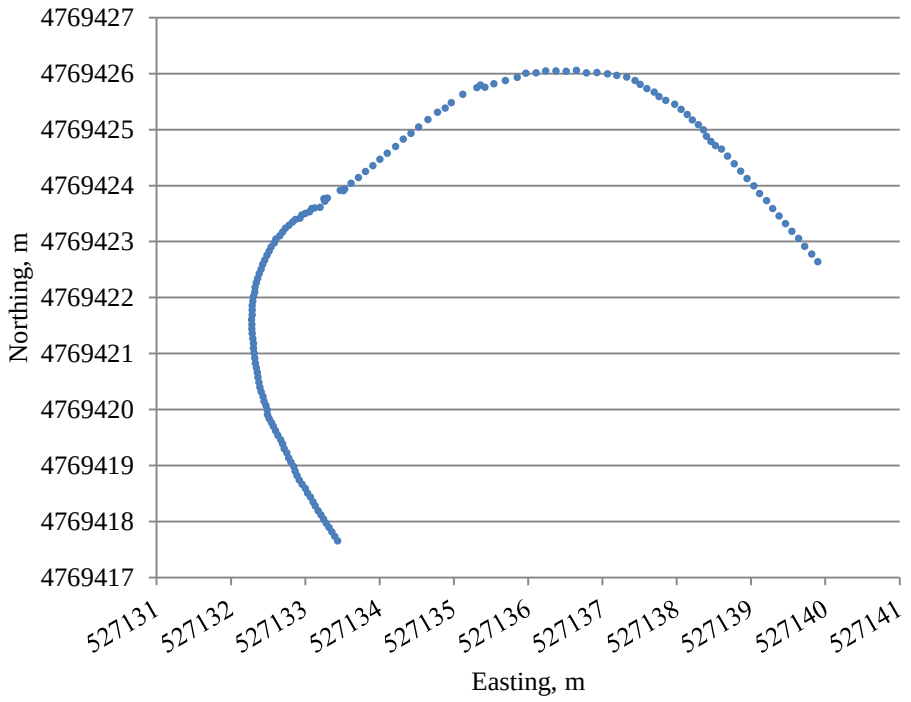

Figure 5-12 Corrected data of turning with forward movement

It is obvious that the data recorded in Figure 5-11 is totally different from the proposed one shown in Figure 5-2-(1) in shape. This is because that the GPS receiver is on top of cabin, not on top of the center of the crawlers. As a result, the recorded data should be corrected so as to show the trajectory of the crawlers, e.g. the trajectory of the vehicle. Figure 5-12 shows the data after correction.

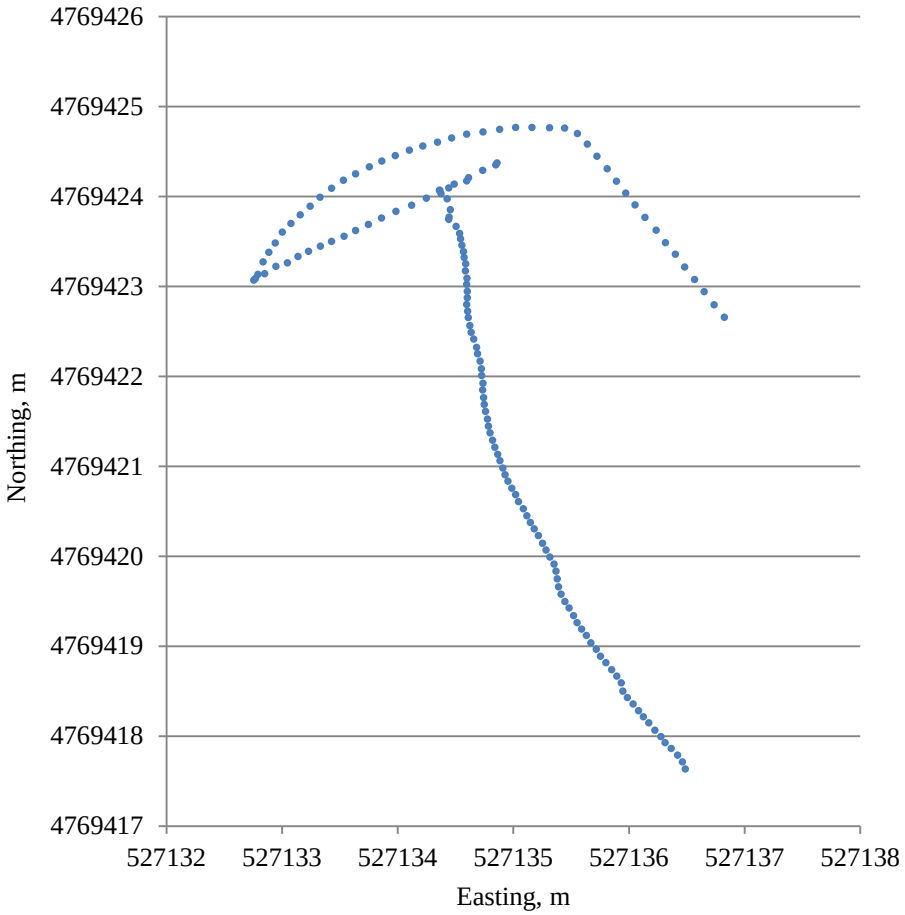

Figure 5-13 Data of turning with backward movement

After correction, it can be seen that the trajectory of the turning is similar to that of the proposed one, in which the combine harvester went a certain distance then turned left for around 90 deg; after turning, it went a straight line forward; then it turned left and found its way to the next path. There were also some problems in the turning. For

example, due to the delay of mechanical response, the combine harvester could not turn exactly 90 deg. Instead, it turns a little more than 90 deg, as shown in Figure 5-12. In addition, the points at the second turning are denser than the points at the first turning. This is because that when the vehicle was doing the second turning, its speed was slower than the first turning. Finally, the vehicle could find its way to enter the next path. This proved that the turning for the vehicle was successfully developed.

By using the same method, turning with back movement was also tested. The recorded data are shown in Figure 5-13.

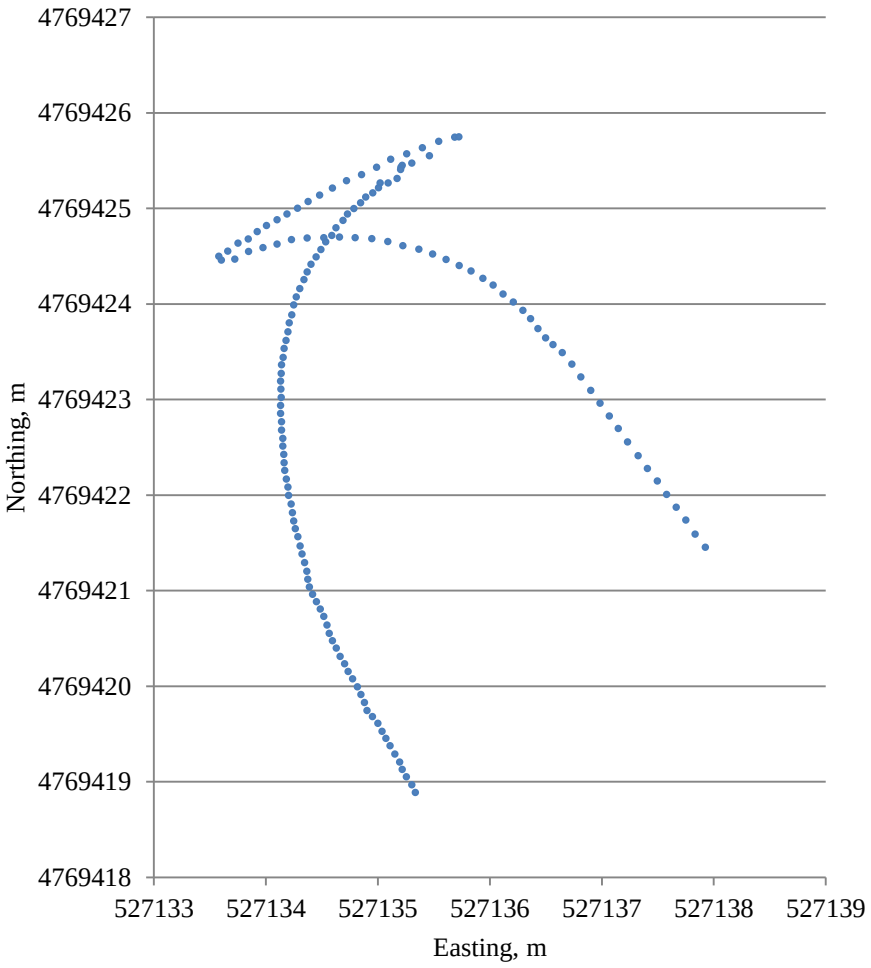

Figure 5-14 Corrected data of turning with backward movement

Corrected data are shown in Figure 5-14. It can be seen that the shape of the recorded data is similar to that of the proposed one shown in Figure 5-2-(2).

Results of the test showed that the vehicle found its way to the next path and went into the path smoothly – without noticeable oscillation.

5.3.2 Experiments of high-efficiency path plan

Before read field experiments, the human-like plan was tested in the experimental field in Memuro Town in Hokkaido, Japan. Although the proposed navigation map was made of 18 paths, in the experiment, due to the size of the experiment field, only 14 paths were made. The result of the test is shown in Figure 5-15. Results of the

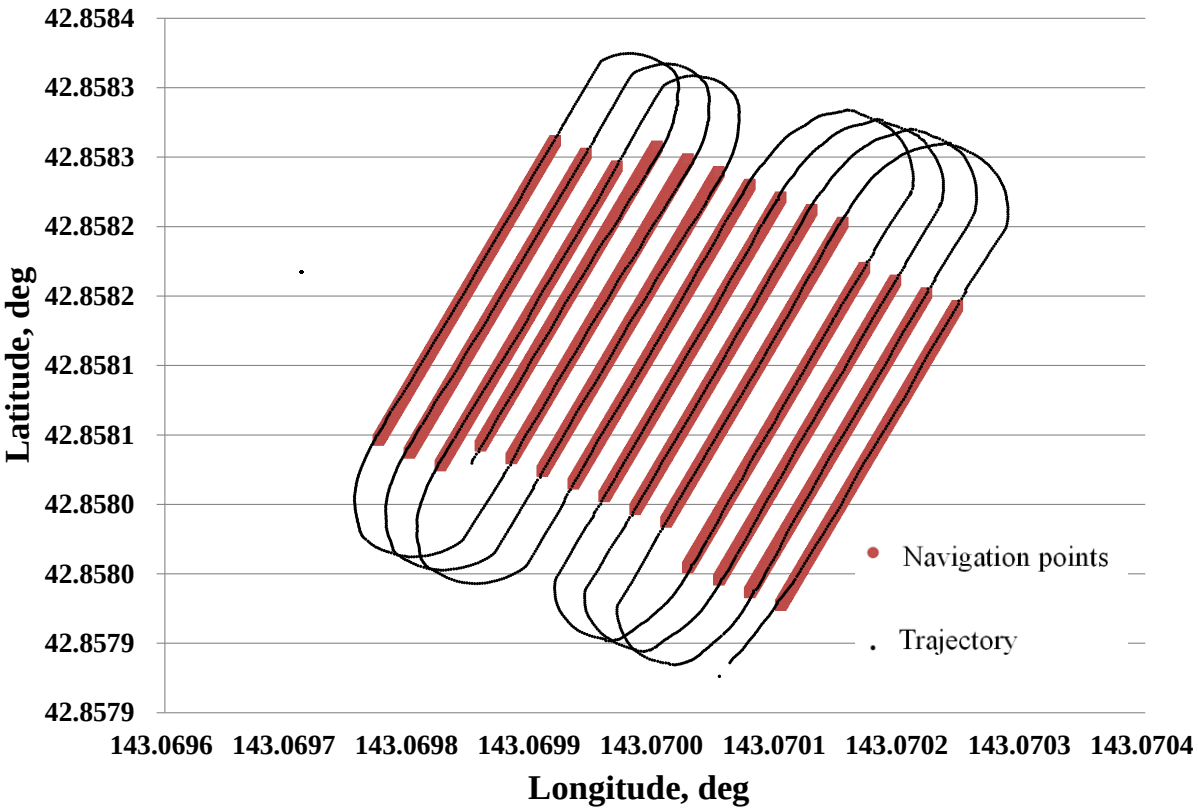

Figure 5-15 Experiment for the high-efficiency path plan

experiment indicated that the robot combine harvester was able to complete the high-efficiency path plan. At the end of each path, the robot combine harvester turned without decreasing its speed. Compared with the human-like path plan, when harvesting a field consisting 18 paths, the high-efficiency can save up to 10 minutes in turning.

5.4 Conclusions

Two path plans, the human-like path plan and the high-efficiency path plan, were proposed and verified in this chapter. These two path plans can be used for different types of field. The high-efficiency path plan proved that the robot combine harvester can perform the harvesting in a method that is impossible for human beings to perform.

However, since these experiments were conducted in the experimental field, more experiments are considered to be necessary to verify the feasibility in the real field, which is usually with rough ground. In addition, in the real field test, safety issues should also be taken into account.

CHAPTER 6

FIELD AND FEASIBILITY TESTS FOR THE ROBOT COMBINE HARVESTER

6.1 Introduction

The objective of this chapter was to test and evaluate the robot combine harvester's field performance. The difference between Chapter 6 and Chapter 5 is that in Chapter 5, the robot combine harvester was tested in the experimental field in Hokkaido University. However, in this chapter, the combine harvester was tested in the real field. In the experimental field introduced in Chapter 5, the surface of the ground was even enough, so that there is no much interference. This chapter introduces how the robot combine harvester was prepared for, developed and tested in the real field.

In order to deal with the rough ground, a correction to the navigation software was added. This chapter introduces how it works and it was realized. Moreover, a laser scanner was added to the robot combine harvester to prevent the vehicle from colliding to obstacles such as a human being. The principle of the laser scanner is introduced and they were also tested to ensure that the robot combine harvester will stop when there are people standing in front of it, especially during turning.

The combine harvester was developed for not only harvesting paddy rice and wheat, but also for soybean. Harvesting of paddy rice and wheat was tested with ordinary header, while soybean harvesting was tested with the header changed to a row-crop header. For paddy rice and wheat test, the perimeter of the field was harvested by an experienced farmer, usually for three to four cycles. This is extremely important for the

robot, for it prepares the space for turning. Then the combine harvester performed the automatic navigation and harvested the paddy rice or wheat. For the soybean harvest, since there was a slope at the end of the paths, it was dangerous to perform the turning by the robot. As a result, navigation was conducted only in the straight path. And turnings were conducted by a human being.

Results of the field tests showed that the robot combine harvester developed in this study can be used for harvesting paddy rice, wheat and soybean. However, minor improvements are still needed so that the robot can perform all the tasks without any involvement of human beings.

6.2 Materials and methods

6.2.1 Combine harvester's posture compensation

When the combine harvester works in the field, it is likely to be interfered by the landform. This is especially obvious when the robot relies on GPS receiver for its position data.

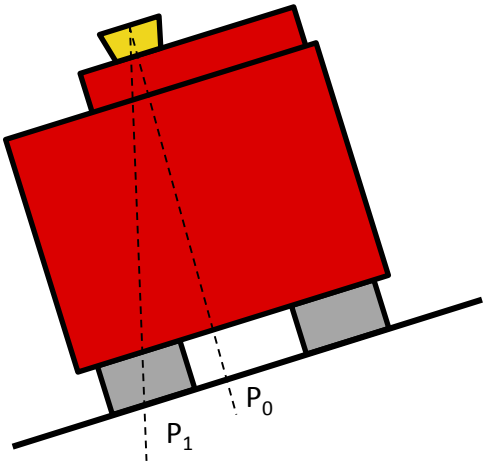

Figure 6-1 Position affected by roll angle of the robot

Figure 6-1 shows how the combine harvester's position can be affected by its roll angle. When the combine harvester move on a slope, its position is usually considered to be P_0, which is perpendicular to the surface of the ground. However, when the robot has a roll angle, its position indicated by a GPS receiver is P_1. The difference between P_1 and P_0 increases as the roll angle increase.

Accordingly, the robot's position can also affected by its pitch angle. Figure 6-2 shows how the GPS position can be different from the combine harvester's real position. This difference also increases when the pitch angle of the robot combine harvester increases.

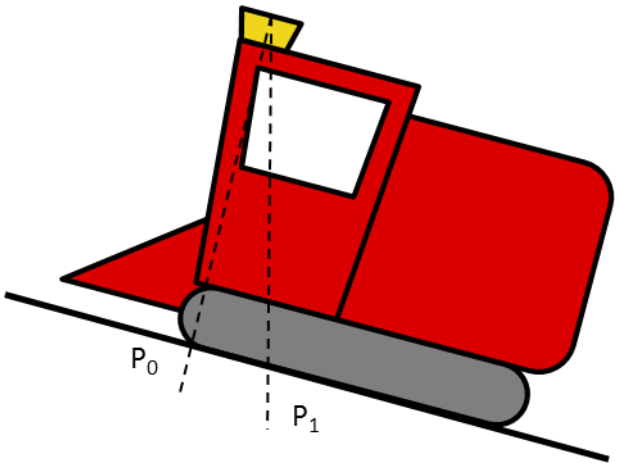

Figure 6-2 Position affected by roll angle of the robot

In this study, the position error caused by the vehicle's roll and pitch angle are called error by inclination. This error can be corrected by compensating the vehicle's position by Eq. (6-1)

$$\mathbf{P}' = \mathbf{P} - \mathbf{E} \cdot \mathbf{A} \tag{6-1}$$

$$\mathbf{P}' = [x', y', z']^T \tag{6-2}$$

$$\mathbf{P} = [x, y, z]^T \tag{6-3}$$

$$\mathbf{A} = [a, b, h]^T \tag{6-4}$$

$$\mathbf{E} = \begin{bmatrix} \cos\theta_r \cos\phi + \sin\theta_r \sin\theta_p \sin\phi & \cos\theta_p \sin\phi & -\cos\theta_r \sin\theta_p \sin\phi + \sin\theta_r \cos\phi \\ -\cos\theta_r \sin\phi + \sin\theta_r \sin\theta_p \cos\phi & \cos\theta_p \cos\phi & -\cos\theta_r \sin\theta_p \cos\phi - \sin\theta_r \sin\phi \\ -\sin\theta_r \cos\theta_p & \sin\theta_p & \cos\theta_r \cos\theta_p \end{bmatrix} \tag{6-5}$$

where $\mathbf{P}'$ is the compensated position data; $\mathbf{P}$ is the raw position data received from the GPS receiver; a, b and h are the offset of GPS antenna from the pivot of the vehicle; θ_r, θ_p and ϕ are the roll, pitch and yaw angle received from the IMU embedded in the GPS receiver.

After compensation, the lateral error d and heading error $\Delta\phi$ can be calculated and by using Eq. (3-12), steering angle of the robot can also be calculated.

6.2.2 Safety device based on a laser scanner

By using the laser scanner introduced in Chapter 2, a safety device for the robot combine harvester was made. The laser scanner detects obstacles by measuring distance from -135 deg to 135 deg, and within a distance of 30 meters. The principle of the laser scanner is shown in Figure 6-3. When there is an obstacle, the laser scanner is able to detect it due to the change of distance.

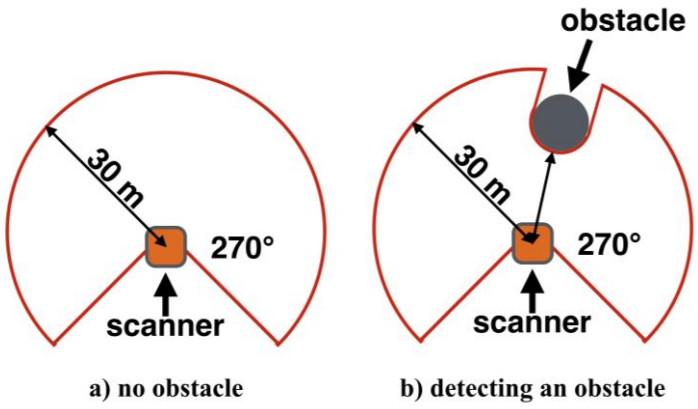

Figure 6-3 Principle of laser scanner detecting an obstacle

When the laser scanner is mounted on top of the cabin, Figure 6-4 shows how the robot can detect the human being in the field without interfered by the crops. A prerequisite is that the human being should be taller than the crops.

Figure 6-4 Robot detecting a human being in the field

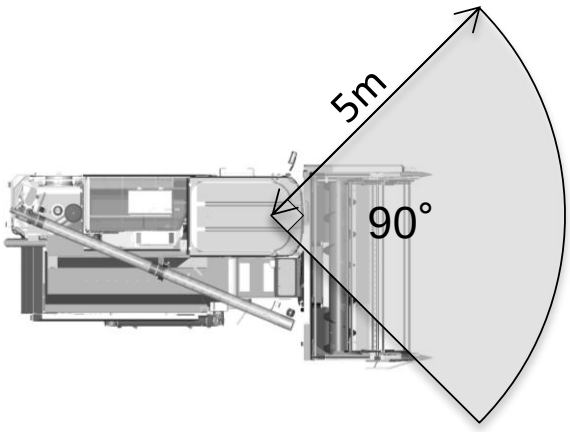

Figure 6-5 Range of the laser scanner

Range of the laser scanner is shown in Figure 6-5. Radius of the range is 5 m and its angle is 90 deg. This ensures that the combine harvester can detect an obstacle taller than 1.55 m without being interfered by the crops.

6.2.3 Field experiments for wheat

The field experiment for wheat was conducted in Memuro Town, Hokkaido, Japan. Since the width of the field was approximately 50 m, a map 18 paths were made, with

2.3 m wide for each path. Before the harvesting experiment, an experienced farmer harvested the perimeter of the field for four times, as shown in Figure 6-6 marked by "X". The rest of the field was all harvested by the robot combine harvester. The direction to enter each path is shown by the arrows and the order of the paths is shown by the numbers. Corrections to the vehicle's position were applied so that when there is inclination, the position could be corrected and it prevented the vehicle from oscillation. Safety control of the vehicle was also included, so when there is a human being detected in front of the robot, the vehicle will immediately stop.

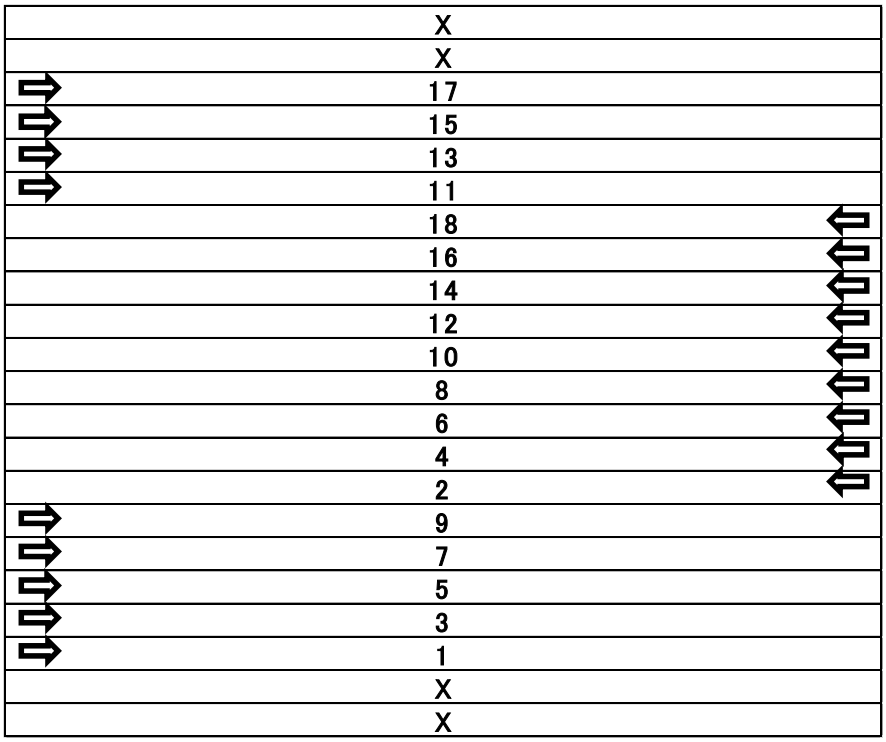

Figure 6-6 Field experiment path plan for wheat harvesting

6.2.4 Field experiments for paddy rice

Field experiments for the rice were conducted in Nanporo Town, Hokkaido, Japan. In these experiments, the human-like path plan was used. There were totally 8 paths and

each path was about 70 m in length. In the test, the surface of the ground was soft and muddy. However, with proper steering, the robot combine harvester could navigate with a high accuracy and complete the harvesting work without causing much damage to the ground.

6.2.5 Field experiment for soybean

The soybean test was performed in Memuro Town, Hokkaido, Japan. This test was different from the wheat and paddy rice test mainly in that this experiment was conducted in a small soybean field. At the end of the paths, there was a slope. If the combine harvester were to turn at the slope, it is possible that the combine harvester may turn over. Thus to avoid the accident, the robot combine harvester only conducted the harvesting work but did not perform the turning. Its path plan in this test was shown in Figure 6-7.

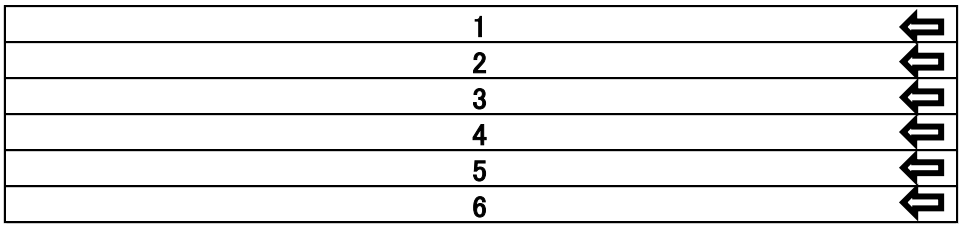

Figure 6-7 Field experiment path plan for soybean

Moreover, since the row crop header was used this time, it was necessary that the combine harvester follow the soybean plant strictly. As a result, the navigation map was not a straight line determined by two points. Instead, it was logged by people who carried GPS receivers on a pole that pointing at crops and followed the crop lines.

6.3 Results and discussions

6.3.1 Laser scanner test

In order to test the ability of the laser scanner to detect obstacle, experiments were conducted in the laboratory. In the experiment, the laser scanner was mounted on the top of the robot combine harvester and an obstacle made of cardboard was used. The obstacle was 1.8 m tall.

In the first experiment, data were recorded without obstacle. The result is shown in Figure 6-8. When there is no obstacle in front of the vehicle, the data of the laser scanner show a triangle.

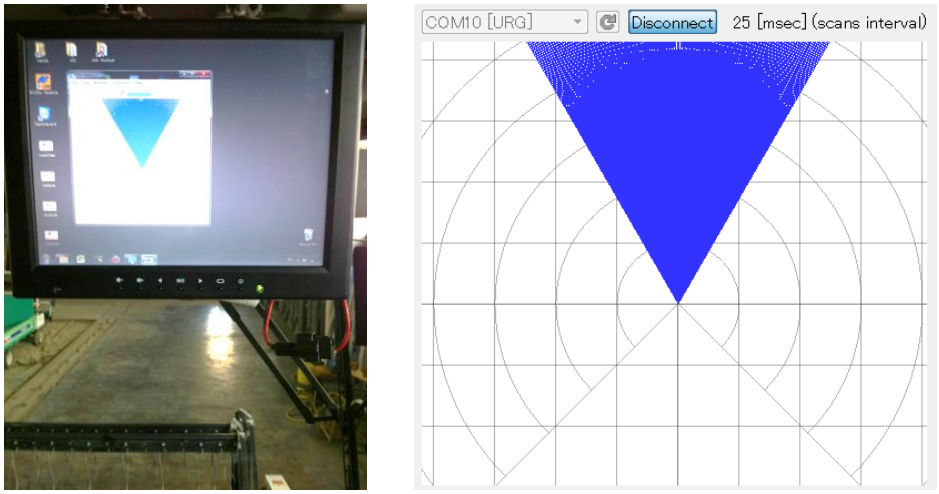

a) No obstacle in front of the vehicle b) Data of the laser scanner

Figure 6-8 Data of the laser scanner when no obstacle

Then, an obstacle was placed 3 m in front of the vehicle, and the result is shown in Figure 6-9. When there is an obstacle 3 m in front of the vehicle, the laser scanner was able to detect it and it can send a data to the controller of the robot combine harvester and stop the vehicle.

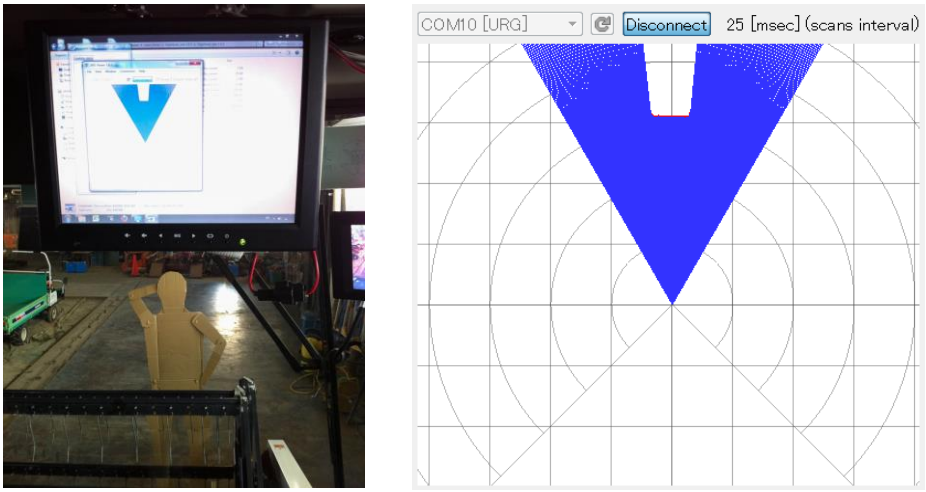

a) An obstacle in front of the vehicle b) Data of the laser scanner

Figure 6-9 Data of the laser scanner when the obstacle is 3 m ahead

6.3.2 Field experiment for wheat

As stated before, the field experiment for wheat used the high-efficiency path plan. There are totally 18 paths and the navigation map is shown in Figure 6-10. The red points are the navigation points. Since they are too close to each other, in the figure, it seems that they have formed 18 lines. The distance between adjacent paths is 2.3 m and the length of each path is approximately 50 m. The map was shifted according to the robot's traveling direction by using the method introduced in Chapter 3. The black points are the trajectory of the vehicle. It can be seen in the figure that with the position compensation, the robot combine harvester's trajectory followed the paths in a high accuracy. Moreover, with the steering angle set to a proper value, the turning from one path to the next path was smooth. Turning radiuses in this field experiment were 5.75 m and 4.6 m. The robot combine harvester did not cause damage to the field with these turning radiuses. Besides, it was not necessary for the robot to slow down either. So this path plan could also save a lot of time in harvesting.

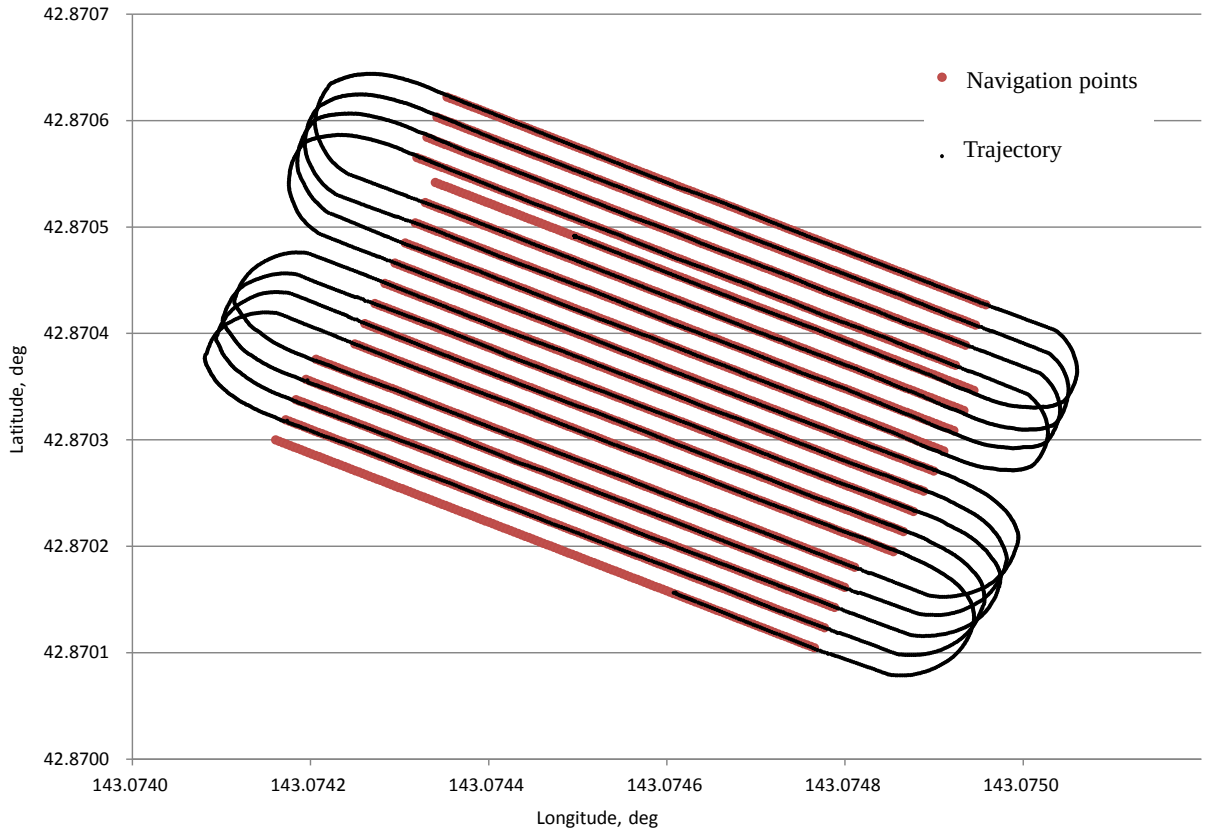

Figure 6-10 Wheat field navigation map and trajectory

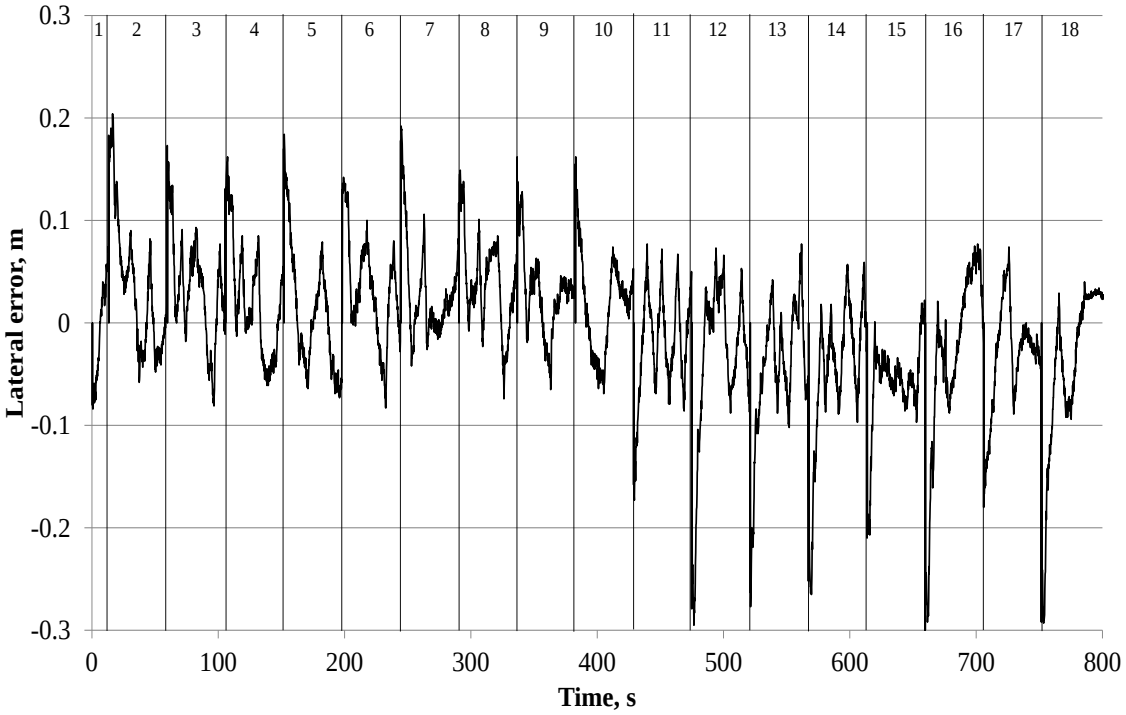

Figure 6-11 Lateral error of wheat field navigation

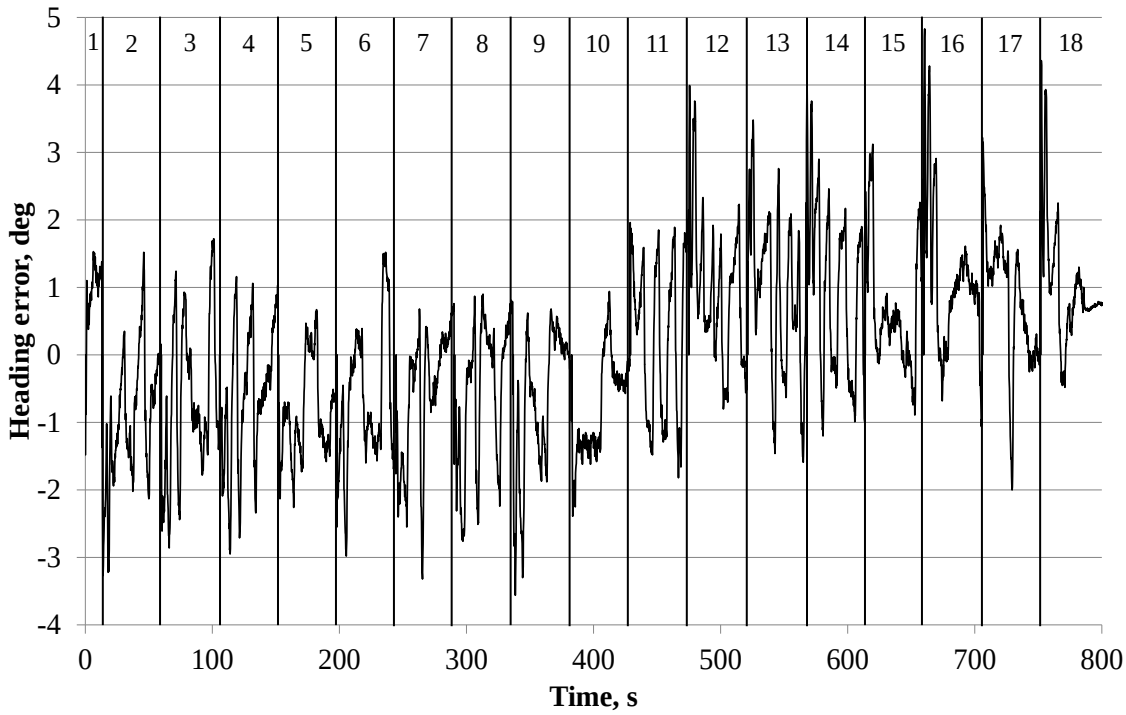

Figure 6-12 Heading error of wheat field navigation

Figure 6-11 shows the lateral error in the whole wheat field test. The figure also shows the path numbers. The first path was a little short, but all the other paths were of the same length. The robot combine harvester navigated at a speed of 1.2 m/s and the largest lateral error was about 0.15 m for the first 10 paths and 0.2-0.3 m for the last 8 paths. Since the robot combine harvester turned left in the first 10 paths and turned right in the other 8 paths, it can be concluded that when the combine harvester turns left to enter the next path, its accuracy is better than when it turned right. This is considered to be caused by the position of the GPS receiver, since it is not on the symmetrical line of the vehicle, rather it is on the left of that line. Moreover, the large lateral error only happened the moment when the vehicle entered a new path. After the vehicle fully entered a path, it navigated with a lateral error no more than 0.07 m in most of the time. The RMS value of the lateral error in the whole test was 0.066 m. As for the heading error in this test, it is shown in Figure 6-12. It can be seen that in the first 10 path, the heading error was relatively small, while in the last 8 paths, the heading error was larger. This was especially true when the vehicle was entering a new path, like from path 15 to path 16. The position of the GPS receiver was considered to be the main cause of this phenomenon. However, due to the structure of the robot combine harvester, it is impossible to mount the GPS receiver to the center of the crawlers. On the other hand, most of the time, the robot's heading error was smaller than 1 deg in the first 10 paths. In the last 8 paths, it ranged from -1 deg to 2 deg. The RMS value of the heading error in the whole test was 1.243 deg. When the lateral error and heading error are compared, it is manifest that the heading error is not as stable as the lateral error. This was considered to be caused by the property of crawler – the heading of the crawler-type vehicle can easily be changed.

Finally, since it is obvious that the performance when the vehicle was turning left was better than that when the vehicle was turning right, two typical paths were selected to make comparison.

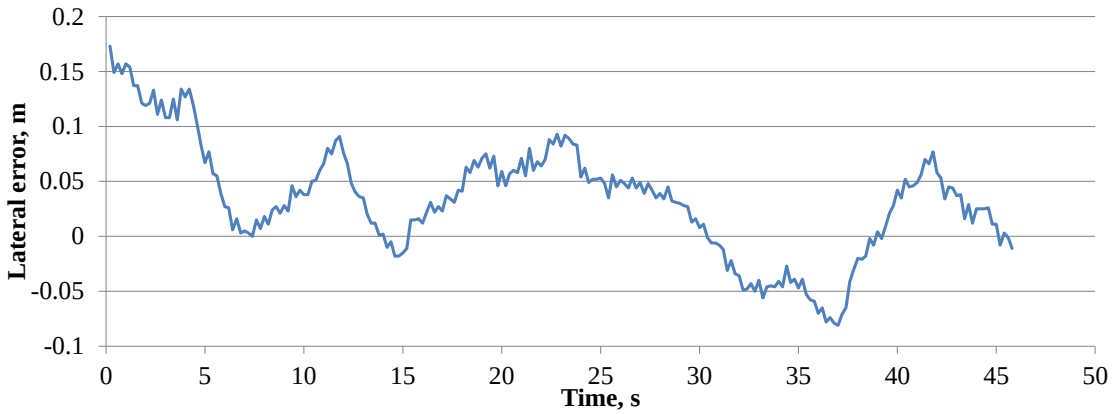

Figure 6-13 Lateral error in a typical path with left turn

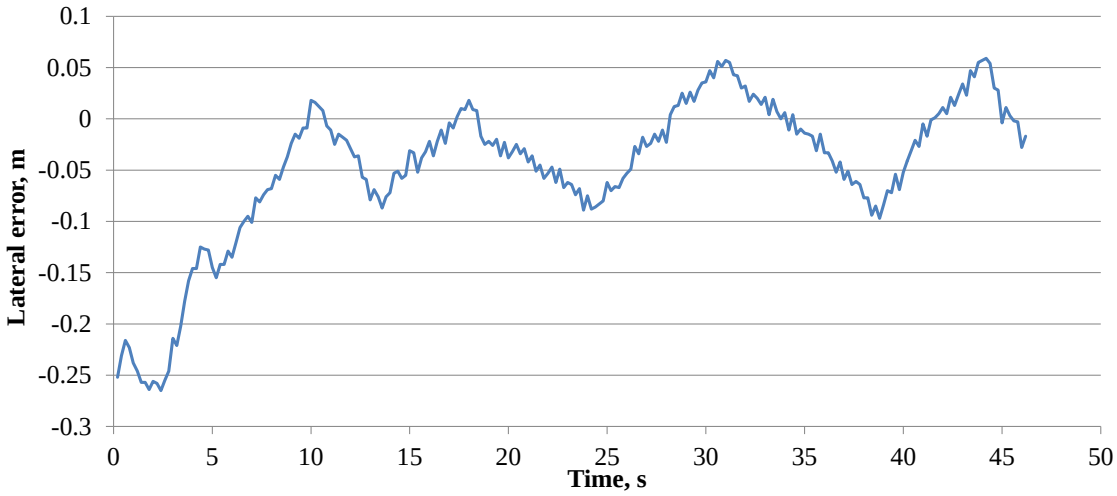

Figure 6-14 Lateral error in a typical path with right turn

Figure 6-13 and Figure 6-14 show the lateral error in path 2 (a typical path with a left turn) and path 12 (a typical path with a right turn) in the wheat field test respectively. The initial error in path 2 was moderately smaller than that in path 12. Apart from that, the performances in the two paths were nearly the same, especially the oscillation. In path 2, the RMS value of the lateral error was 0.061 m and in path 12, the RMS value

was 0.086 m. However, after the vehicle entered the stable state, the RMS value of path 2 was 0.046 m and that of path 12 was 0.043 m. In a stable state, the lateral error in path 12 was even smaller. Thus the large initial offset was the main cause to the large RMS value of lateral error.

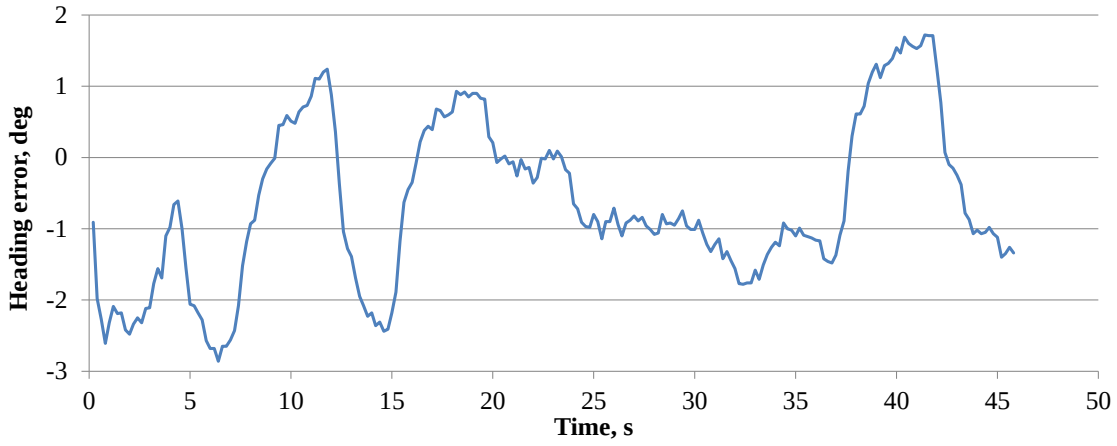

Figure 6-15 Heading error in path 2 of wheat field

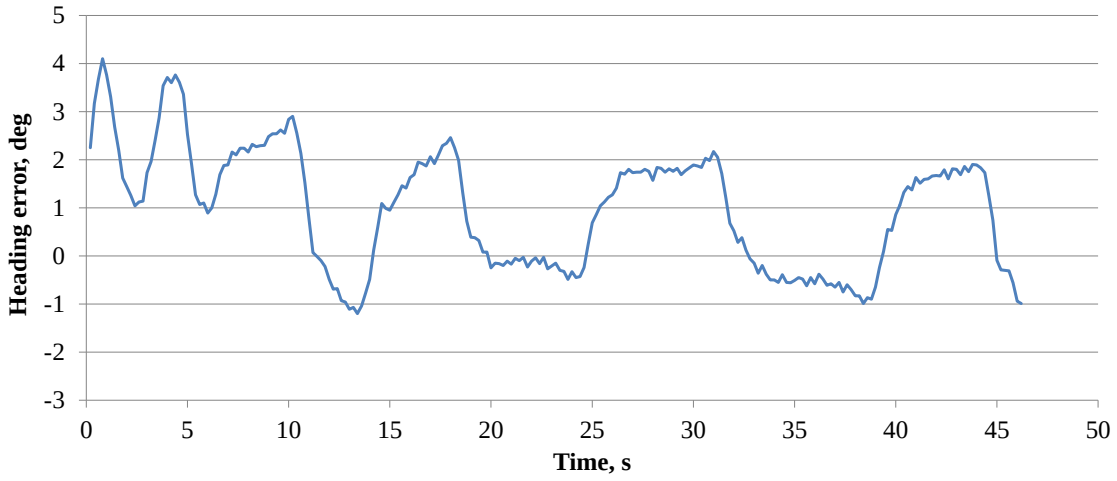

Figure 6-16 Heading error in path 12 of wheat field

Figure 6-15 and Figure 6-16 show the heading error in path 2 and path 12. It is obvious that the heading error in path 2 is smaller than that in path 12. Respectively, the RMS value of the heading errors were 1.32 deg and 1.58 deg.

To sum up, in the field test for wheat, the robot combine harvester navigated in a high accuracy and it successfully finished the high-efficiency path plan.

6.3.3 Field experiment for paddy rice

The field experiment for paddy rice was conducted in the Nanporo Town, Hokkaido, Japan. In the experiment, the human-like path plan was used. There are totally 8 paths and the length of each path is approximately 70 m. The map and trajectory of the experiment is shown in Figure 6-17, with the map in blue and trajectory in black points. The paths were shifted according to the traveling direction of the vehicle. It is obvious that for most of the black points, they are at the center of the blue points, which indicates that the vehicle was following the navigation map at a high level of accuracy. However, at the beginning of each path, the lateral was a little large. The lateral error in each path is shown in Figure 6-18.

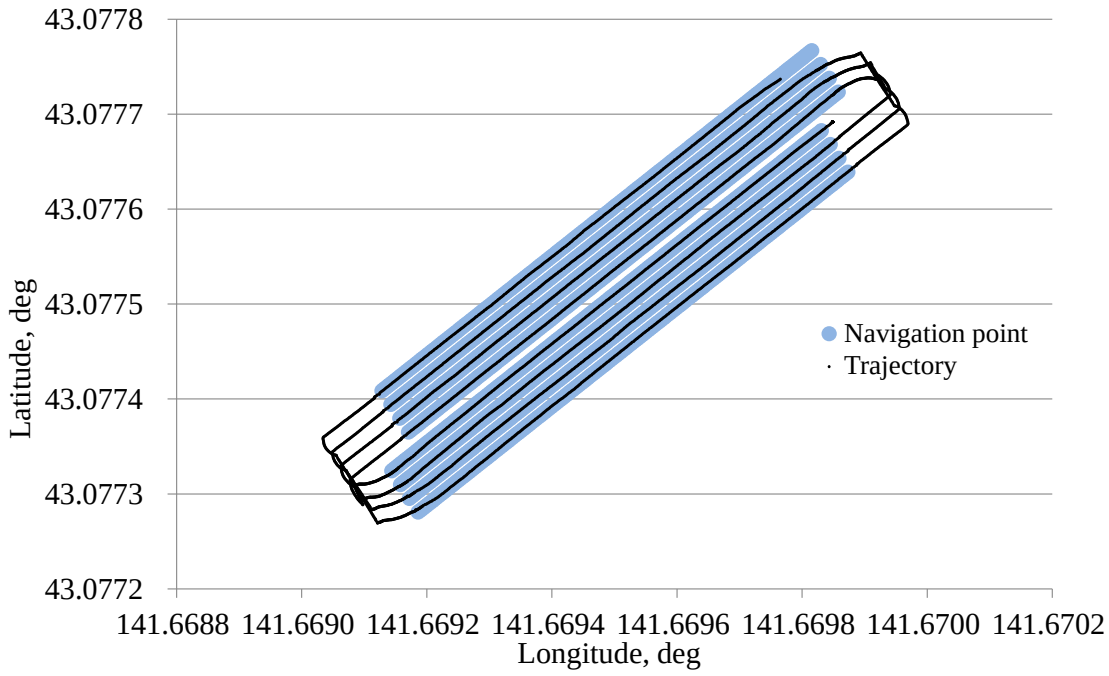

Figure 6-17 Paddy rice field map and trajectory

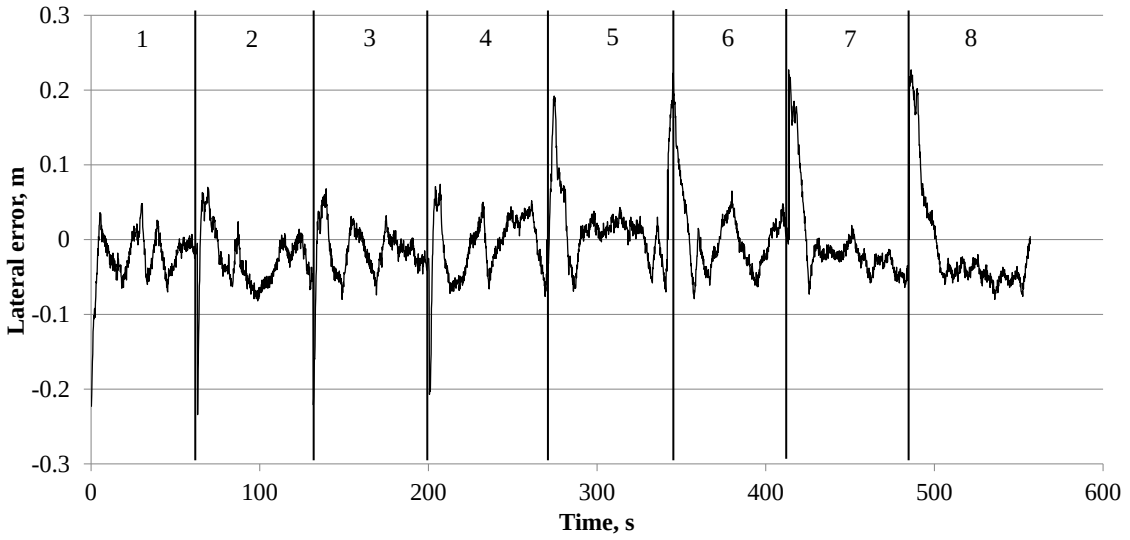

Figure 6-18 Lateral error of paddy rice field test

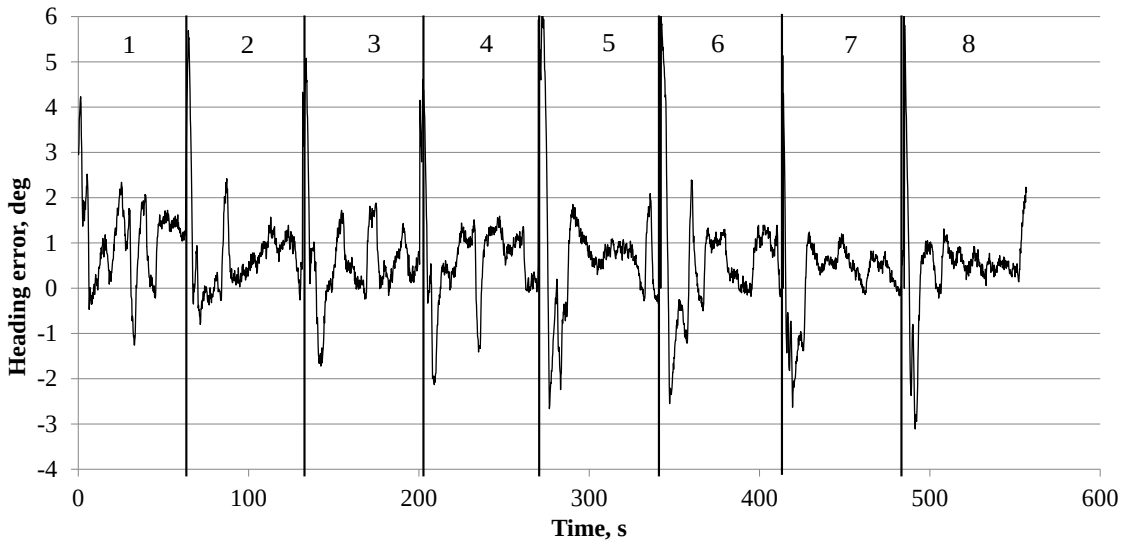

Figure 6-19 Heading error of paddy rice field test

As shown in Figure 6-18, the maximum of the lateral error was at the beginning of each path, just as the result of wheat field experiment. In the paddy rice experiment, the maximum was up to 0.22 m. However, the time for this large lateral error is very short, usually 2-3 s. After this period of time, the robot could navigate with a lateral error less than 0.05 m. Given that the distance between adjacent plant lines is 0.33 m, accuracy of

this robot combine harvester is absolutely satisfactory. Comparing the field data with those taken in Hokkaido University, it is manifest that the inclination compensation worked well for the robot combine harvester and the accuracy of the robot in the field was as good as it in Hokkaido University test. Specifically, RMS value of the lateral error in the paddy rice field test is 0.053 m.

The heading error of the paddy rice field experiment is shown in Figure 6-19 and the RMS value of the heading error is 1.31 deg.

6.3.4 Field experiment for soybean

The field experiment for soybean was conducted in the Agricultural Research Center in Memuro Town, Hokkaido, Japan. In the experiment, there were 6 paths in total. The length of each path was approximately 75 m. Since there was a slope at the end of the paths, it was difficult and dangerous for the robot combine harvester to turn. As a result, in the field experiment, the robot combine harvester only performed the harvesting and after each path, the robot combine harvester was driven by a human being to the beginning of the next path. Moreover, since the row crop header was used in the experiment, the navigation map was made by the researchers by holding a GPS receiver and following the crop row to record the GPS data. This is one way to make the navigation map. If the farmer records the GPS data during seeding the GPS data can be modified into a navigation map which can be used when harvesting. The navigation map and the trajectory of the experiment are shown in Figure 6-20. The red arrows in the figure show the start direction of each path. The blue points are navigation points and the black points are the trajectory recorded in the navigation.

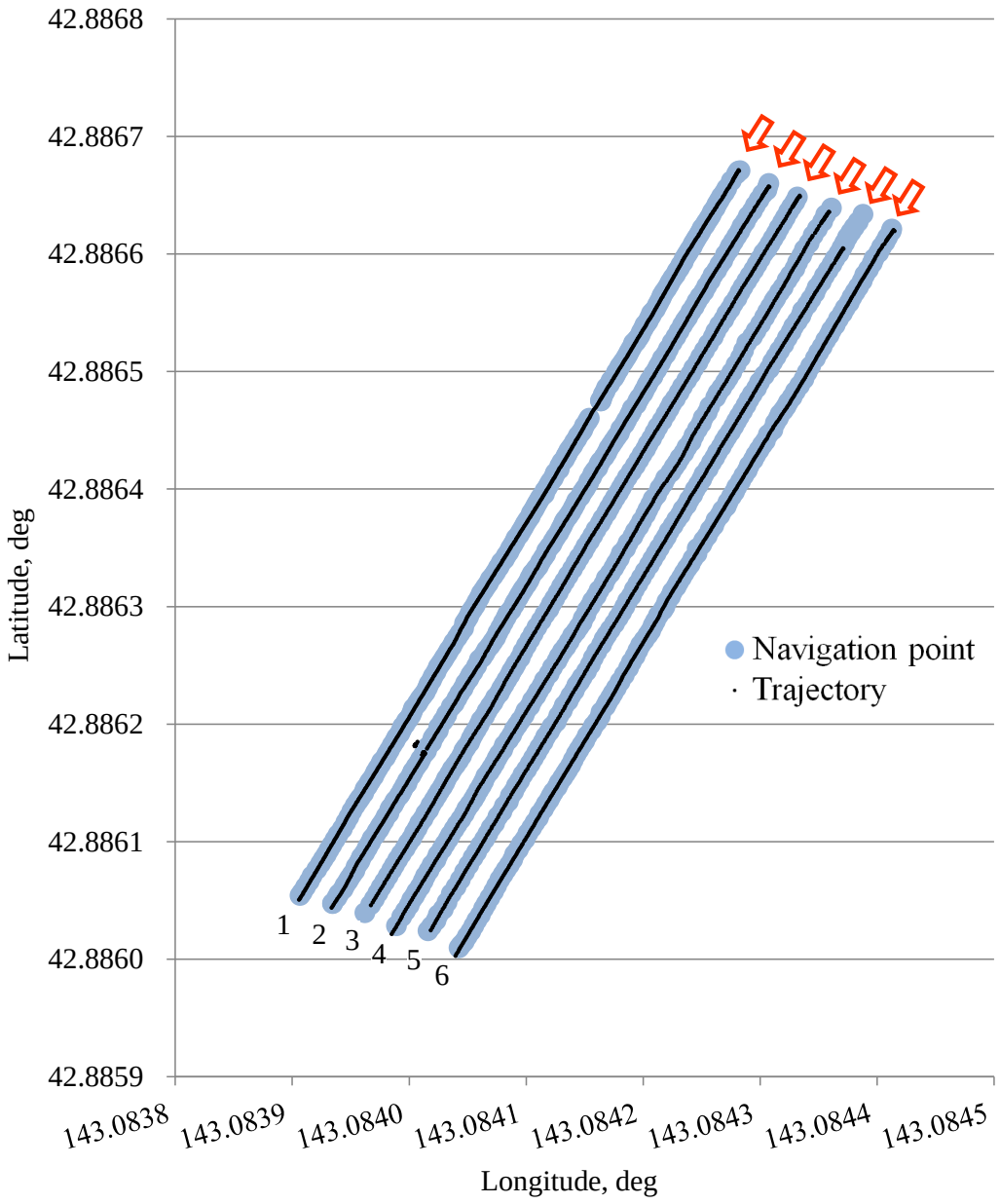

Figure 6-20 Soybean field map and trajectory

The order of the paths was one by one and the top left path was the first one. It can be seen in the map that the first path was broken into two separate ones. This is because that when the paths were recorded, there was some data recorded when the GPS was in "float" status. However, since there is a look-ahead-distance in the navigation algorithm, the robot combine could still find its way and successfully connected the two parts of

the path. In path two, there were some points off the paths. This, however, does not indicate that the robot combine harvester was running off the path. In fact, at those points, the GPS was in "standalone" status. Thus the combine harvester stopped and waited until the GPS became "fixed" status. In all the paths, the robot combine harvester proved to navigate in a high accuracy, because the black points run through the blue points from the center.

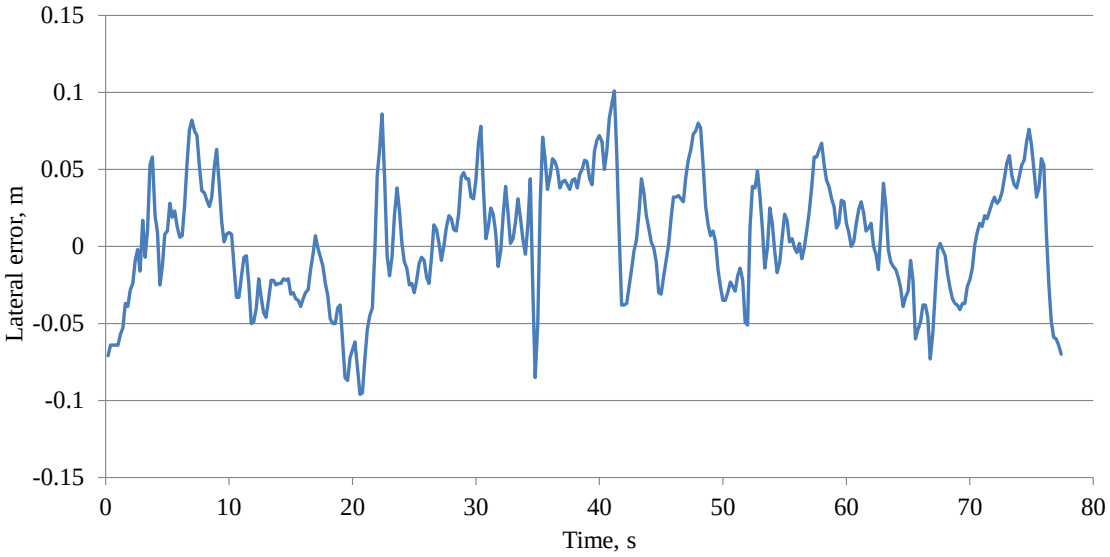

Figure 6-21 Lateral error of the first path in soybean field test (0.8 m/s)

Figure 6-21 shows the lateral error of the first path in soybean field test. In the field test, the vehicle started with a lateral error of nearly 0.07 m. Then it went towards the target path. In the middle of the path, the robot combine harvester's lateral error exceeded 0.05 m and the largest one was about 0.1 m. However, this does not mean that the robot combine harvester's accuracy is not good. In this test, the paths in the navigation map were recorded by a hand-held GPS receiver and the receiver was mounted on a long pole. Thus, a small inclination could result in an offset in the navigation path. When the combine harvester navigated with the navigation map, it

might cause a larger lateral error. However, this did not have an adverse impact on the field experiment itself. Specifically, the RMS value of the lateral error was 0.039 m.

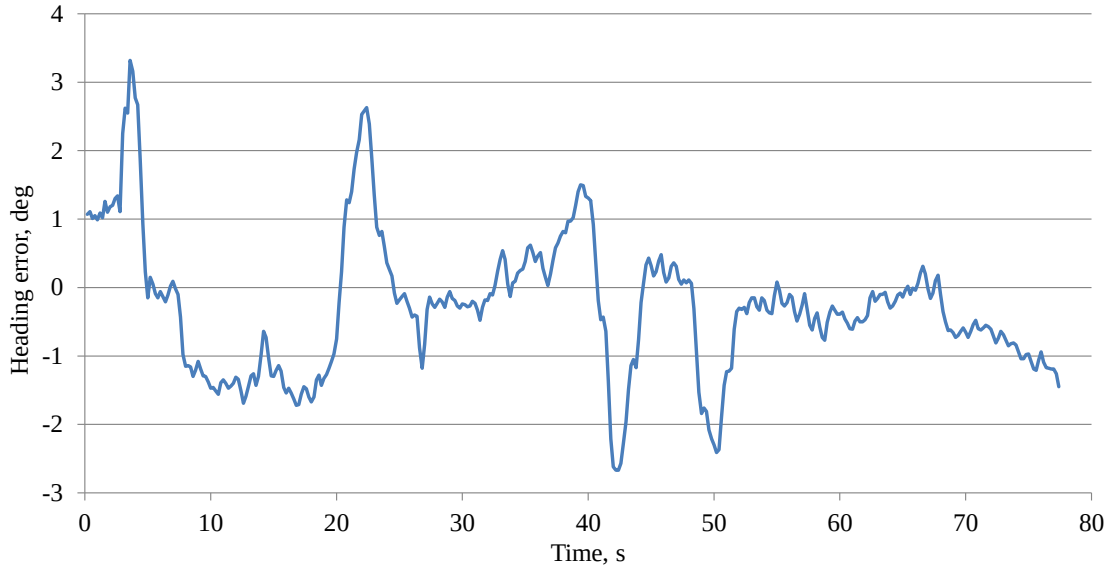

Figure 6-22 Heading error of the first path in soybean field test (0.8 m/s)

Accordingly, the heading error of the same path is shown in Figure 6-22. It can be seen that the heading error of the robot combine harvester was less than 1 deg in most of the time. From the field experiment, no noticeable oscillation happened. Thus, the vehicle was moving and steering smoothly. Specifically, the RMS value of the heading error was 1.034 deg.

Moreover, in the first two paths of the field test, the robot vehicle navigated at a speed of 0.8 m/s. This was lower than the ordinary speed of 1.0 m/s for soybean, so as to test whether the robot combine harvester could navigate stably with the row crop header. After the tests of the first two paths, it was proved that the robot vehicle could navigate at a speed of 0.8 m/s. Thereby, the speed was increased to 1.0 m/s for path 3 and path 4. Finally, in the last two paths, the vehicle speed was further increased to 1.2 m/s. The lateral error and heading error when the vehicle navigate at the speed of 1.2

m/s are shown in Figure 6-23 and Figure 6-24.

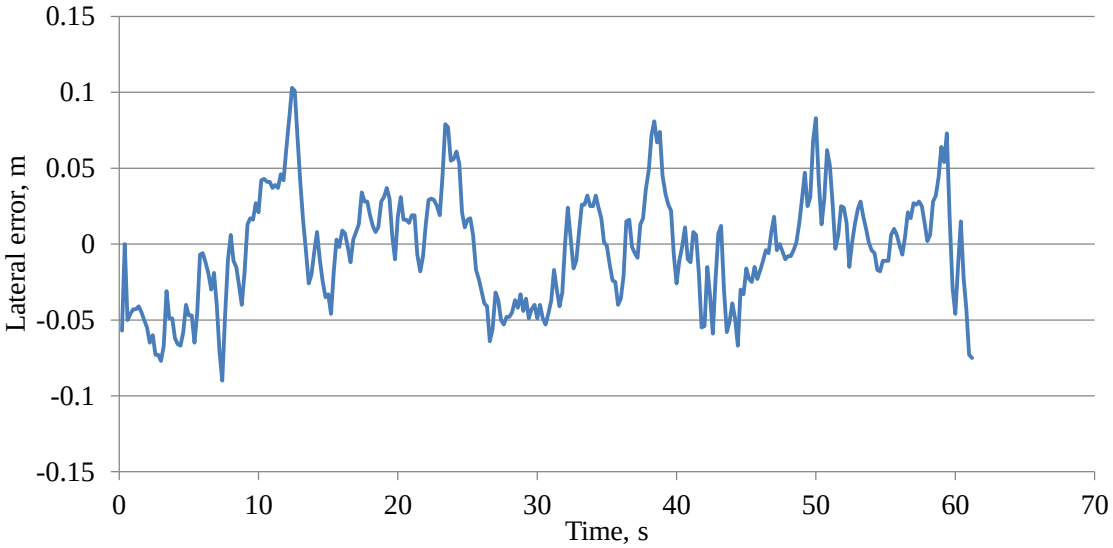

Figure 6-23 Lateral error of the last path in soybean field test (1.2 m/s)

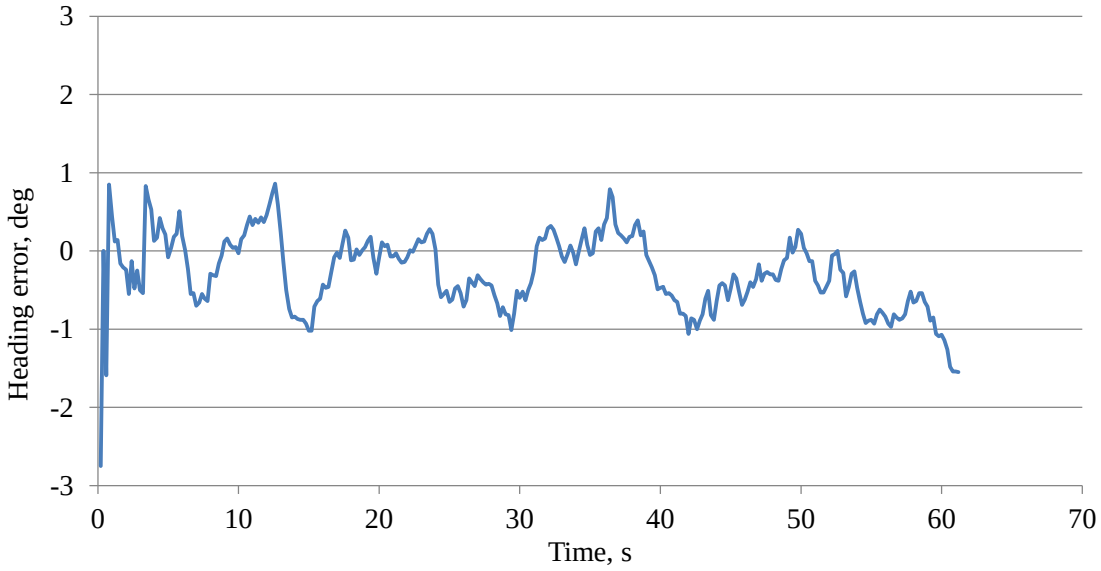

Figure 6-24 Heading error of the last path in soybean field test (1.2 m/s)

The lateral error of the test shows that most of the time the vehicle's lateral error ranged from -0.05 m to 0.05 m. The RMS value of the test was 0.037 m. The heading error of the test shows that apart from the beginning and the end of the path, the robot combine harvester navigated with its heading error ranging from -1 to 1 deg. The RMS

value of the heading error was 0.56 deg. The results indicated that when the robot combine harvester's speed increased, it could still navigate in a high level of accuracy.

6.4 Conclusions

In this chapter, the robot combine harvester was tested in the real field for wheat, paddy rice and soybean. To ensure a high level of accuracy, a correction algorithm was used. And to ensure the safety, a 2D laser scanner was modified into the safety device. Results in the field showed that the robot combine harvester can be used in the harvesting of wheat, paddy rice and soybean.

CHAPTER 7

RESEARCH SUMMARY

7.1 Introduction

Robots were invented to replace human beings in doing the repeated or dangerous work in military, industry and agriculture. It is also an effective solution to the problems of shortage and high cost of the labor force in various disciplines. The shortage of agricultural labor force has become a serious problem in the developed countries. Agricultural robot vehicles were proposed as a solution to it. So far, many agricultural robot vehicles have been developed, including robot tractors, robot transplanting machines and so on. These robots use various algorithms for navigation, among which a popular means is to use GNSS (Global Navigation Satellite System). Besides, an IMU is usually used as a complement to the GNSS to ensure higher level of control accuracy. Based on this idea, this study proposed, developed and verified a robot combine harvester.

The combine harvester used in this study is controlled by a computer via a CAN bus and through the same CAN bus, status data of the combine harvester can be sent back to the computer. As for the navigation sensor, the robot combine harvester used an RTK-GPS receiver embedded with an IMU. In order to improve the robot vehicle's safety, a laser scanner was used as the safety device. The level of accuracy was promoted by using the kinematic model of the vehicle and two path plans were realized to meet various harvesting requirements.

Moreover, the robot combine harvester was tested in various conditions, such as the

experimental field in Hokkaido University and fields owned by farmers in Hokkaido.

7.2 Research platform and materials

This research was conducted on a Yanmar AG1100 combine harvester, as shown in Figure 2-1. Before developed into a robot, it was modified from an ordinary combine harvester to a machine that can be fully controlled by sending commands via a CAN bus interface. Also, the combine harvester's status can be sent to the computer by the same CAN bus. In addition, the robot relies on an RTK-GPS receiver for its position data. Its posture data are from an IMU embedded in the RTK-GPS receiver, as shown in Figure 2-2. To ensure the safety of the robot, a 2D laser scanner was installed, as shown in Figure 2-10. This laser scanner can detect obstacle by measuring distance. It can also detect human beings if installed in a proper angle.

7.3 Navigation algorithm of the robot combine harvester

The robot combine harvester is a navigation-map-based robot. A navigation map was designed to be made up of a series of points, called navigation points, as shown in Figure 3-1. In a navigation point, there are coordinates and a code that designates the task that the robot should perform at the point. The accuracy of the robot combine harvester is affected by its accuracy of steering. In this study, the robot was designed to calculate its steering by measuring its distance to the navigation map and the difference between its yaw angle and direction of the navigation map, as shown in Figure 3-2. Besides, since there is a difference between the GPS receiver and the combine harvester's cutter, a compensation method was designed to make corrections to the navigation map, as shown in Figure 3-6.

7.4 Improvement of the navigation accuracy based on the combine harvester's kinematic model

In order to improve the level of navigation accuracy of a robot vehicle, usually repeated field trials are necessary. In this study, to free developer of robot vehicles from endless trials in the field, a kinematic model was developed and used in the simulation to improve the level of the robot combine harvester's navigation accuracy. The optimization of the control parameters included two steps. In the first step, the vehicle was optimized so that it could approach a target path in the shortest time. In the second step, when the vehicle was close enough to the target path, the control parameters were optimized and it successfully followed the target path without severe oscillations. By using this method, the efficiency of tuning control parameters of a robot vehicle can be improved to a great extent. After the optimizations on a computer, field experiments were conducted to verify the optimized control parameters. Results of the experiments showed that with the initial lateral error set to 0.15 m, 0.3 m and 0.7 m, RMS values of the lateral error were 0.022 m, 0.025m and 0.025 m when the robot navigated at the speed of 1.2 m/s. This indicated that the optimization results were satisfactory to the requirements of all the farms in Japan.

7.5 The robot combine harvester's path plan for field work

There are usually several path plans that can be applied to harvest a field. In this study, two path plans for the robot combine harvesters were verified. One of the path plans was named human-like path plan, in which the robot combine harvester imitates what farmers do in the field and harvests from the perimeters of a field to the center. Another path plan was named high-efficiency path plan, which can only be performed

by a robot with a GNSS receiver. By using this path plan, the robot vehicle did not need to decrease its speed when it turned from one path to another. And comparing to the human-like path plan, there is no straight movement in turning. Thus it can save a great amount of time in the turning of the vehicle. This method can improve the harvesting efficiency especially in small fields, like the ones in Honshu, Japan. Field experiments showed that the robot combine harvester could perform the two path plans in the experimental field of Hokkaido University.

7.6 Field verifications of the robot combine harvester

Field verifications were conducted in different areas in Japan so as to test the robot combine harvester's feasibility. In the field experiments for wheat, the high-efficiency path plan was applied. There were totally 18 paths in the navigation map and results showed that the RMS values of the lateral error and heading error of the test were 0.066 m and 1.24 deg respectively. In the paddy rice field test, the human-like path plan was used. There were 8 paths in total and the RMS values of the lateral error and heading error were 0.053 m and 1.31 deg. Finally, in the soybean harvesting test, the RMS values of lateral error and heading error were 0.039 m and 1.03 deg.

7.7 Conclusions

A robot combine harvester based on GNSS was developed in this study. An IMU was used as a complement to the GNSS. To improve the level of accuracy, a kinematic model was constructed and optimization of control parameters was conducted. To apply the robot to the harvesting of different crops, two path plans were developed and verified. They are the high-efficiency path plan and the human-like path plan. Field

experiments showed that the robot combine harvester can perform the two path plans and navigate in a high level of accuracy. The field experiments also showed that the robot combine harvester can perform harvesting tasks for wheat, paddy rice and soybean. The RMS values of lateral error and heading error were 0.066 m and 1.24 deg for wheat, 0.053 m and 1.31 deg for paddy rice and 0.039 m and 1.03 deg for soybean. The data indicated that the robot combine harvester can be applied to practical use in Japan.

REFERENCE

Backman, J., Oksanen, T., Visala, A.: Navigation system for agricultural machines: Nonlinear Model Predictive path tracking, Computers and Electronics in Agriculture, 82, 32-43, 2012a

Backman, J., Oksanen, T., Visala, A.: Path generation method with steering rate constraint, ICPA 2012, Indianapolis, USA, 15, 2012b

Backman, J., Oksanen, T., Visala, A.: Front Wheel Skidding Compensation System in Snow Ploughing. In: Agricontrol 2013, Helsinki, Finland, 2013

Barawid, O.C., Mizushima, A., Ishii, K., Noguchi, N.: Development of an autonomous navigation system using a two-dimensional laser scanner in an orchard application, Biosystems Engineering, 96(2), 139-149, 2007

Bell. T.: Automatic tractor guidance using carrier-phase differential GPS, Computer and electronics in agriculture, 25(1-2), 53-66, 2000

Benson, E.R., Reid, J.F., Zhang, Q.: Machine vision based steering system for agricultural combines, 2001 ASAE Annual Meeting, 011159, 2001

Bevly, D.: High Speed, Dead Reckoning and Towed Implement Control for Automatically Steered Farm Tractors Using GPS. Ph.D. Thesis, Stanford University, 2001

Buick, R. (2006). GPS Guidance and Automated Steering Renew Interest In Precision Farming Techniques, Agriculture Division, Westminster, Colorado, USA, Available at: www.trimble.com

Cariou, C., Lenain, R., Thuilot, B., Maritinet, P.: Path following of a vehicle-trailer system in presence of sliding: Application to automatic guidance of a towed agricultural implement, In IEEE/RSJ International Conference on Intelligent Robots and Systems (IROS), 4976-4981, Taipei, 2010

Coen, T., Vanrenterghem, A., Saeys, W., De Baerdemaeker, J.: Autopilot for a combine harvester. Computers and Electronics in Agriculture, 63, 57-64, 2008

Cho, S.I., Ki, N.H.: Autonomous speed sprayer guidance using machine vision and fuzzy logic, Transactions of the ASAE, 42(4), 1137-1143, 1999

Daly, P. "Navstar GPS and GLONASS: global satellite navigation systems", 1993

Gan-Mor, S., Clark, R. L., Upchurch, B. L.: Implement lateral position accuracy under RTK-GPS tractor guidance, Computer and Electronics in Agriculture, 59, 31-38, 2007

Han, S., Zhang, Q., Noh, H., Sin, B.: A dynamic performance evaluation method of DGPS auto guidance systems under linear parallel-tracking applications, Transactions of the ASAE, 47(1), 321-329, 2004

Iida, M., Ymada, Y.: Rice harvesting operations using an autonomous combine harvester with a GPS and FOG, Paper presented at the Automation Technology for Off-road Equipment, Bonn, Germany, 2006

Iida, M., Uchida, R., Zhu, H., Kurita, H., Suguri, M., Masuda, R.: Development of robotic head-feeding combine, Proceedings CD of the CIGR International Symposium on “sustainable Bioproduction – Water, Energy, and Food”, Tokyo, Japan, 20HOS3-06, 2011

Iida, M., Uchida, R., Zhu, H., Kurita, H., Suguri, M., Masuda, R.: Path-following control of a head-feeding combine robot, Engineering in Agriculture, Environment, and Food (EAEF), 6(2), 61-67, 2013

Inoue, K., Otsuka, H., Sugimoto, H., Murakami, N.: Sensor fusion of GPS and gyroscope by using Kalman Filter for automatic navigation (Part 1), Journal of the Society of Agricultural Machinery, 61(4), 103-114, 1999

Ishii, K., Terao, H., Noguchi, N.: Studies on Self-learning Autonomous Vehicles (Part 1), Journal of the Society of Agricultural Machinery, 56(4), 53-60, 1994 (Japanese)

Ishii, K., Terao, H., Noguchi, N.: Studies on Self-learning Autonomous Vehicles (Part 2), Journal of the Society of Agricultural Machinery, 57(6), 61-67, 1995 (Japanese)

Ishii, K., Terao, H., Noguchi, N.: Studies on Self-learning Autonomous Vehicles (Part 3), Journal of the Society of Agricultural Machinery, 60(1), 51-58, 1998 (Japanese)

Ishii, K., Terao, H., Noguchi, N.: Studies on Self-learning Autonomous Vehicles (Part 4), Journal of the Society of Agricultural Machinery, 60(2), 53-58, 1998 (Japanese)

Kaizu, Y., Imou, K.: A dual-spectral camera system for paddy rice seedling row detection, Computer and Electronics in Agriculture, 63, 49-56, 2008

Keskin, M., Say, S.M.: Feasibility of low-cost GPS receivers for ground speed measurement, Computer and Electronics in Agriculture, 54, 36-43, 2006

Kataoka, T., Al-Mallahi, A. A., Tamaki, K., Nagasaka, Y., Saito, M., Noguchi, N.: Introduction of autonomous agriculture vehicle development in Japan, Proceeding of the 2nd Eurasia Agricultural Machinery Summit Istanbul, Turkey, 1-9, 2013

Kise, M., Noguchi, N., Ishii, K., Terao, H.: Field mobile robot navigated by RTK-GPS and FOG (Part2), Journal of JSAM, 63(5), 80-85, 2001

Kise, M., Noguchi, N., Ishii, K., Terao, H.: Field mobile robot navigated by RTK-GPS and FOG (Part3), Journal of JSAM, 64(2), 102-110, 2003

Li, M., Imou, K., Wakabayashi, K., Yokoyama, S.: Review of research on agricultural vehicle autonomous guidance. International Journal of Agricultural & Biological Engineering, 2(3), 1-16, 2009

Mizushima, A., Noguchi, N., Ishii K.: Automatic guidance system based on sensor fusion with geomagnetic direction sensor and gyroscope. In Proceedings of The Fourth IFAC Symposium on Intelligent Autonomous Vehicles, 109-114, 2001

Nagasaka, Y., Taniwaki, K., Otani, R., Shigeta, K., Sasaki, Y., The Development of Autonomous Rice Transplanter.(Part 1): The Location of the Rice Transplanter by a Real-Time Kinematic GPS. Journal of the Society of Agricultural Machinery, 61(6), 179-186, 1999

Nagasaka, Y., Umeda, N., Kanetai, Y., Taniwaki, K., Sasaki, Y.: Autonomous guidance for rice transplanting using global positioning and gyroscopes, Computers and Electronics in Agriculture, 43, 223-224, 2004

Nagasaka, Y., Saito, H., Tamaki, K., Seki, M., Kobayashi, K., Taniwaki, K.: An autonomous rice transplanter guided by global positioning system and inertial measurement unit, Journal of Field Robotics, 26(6-7), 537-548, 2009

Nagasaka, Y., Tamaki, K., Nishiwaki, K., Saito, M., Kikuchi, Y., Motobayashi, K.: A global positioning system guided automated rice transplanter, Proceedings of 4th

IFAC Conference on Modelling and Control in Agriculture, Horticulture and Post Harvest Industry, 41-46, 2013

National Research Council (U.S.). Committee on the Future of the Global Positioning System; National Academy of Public Administration (1995). The global positioning system: a shared national asset: recommendations for technical improvements and enhancements. National Academies Press. p.16. ISBN 0-309- 05283-1. Retrieved 2013-08-16., Chapter 1, p. 16

Noguchi, N., Reid, J.F., Benson, E., Stombaugh, T.: Vehicle automation system based on multi-sensor integration. ASAE Paper, 983111, St. Joseph, MI, 1998

Noguchi, N., Will, J., Reid, J. Zhang, Q.: Development of a master-slave robot system for farm operations. Computers and Electronics in Agriculture, 44, 1-19, 2004

Noguchi, N., Barawid, O.: Robot farming system using multiple robot tractors in Japan Agriculture, Preprints of the 18th IFAC World Congress, 633-637, 2011

Northern Advancement Center for Science & Technology: File of 3rd Meeting of Research and Development Committee Member in 2000

Oksanen, T., Visala, A.: Coverage Path Planning Algorithms for Agricultural Field Machines, Journal of field robotics. 26 (8), 651-668, 2009

Perez-Ruiz, M., Slaughter, D.C., Gliever, C., Upadhyaya, S.K: Tractor-based Real-time Kinematic-Global Positioning System (RTK-GPS) guidance system for geospatial mapping of row crop transplant. Biosystems Engineering, 111, 64-71, 2012a

Perez-Ruiz, M., Slaughter, D.C., Gliever, C., Upadhyaya, S.K: Automatic GPS-based

intra-row weed knife control system for transplanted row crops. Computers and Electronics in Agriculture, 80, 41-49, 2012b

Pinto, F.A.C., Reid, J.F., Zhang, Q., Noguchi, N.: Vehicle guidance parameter determination from crop row images using principal component analysis, Journal of agricultural engineering research, 75, 257-264, 2000

Reid, J.F.: Establishing automated vehicle navigation as a reality for production agriculture, Proceedings of 2nd IFAC/CIGR international workshop on Bio-robotics, Information technology and intelligent control for bio production systems, 33-40, 2000

Reid, J.F., Zhang, Q., Noguchi, N., Dickson, M.: Agricultural automatic guidance research in North America, Computers and electronics in agriculture, 25(1-2), 155-16, 2000

Saito, M., Tamaki, K., Nishiwaki, K., Nagasaka, Y.: Development of an autonomous rice combine harvester using CAN bus system, Journal of the Japanese Society of Agricultural Machinery, 74(4), 312-317, 2012

Stombaugh, T., Benson, E., Hummel, J.W.: Automatic guidance of agricultural vehicles at high field speed, ASAE Paper, 983110, St. Joseph, MI, 1998

Subramanian, V., Burks, T.F., Arroyo, A.A.: Development of machine vision and laser radar based autonomous vehicle guidance systems for citrus grove navigation. Computers and Electronics in Agriculture, 53, 130-143, 2006

Suguri, M., Karita, K., Nishiike, Y.: RTK-GPS based autonomous crawler wagon control, Proceedings of the Automation Technology for Off-road Equipment (ATOE

2004), 360-368, 2004

Takai, R., Barawid, O. Jr., Ishii, K., Noguchi, N.: Development of Crawler-Type Robot Tractor based on GPS and IMU, Preprint of the IFAC International Conference on AGRICONTROL 2010 (CD-R), A3-5, 2010

Takasu, T., Ysuda, A.: Development of the low-cost RTK-GPS receiver with an open source program package RTKLIB, Paper presented at International Symposium on GPS/GNSS 2009, ICC Jeju, Korea, 2009

Tillet, N.D., Hague, T., Marchant, J. A.: A robotic system for plant-scale husbandry, Journal of agricultural engineering research, 69, 169-278, 1998

Tosaki, K., Miyahara, Y., Ichikawa, T., Mizukura, T., Kinoshita, Y.: Unmanned Sprayer Using Induction Cable (Part 1), Journal of the Society of Agricultural Machinery, 58(6), 101-110, 1996 (Japanese)

Tosaki, K., Miyahara, Y., Ichikawa, T., Mizukura, T., Kinoshita, Y.: Unmanned Sprayer Using Induction Cable (Part 2), Journal of the Society of Agricultural Machinery, 59(4), 87-96, 1997 (Japanese)

Tosaki, K., Miyahara, Y., Ichikawa, T., Mizukura, T., Kinoshita, Y.: Unmanned Sprayer Using Induction Cable (Part 1), Journal of the Society of Agricultural Machinery, 60(3), 97-106, 1998

Vougioukas, S. G.: Reactive trajectory tracking for mobile robots based on non linear model predictive control, 2007 IEEE International Conference on Robotics and Automation, ICRA, Barcelona, Spain, 3074-3079, 2007